94p.
X62-11094
Copy
54
CONFIDENTIAL
NASA TM X-655

NASA TM X-655

GROUP 4
Downgraded at 3 year intervals; declassified after 12 years

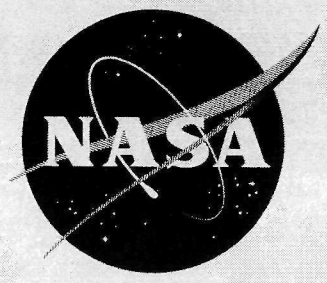

TECHNICAL MEMORANDUM

X-655

CHARACTERISTICS OF A BLUNT HALF-CONE ENTRY CONFIGURATION AT MACH NUMBERS FROM 10.9 TO 21.2 IN HELIUM

By John B. McDevitt and Jack A. Mellenthin

Ames Research Center
Moffett Field, Calif.

CLASSIFICATION CHANGED
UNCLASSIFIED
By Authority of Fed. 72-24 Date 5/15/72

CATEGORY
SPECIAL HANDLING
7

(NASA-TM-X-655) CHARACTERISTICS OF A BLUNT HALF-CONE ENTRY CONFIGURATION AT MACH NUMBERS FROM 10.9 TO 21.2 IN HELIUM J.B McDevitt, et al (NASA) Oct. 1962 94 p

N72-73004

Unclas
00/99 30875

NATIONAL AERONAUTICS AND SPACE ADMINISTRATION
WASHINGTON

October 1962

CONFIDENTIAL

NATIONAL AERONAUTICS AND SPACE ADMINISTRATION

TECHNICAL MEMORANDUM X-655

CHARACTERISTICS OF A BLUNT HALF-CONE ENTRY CONFIGURATION AT MACH NUMBERS FROM 10.9 TO 21.2 IN HELIUM*

By John B. McDevitt and Jack A. Mellenthin

SUMMARY

An experimental investigation of the aerodynamic performance and static stability of a blunt half-cone entry configuration has been made at Mach numbers of 10.9, 17.8, and 21.2 in helium. The configuration is basically one-half of a blunt 30° circular cone with a maximum trimmed lift-drag ratio of about 0.5 at hypersonic speeds. Two sets of trailing-edge controls were investigated with this configuration. The test results indicate that the configuration is statically stable throughout the range of test conditions and that both control systems studied were found to have sufficient effectiveness to trim the vehicle in the range from zero to maximum lift-drag ratio. The effectiveness of the trailing-edge controls was found to be insensitive to Mach number changes in the range from 10.9 to 21.2.

INTRODUCTION

The motion and heating of entry configurations have been studied in considerable detail in recent years. During entry from satellite speeds the vehicle lift can be used to reduce decelerations and heating rates and to increase maneuverability. In entry from supersatellite speeds, a lifting capability deepens the entry corridor and tends to relieve the guidance problem.

A lifting configuration suitable for an entry vehicle has been proposed for study by Eggers and Wong in reference 1. This blunt, near half-cone configuration was designed to have a maximum lift-drag ratio of approximately one-half near its trim attitude at hypersonic speeds. A preliminary evaluation of the aerodynamic performance and stability of this configuration was presented in reference 1 and additional studies

*Title, Unclassified

have been presented in references 2 through 9. Included in the studies of references 1 and 2 were trailing-edge control systems capable of providing trim from zero to maximum lift-drag ratio. The first control set studied consisted of two upper and two lower trailing-edge flaps. However, the aerodynamic lateral-directional and longitudinal control moments are cross coupled for this control set. For this reason an alternative control set was studied in reference 2. The second control set consists of single upper and lower controls for longitudinal control and single flaps at either side of the body base for yaw control. However, no provision is made for aerodynamic roll control about the longitudinal axis.

The previous experimental investigations of the aerodynamic performance and stability of this configuration were confined to tests at Mach numbers up to 6. Additional tests at higher speeds are desirable in order to determine the hypersonic characteristics of this configuration, particularly with regard to control effectiveness at hypersonic speeds. The present report presents experimental results for this configuration, including both control systems, at Mach numbers of 10.9, 17.8, and 21.2 in helium flow.

NOTATION

A base area of vehicle, $1.26\ l^2$

C_D drag coefficient, $\frac{\text{drag}}{q_\infty A}$

C_L lift coefficient, $\frac{\text{lift}}{q_\infty A}$

C_l rolling-moment coefficient, $\frac{\text{rolling moment}}{q_\infty A d}$

C_m pitching-moment coefficient, $\frac{\text{pitching moment}}{q_\infty A l}$

C_n yawing-moment coefficient, $\frac{\text{yawing moment}}{q_\infty A d}$

C_p pressure coefficient, $\frac{p - p_\infty}{q_\infty}$

C_Y side-force coefficient, $\frac{\text{side force}}{q_\infty A}$

d base diameter of vehicle

l length of vehicle

M	Mach number
M_N	nominal Mach number
p	static pressure
P_o	total pressure of helium supply gas (with real-gas correction according to ref. 11)
p_{t_2}	pitot pressure
p_∞	free-stream static pressure
q_∞	free-stream dynamic pressure
Re	Reynolds number
T_o	temperature of helium supply gas
y	lateral distance from tunnel center line
α	angle of attack (measured with respect to vehicle upper surface), deg
β	angle of sideslip, deg
δ	control deflection angle, deg (control is normal to the body base at zero deflection; positive deflections are outward into the airstream)
Δ	incremental change due to control deflection

Subscript

β	derivative with respect to angle of sideslip

CONFIGURATION

The configuration is basically one-half of a blunt 30° circular cone with a flat upper section with circular leading edges, figures 1 and 2. (Note that the reference body axis is parallel to the flat upper surface.) The nose is essentially a portion of a hemisphere-cone, modified slightly as described in reference 2.

CONFIDENTIAL

Two sets of trailing-edge controls were used in conjunction with the basic body. "Control set I" consists of four trailing-edge flaps with an aspect ratio of 0.6, see figure 1(b). "Control set II" consists of two horizontal flaps with aspect ratios of 1 and two vertical flaps with aspect ratios of 0.6, see figure 1(c).

The horizontal flap size of control set II was chosen (based on Newtonian impact calculations) so that the longitudinal control effectiveness would be approximately equal to that for control set I. By definition, the controls are normal to the body base at zero deflection and positive deflections are outward into the oncoming stream.

APPARATUS AND TESTS

The tests were conducted in the Ames 14-Inch Helium Tunnel. A schematic diagram of the helium tunnel is presented in figure 3 and a brief discussion of this facility is presented in the appendix of this report.

The test Mach numbers and test Reynolds numbers (based on model length) are given in the following table:

M	Re
10.9	0.8×10^6
17.8	0.8×10^6
21.2	1.2×10^6

An attempt was made to obtain data at a constant Reynolds number of 0.8×10^6 (based on model length) throughout the speed range. However, satisfactory results could not be achieved with the nozzle having a nominal Mach number of 21 at this Reynolds number for this particular configuration. It was found necessary to operate this nozzle at a somewhat higher total pressure and a test Reynolds number of 1.2×10^6.

Data were obtained in the angle-of-attack range from about -14° to $+14^\circ$ by the use of the model-support pitching mechanism. Some additional data were obtained at angles of attack from about -26° to -14° by use of a bent sting. The lateral-directional characteristics were obtained by rotation of the model and balance assembly 90° and then by use of the support mechanism to obtain sideslip angles from about -8° to $+8^\circ$ for angles of attack of approximately 0°, $\pm7^\circ$, and $\pm14^\circ$.

The aerodynamic forces and moments were measured with a six-component strain-gage balance. The model was supported from the base of the balance, and the exposed portion of the balance was shrouded to eliminate any direct aerodynamic loads on the balance. The force and moment coefficients include the contribution of the base-pressure coefficient. The

CONFIDENTIAL

base-pressure coefficient was measured and found to be small (less than 0.010 for the tests at M = 10.9 and less than 0.005 for the higher Mach numbers).

The body-base area was used as the reference area for all force and moment coefficients. The body length was used as the reference length for the pitching-moment coefficient while the body-base diameter was used as the reference length for the yawing- and rolling-moment coefficients.

The accuracy of the experimental results was affected, primarily, by the uncertainties in the angles of attack, sideslip, and control deflection and in the dynamic pressure used in the reduction of the data. The angles of attack and sideslip were subject to a maximum error of 0.2° while the control deflection angle was subject to a possible error of 2°. The maximum error in dynamic pressure is believed to be less than 1 percent at Mach numbers of 10.9 and 17.8 and less than 1.5 percent at Mach number 21.2.

RESULTS AND DISCUSSION

The experimental results were obtained at free-stream Mach numbers of 10.9, 17.8, and 21.2. The aerodynamic characteristics of the basic body are presented first, followed by presentations of the control effectiveness of two sets of trailing-edge controls. Comparisons are made between the experimental results and estimates obtained by use of simple impact theory with $C_p = 2 \sin^2\varphi$ and modified impact theory with $C_p = C_{p_{max}} \sin^2\varphi$ where the angle φ is the inclination of the local surface with respect to the oncoming flow. (The theoretical estimates were obtained with the assumption that the pressure coefficient was zero on all surfaces shaded from the oncoming flow, and, in addition, skin friction was neglected.) The maximum pressure coefficient, $C_{p_{max}}$, is defined as

$$C_{p_{max}} = \frac{p_{t_2} - p_\infty}{q_\infty}$$

(At high Mach numbers the approximation $C_{p_{max}} = p_{t_2}/q_\infty$ can be used.) Values of $C_{p_{max}}$ for air and helium are tabulated below for various Mach numbers:

M	$C_{p_{max}}$, air	$C_{p_{max}}$, helium
5	1.81	1.74
10	1.83	1.76
20	1.84	1.76
∞	1.84	1.76

At high Mach numbers the coefficients are insensitive to changes in the Mach number and the coefficient for helium is approximately 4 percent less than that for air. It might be expected for those cases where experiment and modified impact theory agree well for air, that reasonably good agreement would also be obtained for similar studies in helium. Some additional information regarding the air-helium simulation problem at hypersonic speeds may be obtained from reference 10 where experimental force and moment data for a wide variety of shapes tested in air and in helium have been compared. In general, good agreement between the air and helium results were obtained and it was concluded in reference 10 that helium tunnels can contribute substantially to configuration studies at hypersonic speeds.

Basic Body

The longitudinal characteristics of the basic body are presented in figure 4 and the lateral-directional characteristics are presented in figure 5. Typical variations of C_l and C_n with angle of sideslip are shown in figure 6. (In all cases the lateral-directional coefficients varied linearly with sideslip angle from about -4° to $+4^\circ$.) The results presented in figure 4, at $M = 10.9$, indicate that the longitudinal characteristics agree better with modified impact theory at negative angles of attack and better with simple impact theory with increasing angle of attack. At the higher Mach numbers the agreement with the modified theory is better over a wider range of angles of attack. The lateral-directional characteristics shown in figure 5 are nearly insensitive to both Mach number and angle of attack. It is also noted that the basic body has somewhat greater directional stability and somewhat smaller effective dihedral than indicated by theory.

The trim characteristics of the basic body are presented in figure 7 and it is noted that the basic body trims near zero angle of attack at all Mach numbers without the use of controls. The force coefficients decrease somewhat with increasing Mach number but in the same manner so that the lift-drag ratio remains constant. The stability derivatives decrease slightly with increasing Mach number and the configuration remains statically stable about all three axes at its trim condition.

Control Effectiveness

The characteristics of the various controls of set I (fig. 1(b)) and set II (fig. 1(c)) were determined with each control tested at deflections of 0°, 30°, and 60° (some limited data were also obtained at $M = 10.9$ for control deflections of 90°). Additional data were obtained at $M = 10.9$, with adjacent controls of set I deflected simultaneously instead of individually, to secure information regarding possible interference effects between adjacent controls.

The basic experimental data obtained with control set I are presented in figures 8 through 15 and the basic data obtained with control set II

are presented in figures 16 through 24. The lateral stability derivatives, evaluated at $\beta = 0^\circ$, which are tabulated in table I, were obtained by tests of the model at sideslip angles from -8° to $+8^\circ$. The coefficients, in all cases, varied linearly with β in the range from about -4° to $+4^\circ$.

Control set I.- This control set consists of two upper and two lower trailing-edge flaps (fig. 1(b)). Because of the particular geometry involved, the aerodynamic lateral-directional and longitudinal control moments are cross coupled for this control set.

The longitudinal characteristics of the basic body with control set I undeflected are presented in figure 25 for Mach numbers of 10.9 and 21.2 in helium (present tests) and Mach numbers of 3 and 5 in air (ref. 2). The force coefficients in general decrease with increasing Mach number and at the highest Mach number agree well with estimated values, particularly for angles of attack near zero. The theory tends to overestimate the force coefficients at negative angles of attack and underestimates the measured values at positive angles of attack. The pitching-moment coefficients agree reasonably well with estimated values throughout the angle-of-attack range. In this case, with the controls undeflected and in the lee of the body, the trim angles of attack do not differ, within the experimental accuracy of the data, from the trim angles of attack presented previously for the body alone (see fig. 7).

The variations of force coefficients and stability derivatives with Mach number at $\alpha = 0^\circ$ for control set I undeflected are shown in figures 26 and 27. The present tests in helium appear to correlate well with the results in air at lower Mach numbers. At the very high Mach numbers the aerodynamic quantities agree almost exactly with estimated values (modified impact theory) with the exception that the effective dihedral is somewhat less than indicated by theory.

The control characteristics at $\alpha = 0^\circ$ for control set I are summarized in figure 28. The Mach number effect is, for the most part, less than the experimental accuracy of the present tests and a single solid line has been faired through the data points. Also presented in figure 28 are estimated values and previous results obtained in air at $M = 5$ (ref. 2). The present results agree closely with the test results obtained in air. In fact, the control effectiveness appears to be substantially the same throughout the speed range from $M = 5$ to $M = 21.2$. The agreement between experiment and theory is reasonably good for deflections of the lower control. However, large deflections of the upper control produce incremental pitching and rolling moments somewhat less than those predicted by impact theory. This is probably due to the fact that deflections of the upper control induce large flow separation effects ahead of the control which are not accounted for in a simple application of impact theory.

The results presented in figure 28 also indicate that, when the upper controls are used for roll controls, large pitching and yawing moments are also provided (see also figs. 8(c), 12(c), and 14(c)). The cross coupling of the lateral-directional and longitudinal control moments is discussed in some detail in reference 2 where it is pointed out that the cross coupling can be eliminated near zero angle of attack by the proper deflection of the controls, but eliminating the cross coupling aerodynamically over a wide range of angles of attack does not appear to be feasible.

As previously mentioned, additional data were obtained at $M = 10.9$ with the adjacent controls of set I deflected simultaneously, instead of individually, to obtain information regarding possible interference effects between adjacent controls. The incremental changes in longitudinal characteristics due to the deflection of adjacent controls and the deflection of single controls are presented in figure 29. The incremental changes for both upper or both lower controls are about twice those for single controls, indicating that the interference effects between adjacent controls are small, or negligible. Also presented in figure 29 are results obtained in air at $M = 5$ and $\alpha = 0^\circ$ for both upper and both lower flaps. These results agree well with the present results obtained in helium at $M = 10.9$.

The longitudinal aerodynamic characteristics at trim for deflections of the upper and lower controls are presented in figure 30 for a Mach number of 10.9. It is apparent that this control system has sufficient effectiveness to trim the vehicle from zero to maximum lift-drag ratio. The maximum lift-drag ratio occurs near zero angle of attack for controls undeflected and zero lift is obtained near $\alpha = -23^\circ$ for lower controls deflected approximately 53°. Static longitudinal stability is maintained at all times. The aerodynamic characteristics at trim for the higher Mach numbers are essentially the same as those presented in figure 30 since, as previously mentioned, the control effectiveness appears to be substantially the same throughout the speed range considered (see fig. 28).

Control set II.- This control set (fig. 1(c)) consists of single upper and lower controls for longitudinal control and single flaps at either side of the body base for yaw control. However, no provision is made for aerodynamic roll control about the longitudinal axis. (It has been suggested in reference 2 that a reaction-type system be used for roll control in this case.) Because of the particular arrangement used, this control set produces yawing and pitching moments largely independent of each other.

The variation of incremental changes of moment and force coefficients with control deflection at zero angle of attack is shown in figure 31. As in the previous case for control set I, these results agree closely with data obtained in air at $M = 5.0$, and indicate that the Mach number effect is insignificant. The longitudinal characteristics at trim are presented in figure 32 for a Mach number of 10.9. It is apparent that

this control system also has sufficient effectiveness to trim the vehicle from zero to maximum lift-drag ratio. The effectiveness of the lower control is almost precisely that for both lower controls of set I. The maximum lift-drag ratio occurs near zero angle of attack for controls undeflected. Zero lift is obtained near $\alpha = -23^\circ$ for the lower control deflected about 53° and static stability is maintained throughout. The aerodynamic characteristics at trim for the higher Mach numbers are essentially the same as those presented in figure 32 for $M = 10.9$.

Schlieren photographs.- Schlieren photographs of the model with the upper and lower controls of set II deflected 30°, 60°, and 90° are presented in figure 33 for various model angles of attack from -12° to $+12^\circ$ at $M = 10.9$. With one exception (fig. 33(b)) two photographs, obtained with different settings of the schlieren knife edge, are presented for each control setting and model angle of attack to indicate most effectively both the flow separation and shock-wave patterns. In the photographs presented on the left side of figure 33 the shock waves in the upper half of each photograph appear as light lines while the shock waves in the lower portion appear as dark lines. The flow separation regions and/or boundaries appear as light intensities opposite to those for the shock waves. On the right and left side of figure 33 the photographs display the flow phenomena with exactly opposite light intensity.

These photographs indicate that large deflections of trailing-edge controls can induce large flow-separation regions forward of the controls. For control deflections of 30° the flow separation regions are small but for control deflections of 60° the separation regions become large and for deflections of 90° extensive regions of highly turbulent, unsteady flow are indicated. Although photographs have been presented as a matter of interest for control deflections of 90°, it should be pointed out that this vehicle can be trimmed from maximum lift-drag ratio to zero lift by lower control deflections in the range from about 0° to 53° (see fig. 32(a)). Consequently, control deflections resulting in highly turbulent, unsteady flow can be avoided.

A comparison of schlieren photographs obtained at Mach numbers of 10.9 and 21.2 for the model with upper and lower controls of set II deflected 60° is presented in figure 34. In general, the flow phenomenon appears to be identical at the two Mach numbers.

Lateral stability derivatives.- The measured lateral stability derivatives at $\alpha = 0^\circ$ for control sets I and II are tabulated in table I. It is evident that variations in Mach number and control deflection angle have very little effect on stability values with the exception that C_{n_β} for the side control of set II increases somewhat with control deflection angles. In general, the presence of the trailing-edge controls perturb but slightly the stability levels shown in figure 5 for the basic body.

CONCLUDING REMARKS

An investigation has been made at Mach numbers from 10.9 to 21.2 in helium flow of the performance, stability, and control characteristics of a high-lift, high-drag, entry configuration. The tests included studies of the basic body and two control systems. The results of these tests indicate the following:

1. The longitudinal characteristics of the basic body change only slightly in the Mach number range from 10.9 to 21.2. The lateral-directional characteristics are insensitive to both Mach number and angle of attack. The measured characteristics agree reasonably well with impact theory over a wide range of angles of attack.

2. The basic body is self-trimming near zero angle of attack at all Mach numbers. The force coefficients at trim decrease somewhat with increasing Mach number but in the same manner so that the lift-drag ratio remains constant. The basic body at trim is statically stable about all three axes although the static stability levels decrease slightly with increasing Mach number.

3. Either of the control systems studied provides trim at lift-drag ratios from zero to the maximum (about 0.55) and the vehicle is statically stable about all three axes.

4. The aerodynamic characteristics of the various controls were found to be insensitive to changes in Mach number in the range from 10.9 to 21.2 and to agree well with previous results obtained in air at $M = 5.0$.

5. For one of the control sets studied (control set I), the lateral-directional and longitudinal control moments are cross coupled. The second control set provides yawing and pitching moments nearly independent of each other but does not provide roll control.

6. The interference effects between adjacent trailing-edge controls of set I are small. Consequently, the control effectiveness of several deflected controls can be estimated closely from the sum of the incremental changes in force and moment coefficients due to the deflection of individual controls.

Ames Research Center
National Aeronautics and Space Administration
Moffett Field, Calif., June 8, 1962

APPENDIX

THE AMES 14-INCH HELIUM TUNNEL

TUNNEL DESCRIPTION

A schematic diagram of the Ames 14-Inch Helium Tunnel is presented in figure 3. Three interchangeable first throats provide nominal Mach numbers M_N of 10, 17, and 21 in the test section. The tunnel is of the blowdown type, discharging into four spheres, each having a volume of 2.23×10^5 cu ft. The pressure in the spheres is reduced to about 0.3 psia for the start of each test run. The helium supply gas is withdrawn from storage tanks pressurized to 3000 psia. Running times exceed 4 minutes at each of the nominal Mach numbers.

After each test run the helium in the downstream spherical reservoirs is reclaimed and returned to the high-pressure storage tanks. A small amount of air is always present in the helium supply gas. However, the ratio of partial pressures of the air-to-helium mixture is maintained constant at 0.005 in the high-pressure storage tanks.

The flow properties in the test section were found to be essentially symmetric about the tunnel axis and the stream angle did not deviate by more than 0.2°. The lateral Mach number distributions in the high-speed central portion of the test section at longitudinal station 116 (see fig. 3) are presented in figure 35. The longitudinal Mach number gradient, per inch, near station 116 was approximately -0.04 for $M_N = 10$, approximately 0.04 for $M_N = 17$, and zero for $M_N = 21$. The Mach number values were determined by measuring the ratio of pitot pressure, p_{t_2}, to total pressure, P_o. (The total pressure P_o is the pressure in the high-pressure settling chamber, see fig. 3, with a real-gas correction applied according to ref. 11.) The effective Mach numbers corresponding to the measured values of p_{t_2}/P_o were then read from the tables of reference 12.

As previously mentioned, a small amount of air is present in the helium supply gas. Since the fluid temperature in the test section is far below the liquefaction temperature for air, most of this small amount of air has condensed and the release of latent heat has altered slightly the test-section Mach number based on the local flow velocity and temperature. However, the condensation phenomenon occurs at very low pressures, the total pressure P_o has been almost completely utilized in performing flow work and imparting momentum to the fluid, and a first-order analysis shows that the quantities p_{t_2} and q at the test section have not been altered because of the presence of a small amount of air. Furthermore the ratio q/p_{t_2} is essentially constant at large Mach numbers (M greater

than about 10). Consequently, it is concluded that the measured values of impact pressure, p_{t_2}, are directly proportional to dynamic pressure and the tables of reference 12 can be used to obtain the "effective" Mach number and corresponding "effective" dynamic pressure for use in the reduction of experimental force data.

The test-section Mach numbers vary somewhat with total pressure P_o. The effect of pressure on Mach number is illustrated in figure 36. The flow Reynolds numbers per inch in the high-speed core of the test section are presented in figure 37 for $T_o = 520^\circ$ R. (The temperature of the supply gas entering the tunnel normally does not extend outside the range of values $T_o = 520^\circ$ R $\pm 15^\circ$ R for test runs up to 2 minutes in length.)

TEST PROCEDURES

The test models are sting mounted and placed near tunnel station 116 (see fig. 3). The model support system provides an angle-of-attack range from -15° to $+15^\circ$. (This range can be extended by the use of bent stings.) Data are recorded automatically with an IBM readout system. A typical force test run, where data are obtained over an angle-of-attack range from $\alpha = -14^\circ$ to $+14^\circ$ by 2° increments, takes about 1.5 minutes.

Since the Mach number varies with lateral distance from the tunnel center line (fig. 35), an average, or effective, Mach number is used. For the present tests the local free-stream Mach number at a lateral location y corresponding to $\pi y^2 = \pi R_{max}^2/2$, where R_{max} is the maximum cross-sectional radius of the test model, was used. The dynamic pressure corresponding to this Mach number (at $y = R_{max}/\sqrt{2}$) was then used in the reduction of the experimental data.

A flow starting problem was encountered during the tests involving the nozzle having a nominal Mach number of 21. Under certain conditions, depending on the model and flap settings, hypersonic flow could not be established. It was necessary therefore to employ the "starting cone" device shown in sketch (a). The cone is strut-mounted and hydraulically

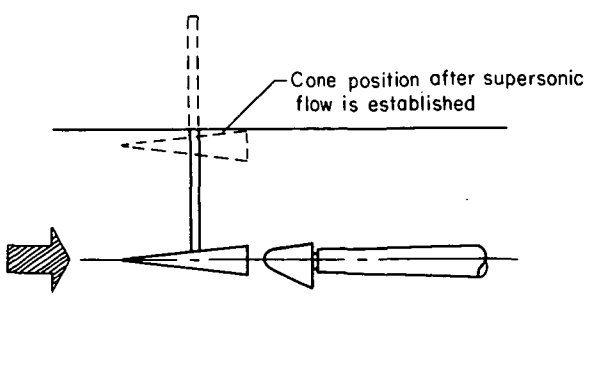

Sketch (a)

operated. The cone is placed at the tunnel center line before commencing the test run. With the cone in this position, hypersonic flow is established without difficulty and the cone is then moved into the boundary layer near the tunnel wall. In the latter position the cone does not alter the characteristics of the high-speed core.

CONFIDENTIAL

REFERENCES

1. Eggers, Alfred J., Jr., and Wong, Thomas J.: Re-entry and Recovery of Near-Earth Satellites, With Particular Attention to a Manned Vehicle. NASA MEMO 10-2-58A, 1958.

2. Sarabia, Michael F.: Aerodynamic Characteristics of a Blunt Half-Cone Entry Configuration at Mach Numbers From 3 to 6. NASA TM X-393, 1960.

3. Dennis, David H., and Edwards, George G.: The Aerodynamic Characteristics of Some Lifting Bodies. NASA TM X-376, 1960.

4. Savage, Howard F., and Tinling, Bruce E.: Subsonic Aerodynamic Characteristics of Several Blunt, Lifting, Atmospheric-Entry Shapes. NASA MEMO 12-24-58A, 1959.

5. Hassell, James L., Jr.: Investigation of the Low-Subsonic Stability and Control Characteristics of a 1/3-Scale Free-Flying Model of a Lifting-Body Reentry Configuration. NASA TM X-297, 1960.

6. Reller, John O., Jr., and Seegmiller, H. Lee: Convective Heat Transfer to a Blunt Lifting Body. NASA TM X-378, 1960.

7. Tunnell, Phillips J.: The Static and Dynamic Stability Derivatives of a Blunt Half-Cone Entry Configuration at Mach Numbers From 0.70 to 3.50. NASA TM X-577, 1961.

8. DeRose, Charles E.: The Aerodynamic Characteristics of a Blunt Half-Cone Entry Configuration Obtained From Ballistic Range Tests at Mach Numbers Near 3. NASA TM X-578, 1961.

9. Holtzclaw, Ralph W.: Static Stability and Control Characteristics of a Half-Cone Entry Configuration at Mach Numbers From 2.2 to 0.7. NASA TM X-578, 1961.

10. Henderson, Arthur, Jr.: Experimental Investigation of the Air-Helium Simulation Problem on Various General and Specific Configurations at Hypersonic Speeds. Proceedings of the Second National Symposium on Hypervelocity Techniques, 1962.

11. Erickson, Wayne D.: Real-Gas Correction Factors for Hypersonic Flow Parameters in Helium. NASA TN D-462, 1960.

12. Mueller, James N.: Equations, Tables, and Figures for Use in the Analysis of Helium Flow at Supersonic and Hypersonic Speeds. NACA TN 4063, 1957.

CONFIDENTIAL

TABLE I.- LATERAL STABILITY DERIVATIVES, $\alpha = 0$

	M	δ, deg	C_{Y_β}	C_{n_β}	C_{l_β}
Control set I	10.9	0	-0.027	0.0050	-0.0027
	10.9	30	-.028	.0053	-.0025
	10.9	60	-.028	.0050	-.0026
	17.8	0	-.027	.0052	-.0026
	17.8	30	-.028	.0058	-.0027
	17.8	60	-.027	.0054	-.0025
	21.2	0	-.026	.0043	-.0026
	21.2	30	-.027	.0053	-.0027
	21.2	60	-.026	.0045	-.0026
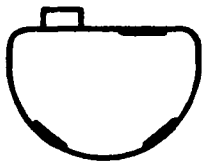 Control set I	10.9	0	-.027	.0050	-.0027
	10.9	30	-.029	.0050	-.0025
	10.9	60	-.028	.0056	-.0023
	17.8	0	-.027	.0053	-.0026
	17.8	30	-.029	.0055	-.0027
	17.8	60	-.030	.0054	-.0023
	21.2	0	-.026	.0043	-.0026
	21.2	30	-.027	.0048	-.0025
	21.2	60	-.026	.0055	-.0023
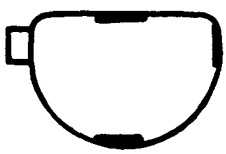 Control set II	10.9	0	-.027	.0050	-.0027
	10.9	30	-.030	.0064	-.0028
	10.9	60	-.033	.0078	-.0028
	17.8	0	-.027	.0052	-.0026
	17.8	30	-.030	.0063	-.0027
	17.8	60	-.031	.0071	-.0025
	21.2	0	-.027	.0048	-.0026
	21.2	30	-.028	.0060	-.0028
	21.2	60	-.028	.0059	-.0027

Page intentionally left blank

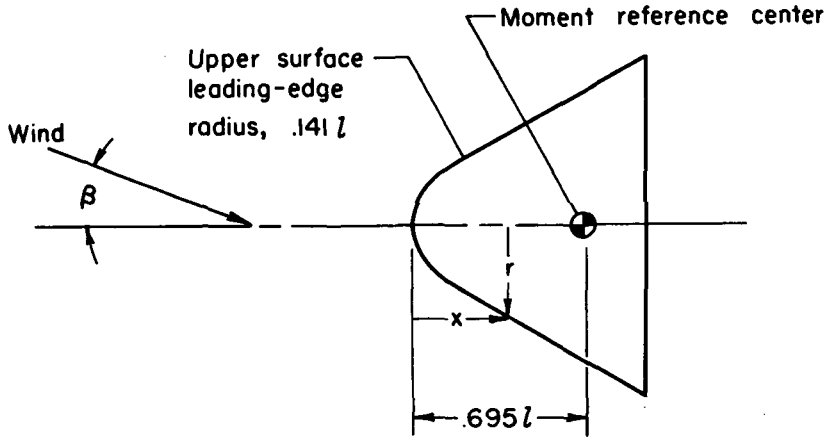

x/l	r/l	x/l	r/l
.0047	.0527	.1168	.2285
.0177	.1016	.1335	.2415
.0234	.1162	.1669	.2652
.0334	.1362	.2003	.2869
.0434	.1523	.2336	.3076
.0534	.1664	.2670	.3273
.0668	.1827	.3003	.3466
.0834	.1998	.4005	.4048
.1001	.2147	1.000	.7510

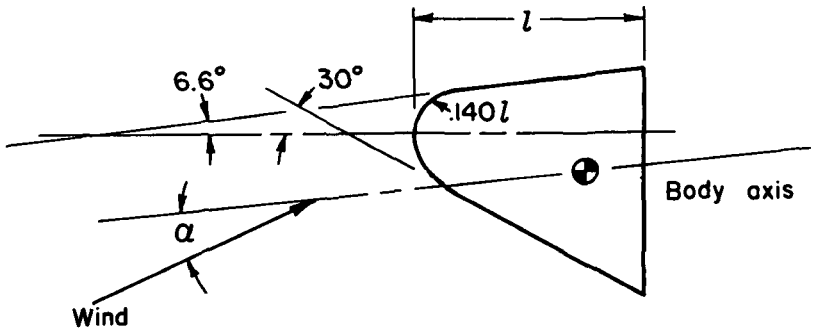

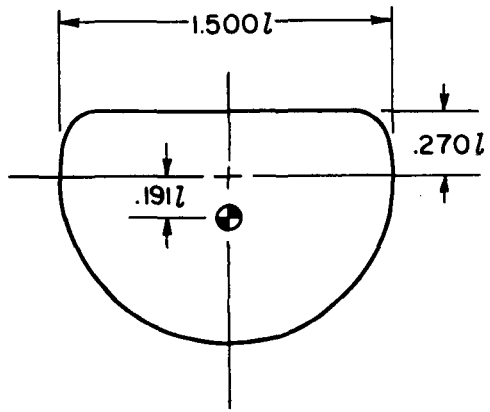

Present tests: l = 1.5 inches

(a) Basic body.

Figure 1.- Dimensions of the blunt 30° half-cone model.

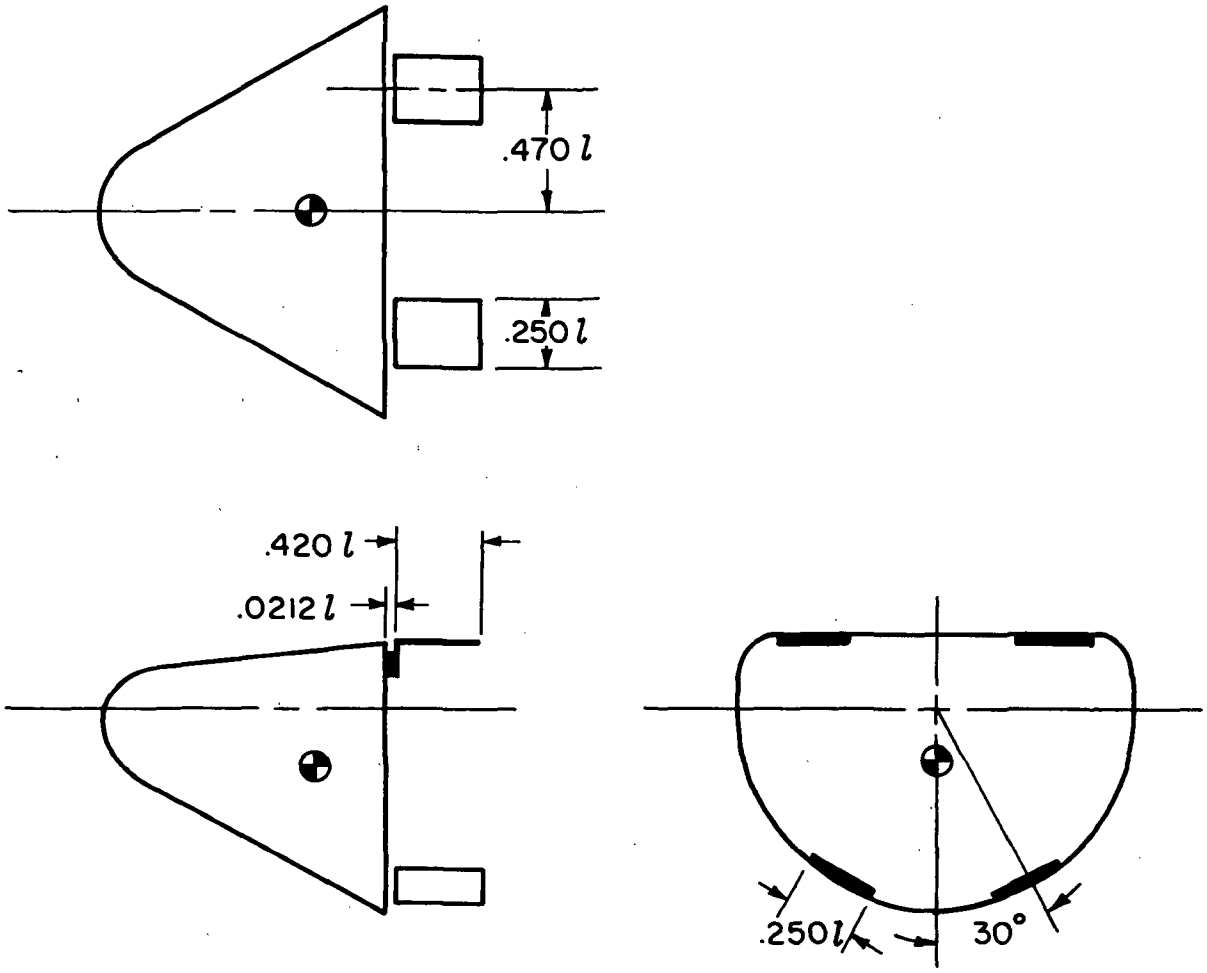

(b) Control set I.

Figure 1.- Continued.

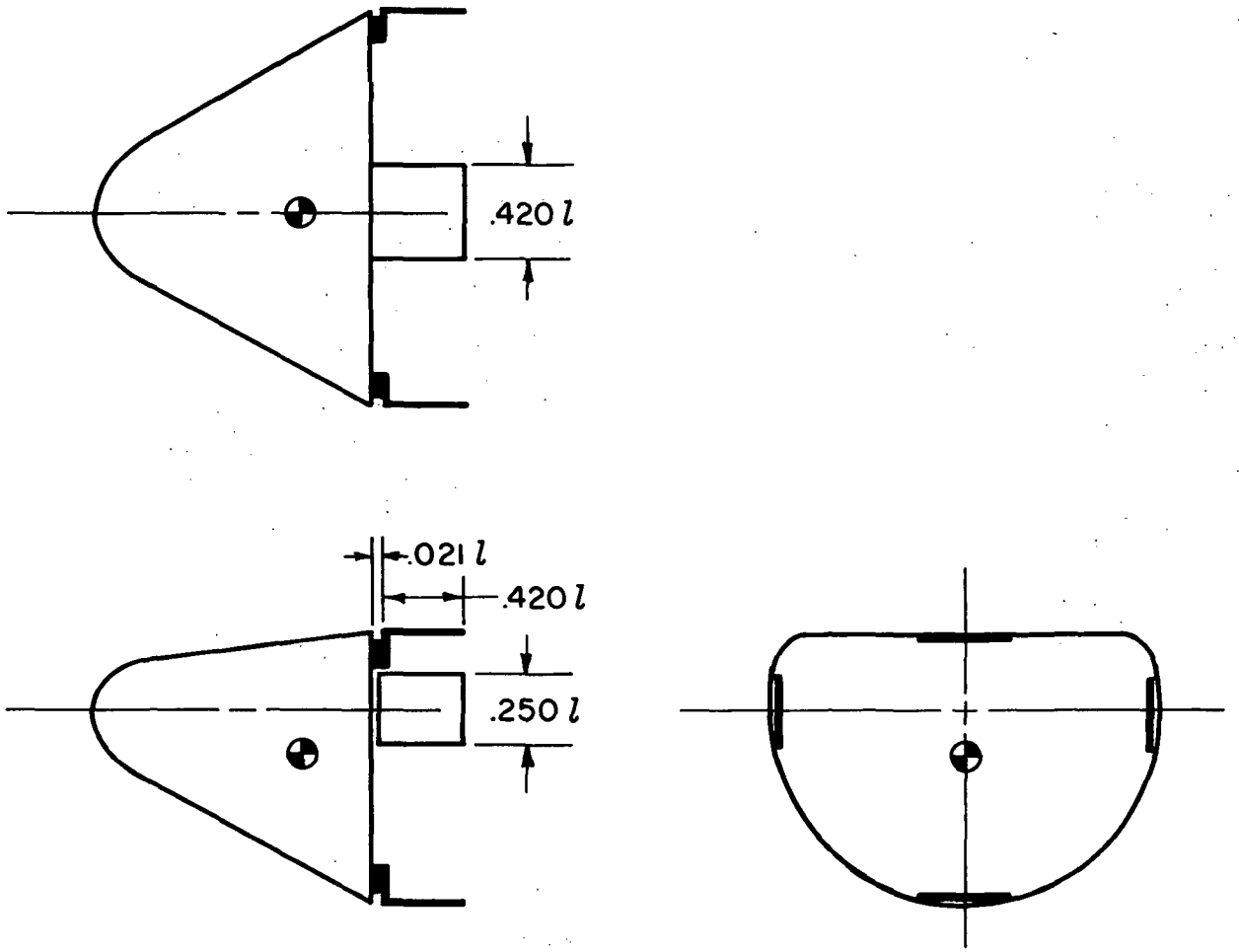

(c) Control set II.

Figure 1.- Concluded.

CONFIDENTIAL

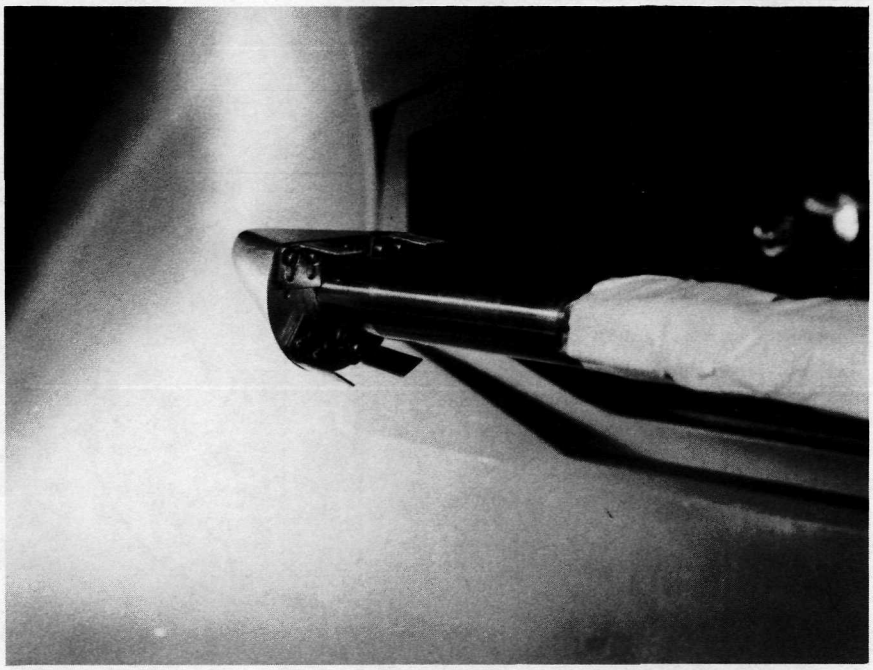

(a) Model with control set I, undeflected. A-29348

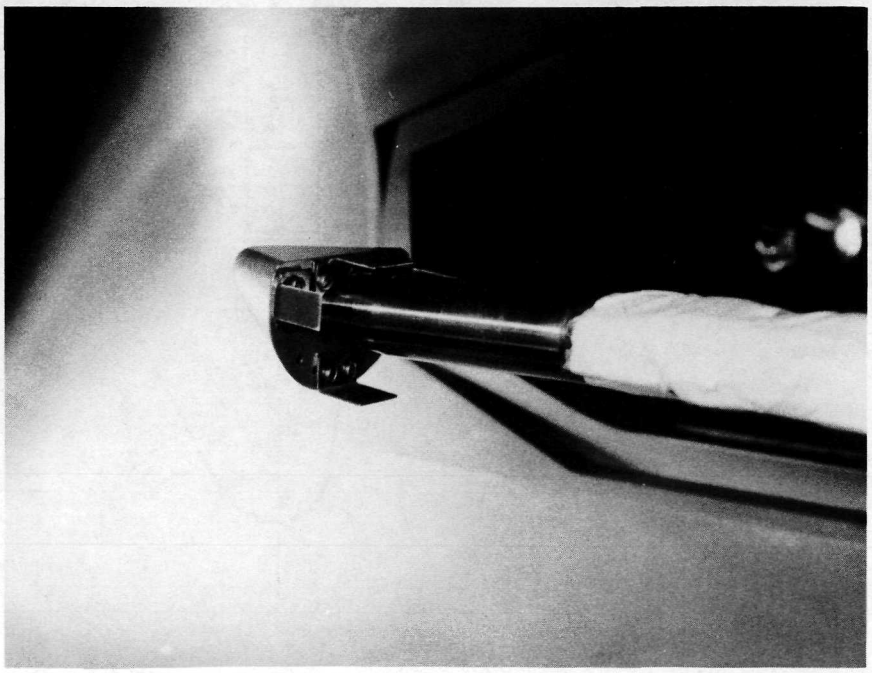

(b) Model with control set II, undeflected. A-29349

Figure 2.- Photographs of the model.

CONFIDENTIAL

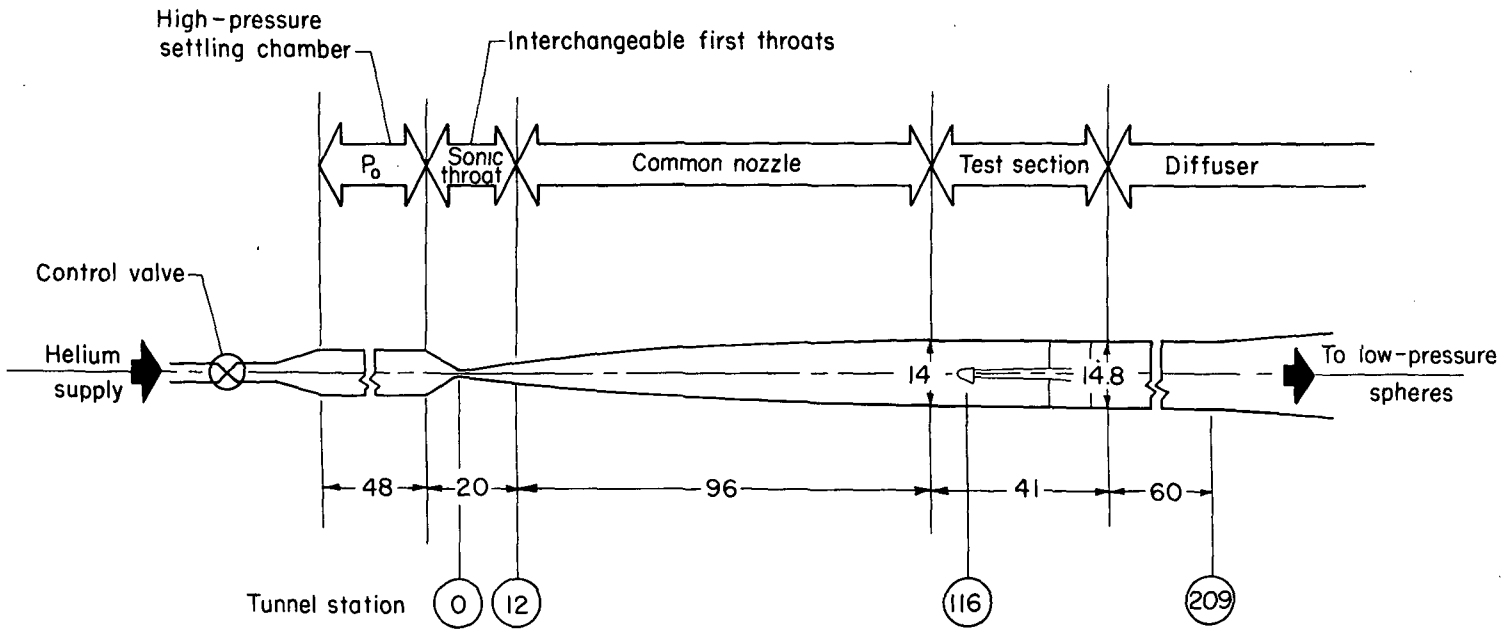

Note: All dimensions in inches

Figure 3.- Schematic diagram of the Ames 14-Inch Helium Tunnel.

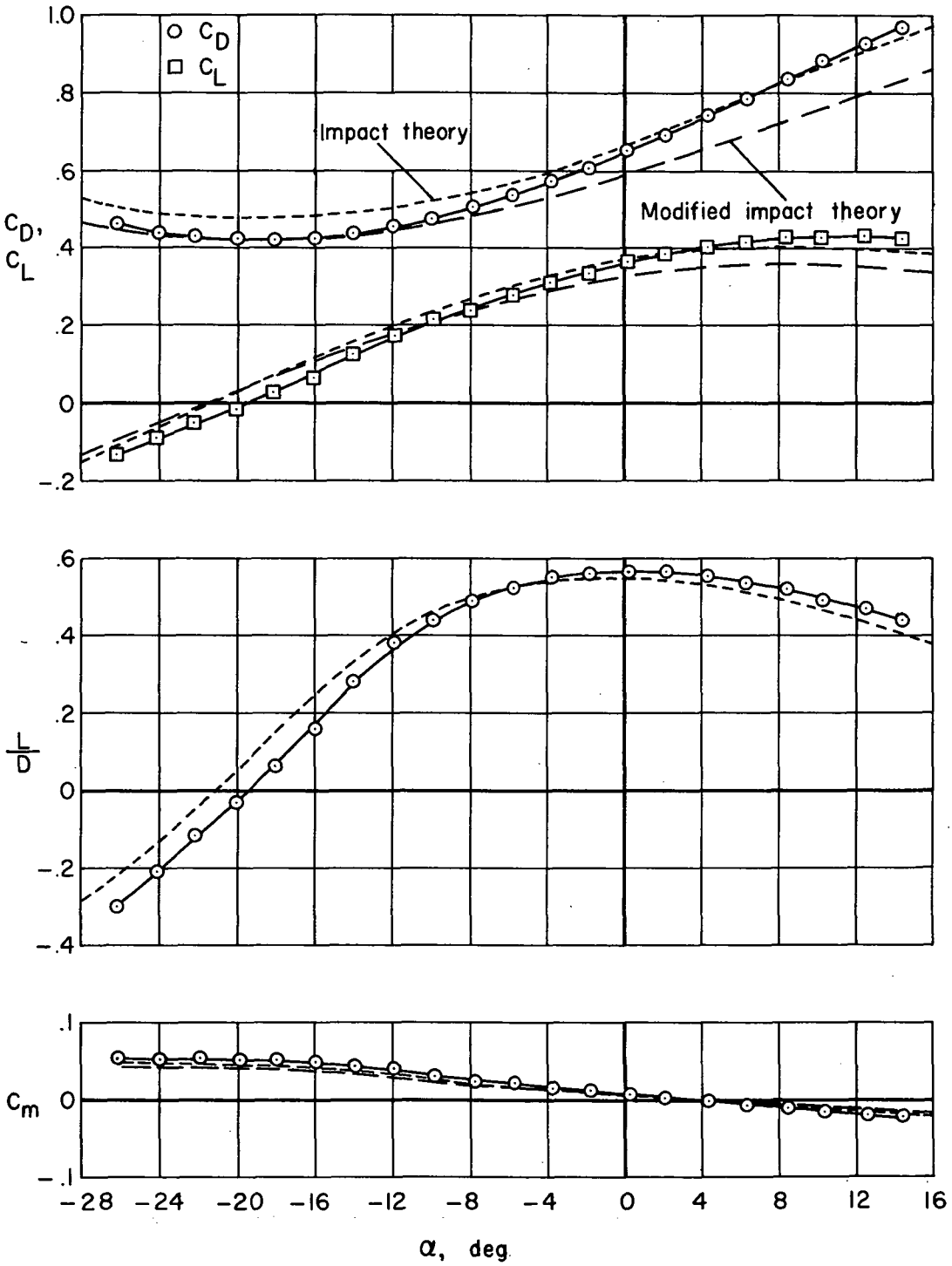

(a) M = 10.9

Figure 4.- Variation of the longitudinal characteristics with angle of attack for the basic body.

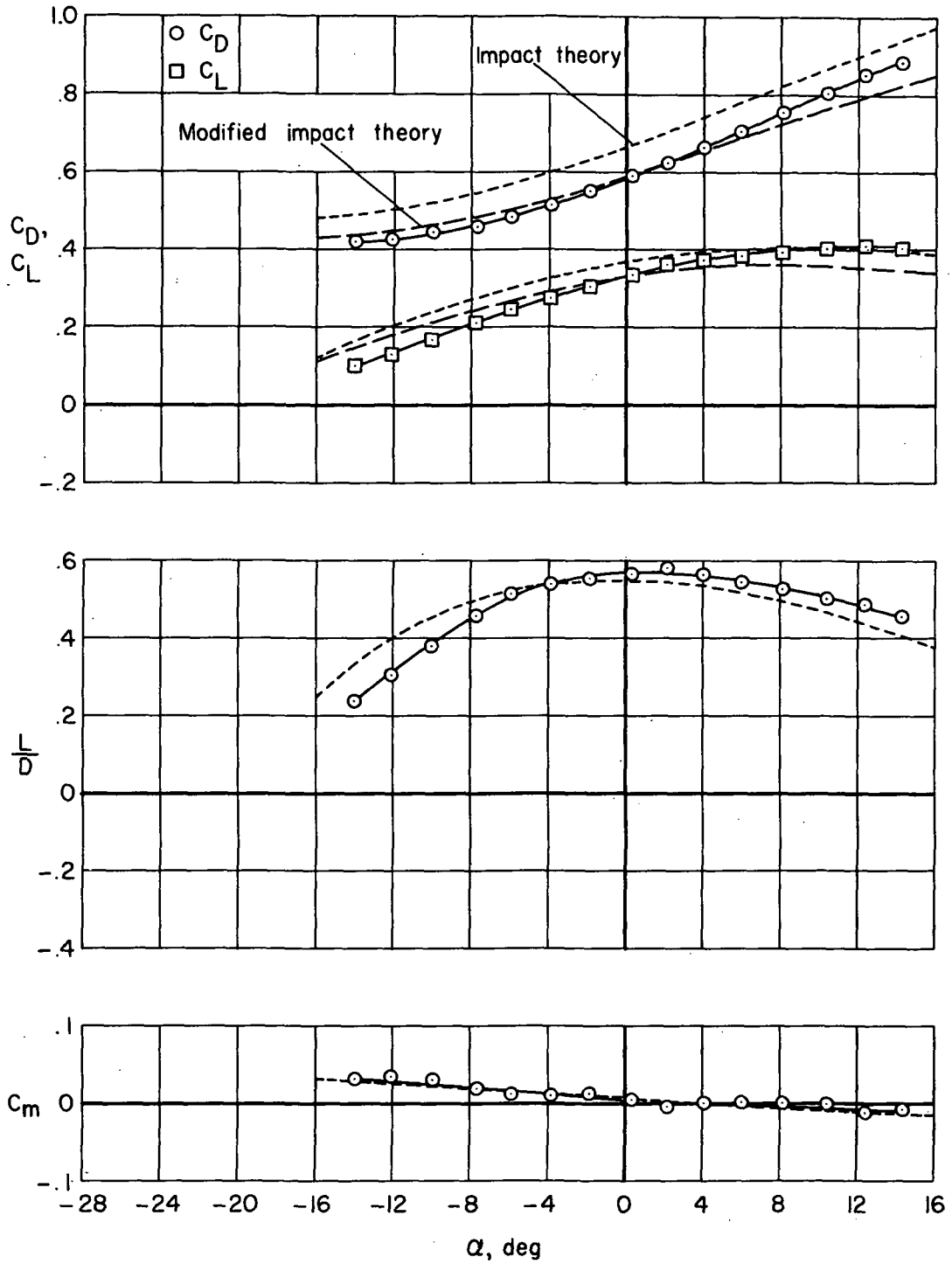

(b) M = 17.8

Figure 4.- Continued.

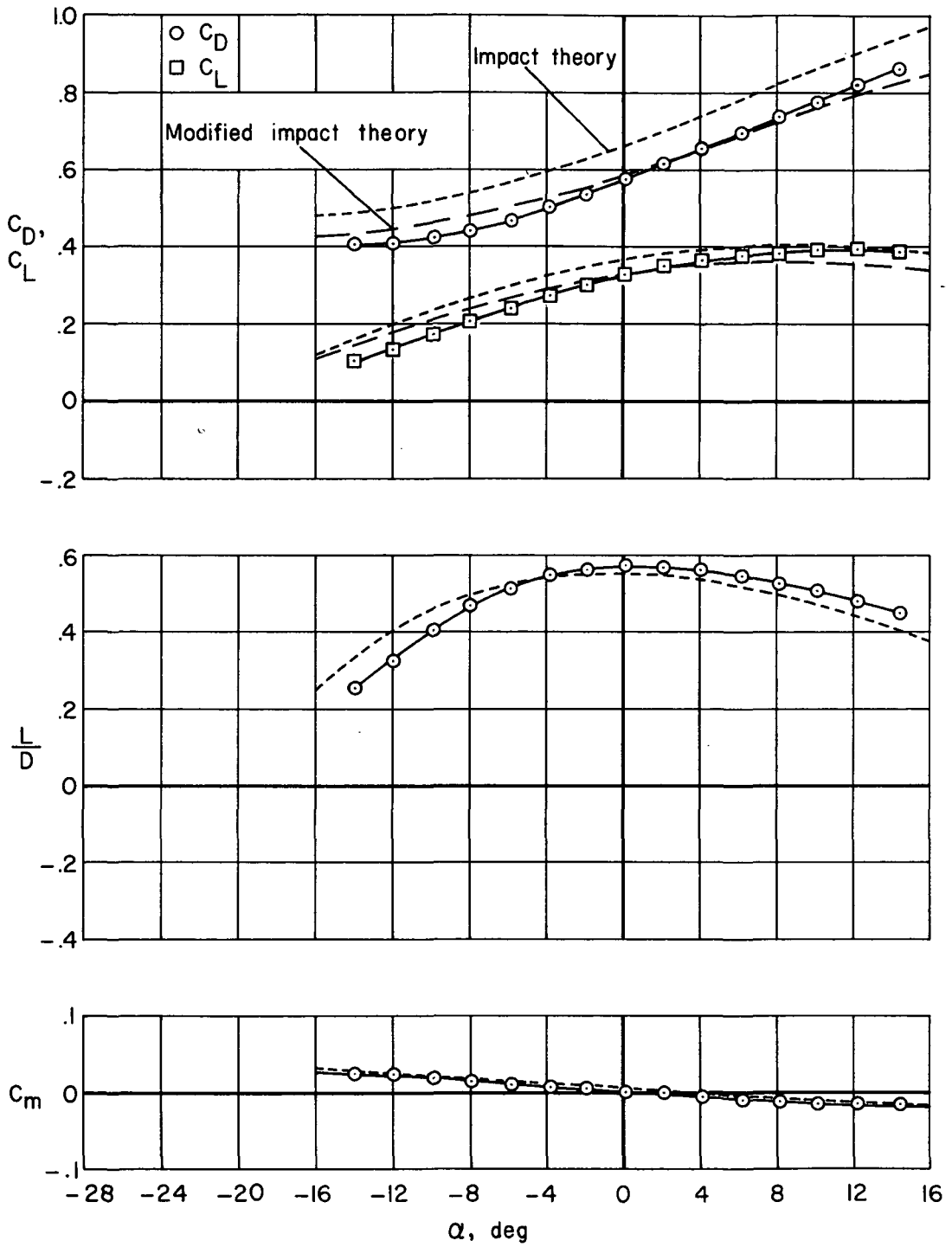

(c) M = 21.2

Figure 4.- Concluded.

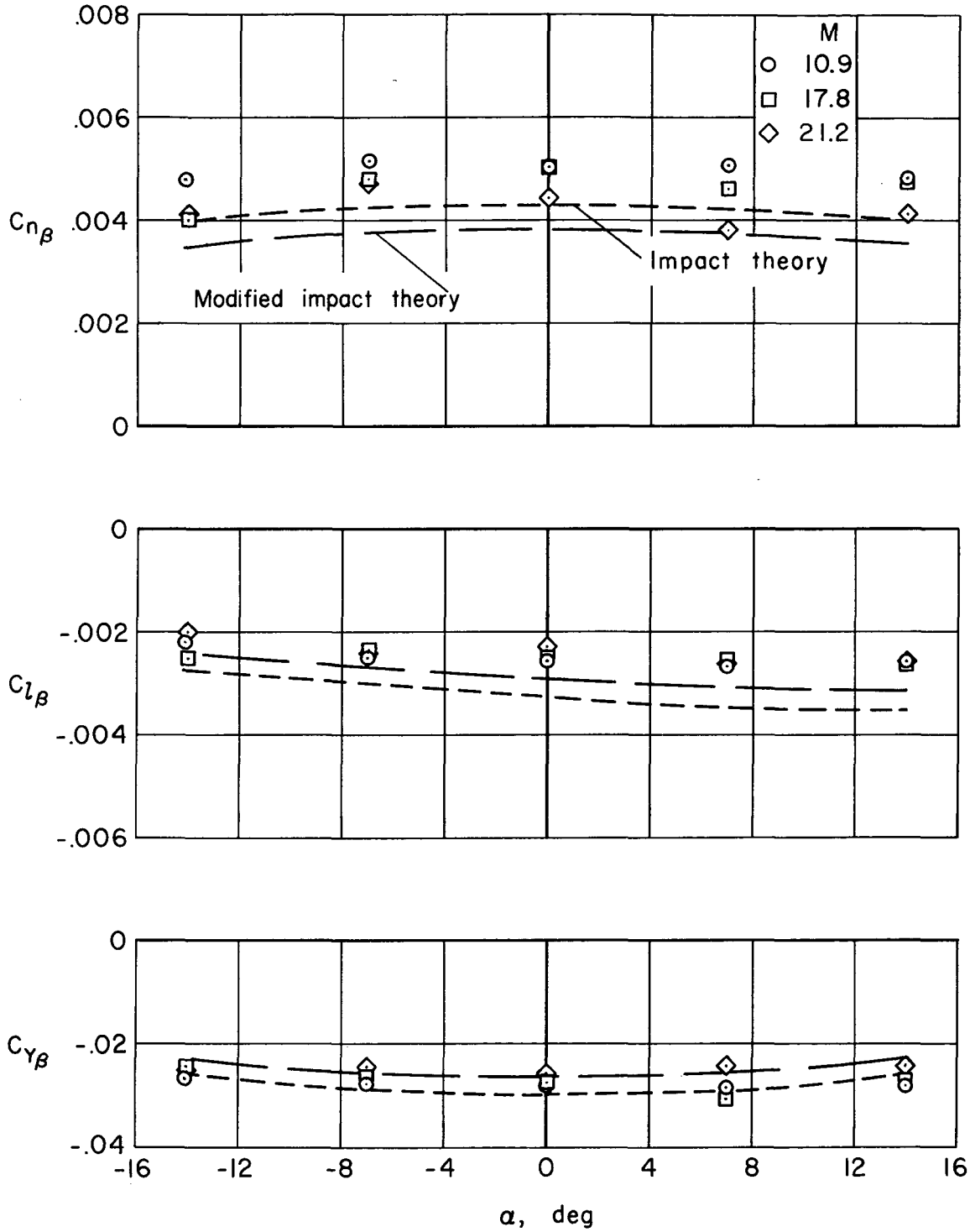

Figure 5.- Variation of the lateral-directional stability derivatives with angle of attack for the basic body.

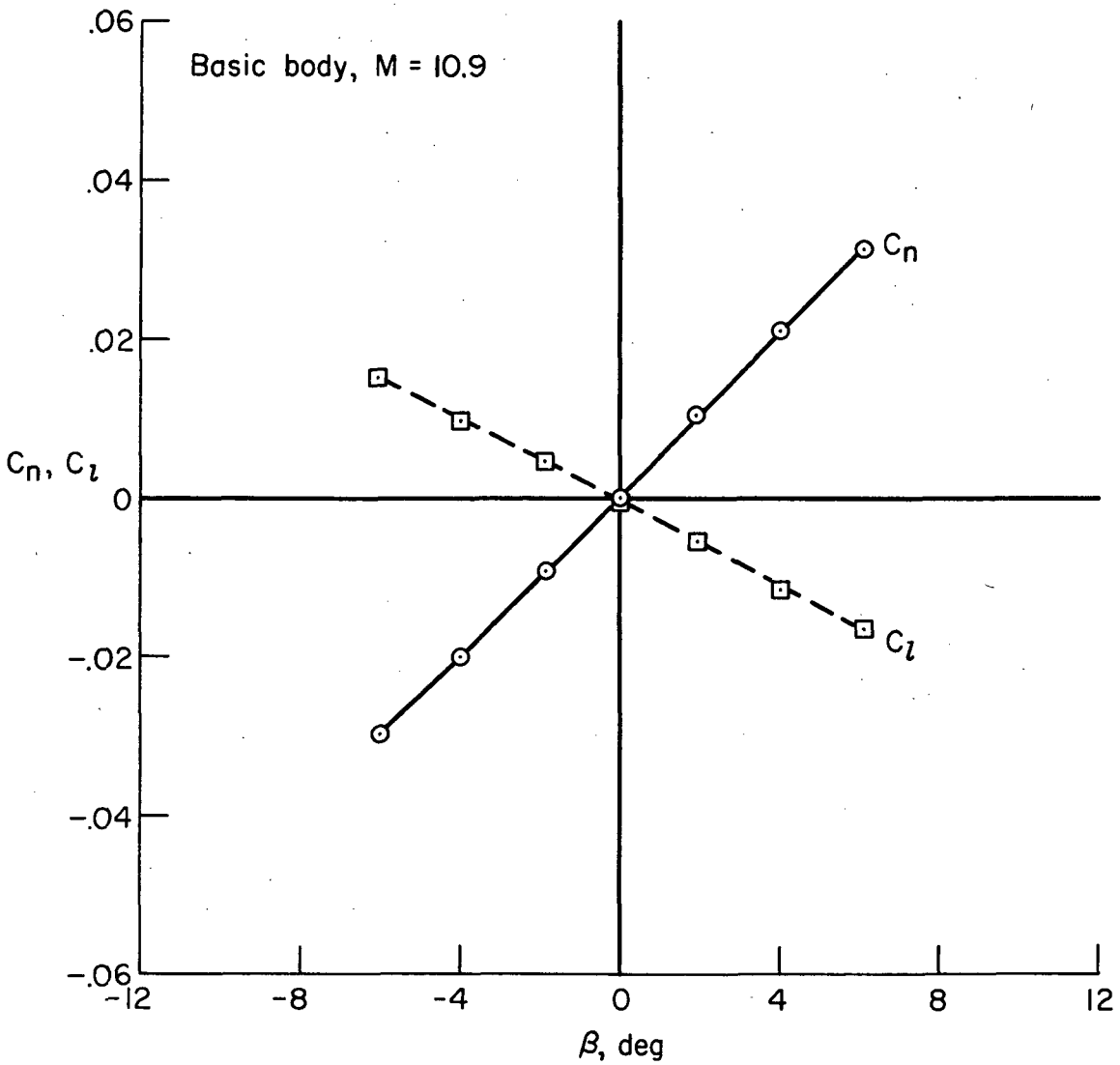

Figure 6.- Typical variations of C_n and C_l with angle of sideslip, M = 10.9.

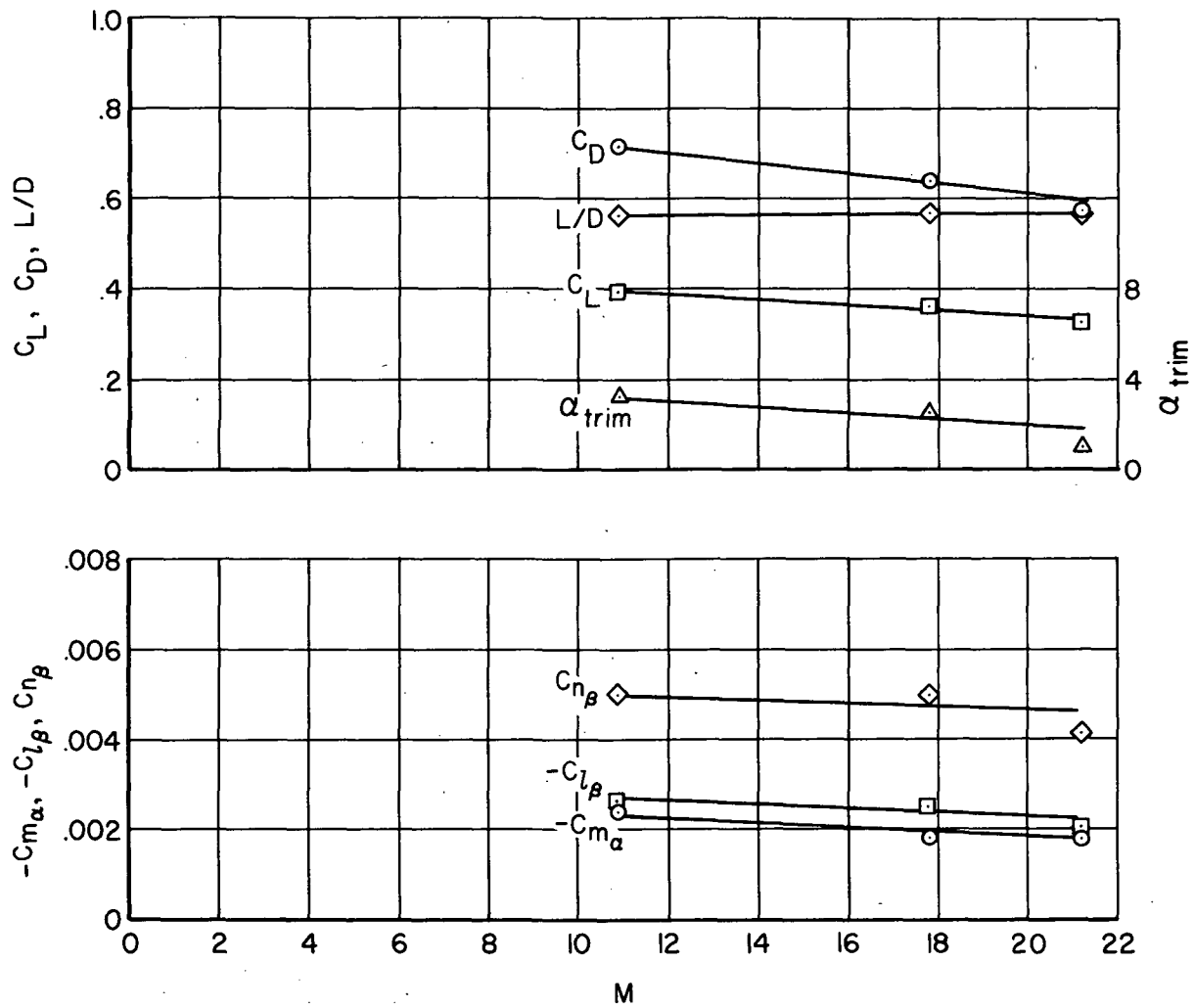

Figure 7.- Variation of the longitudinal aerodynamic and lateral-directional stability characteristics at trim with Mach number for the basic body.

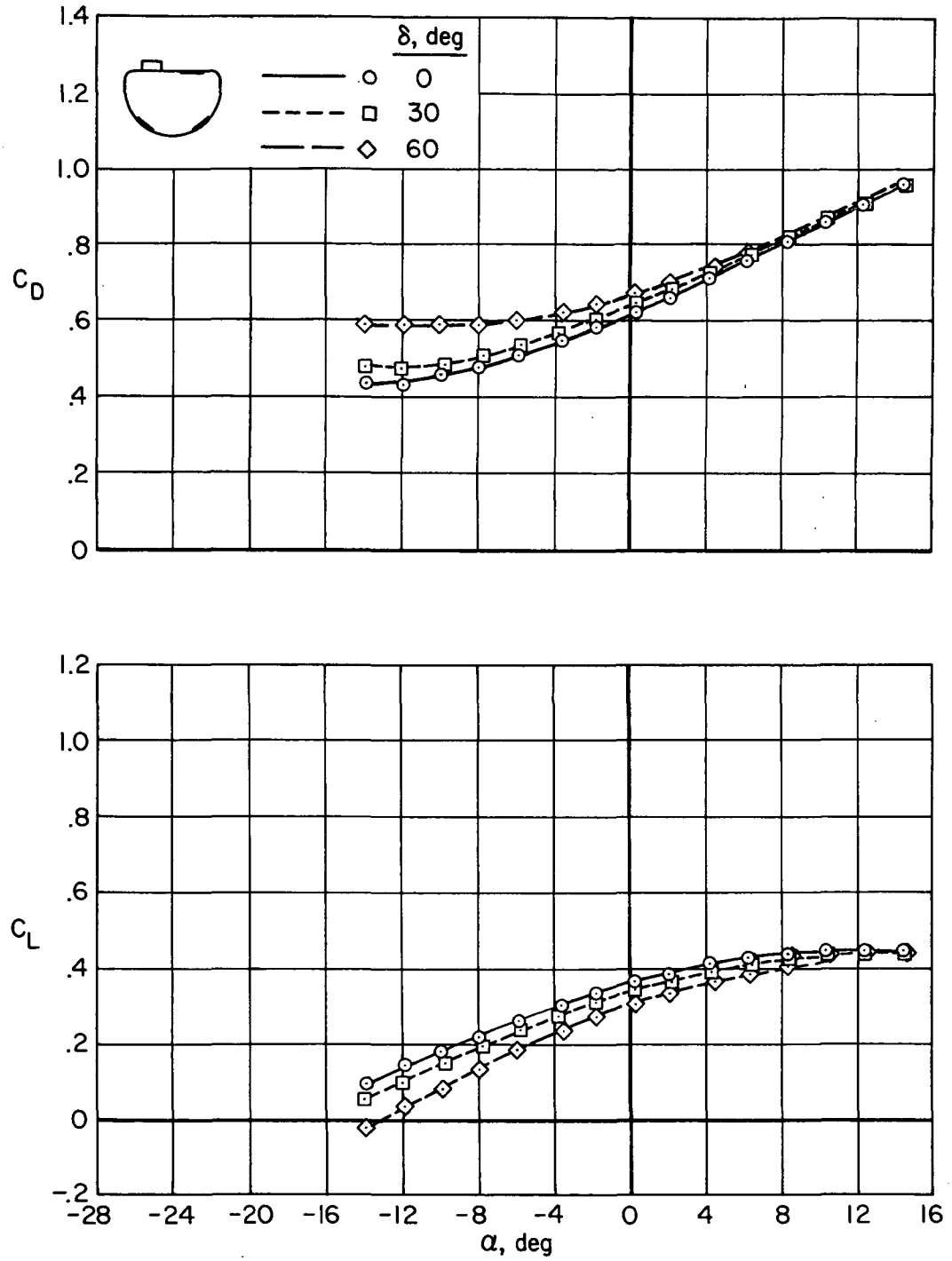

(a) C_D, C_L

Figure 8.- Variation of the longitudinal aerodynamic characteristics with angle of attack for one upper control of control set I deflected, M = 10.9.

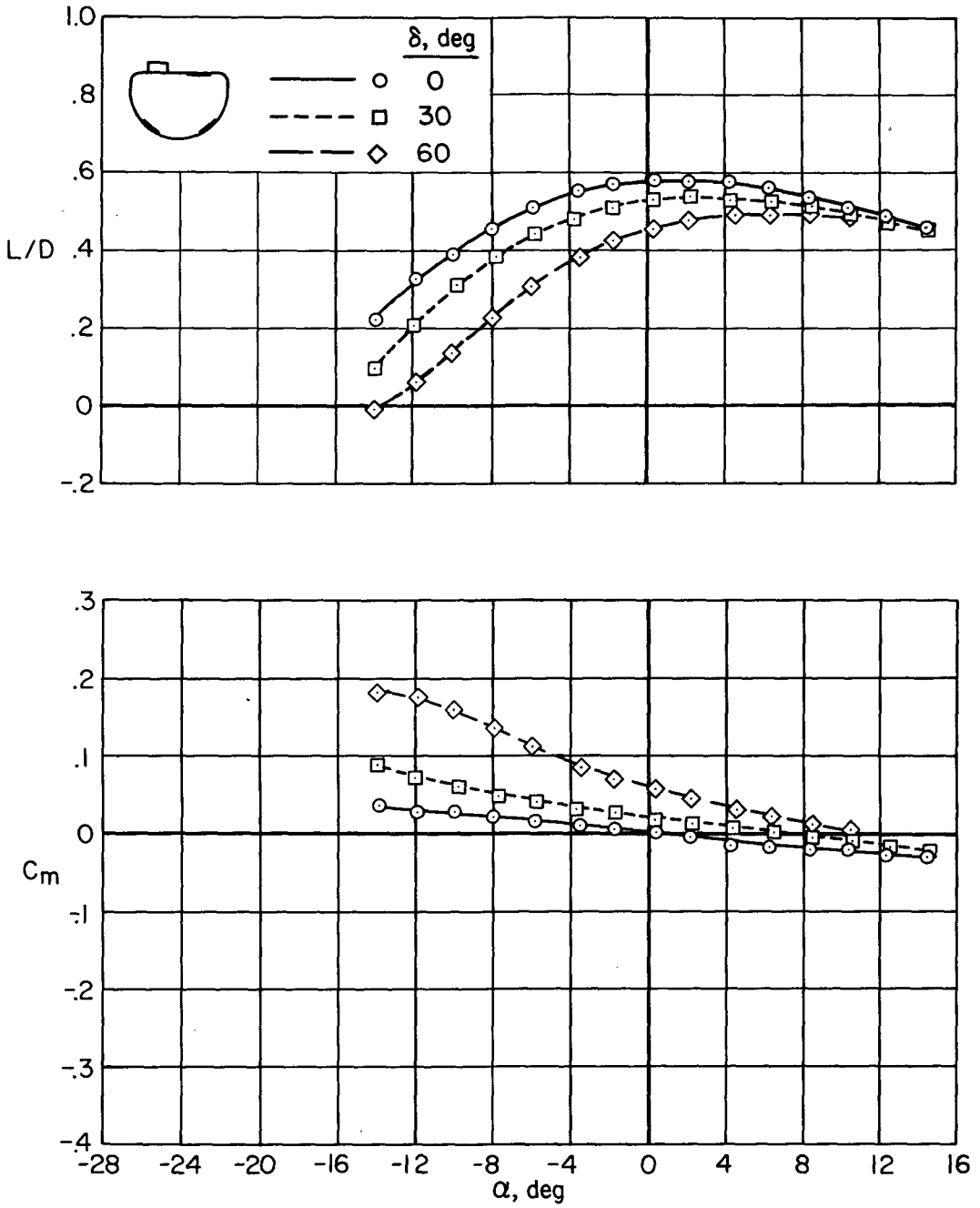

(b) L/D, C_m

Figure 8.- Continued.

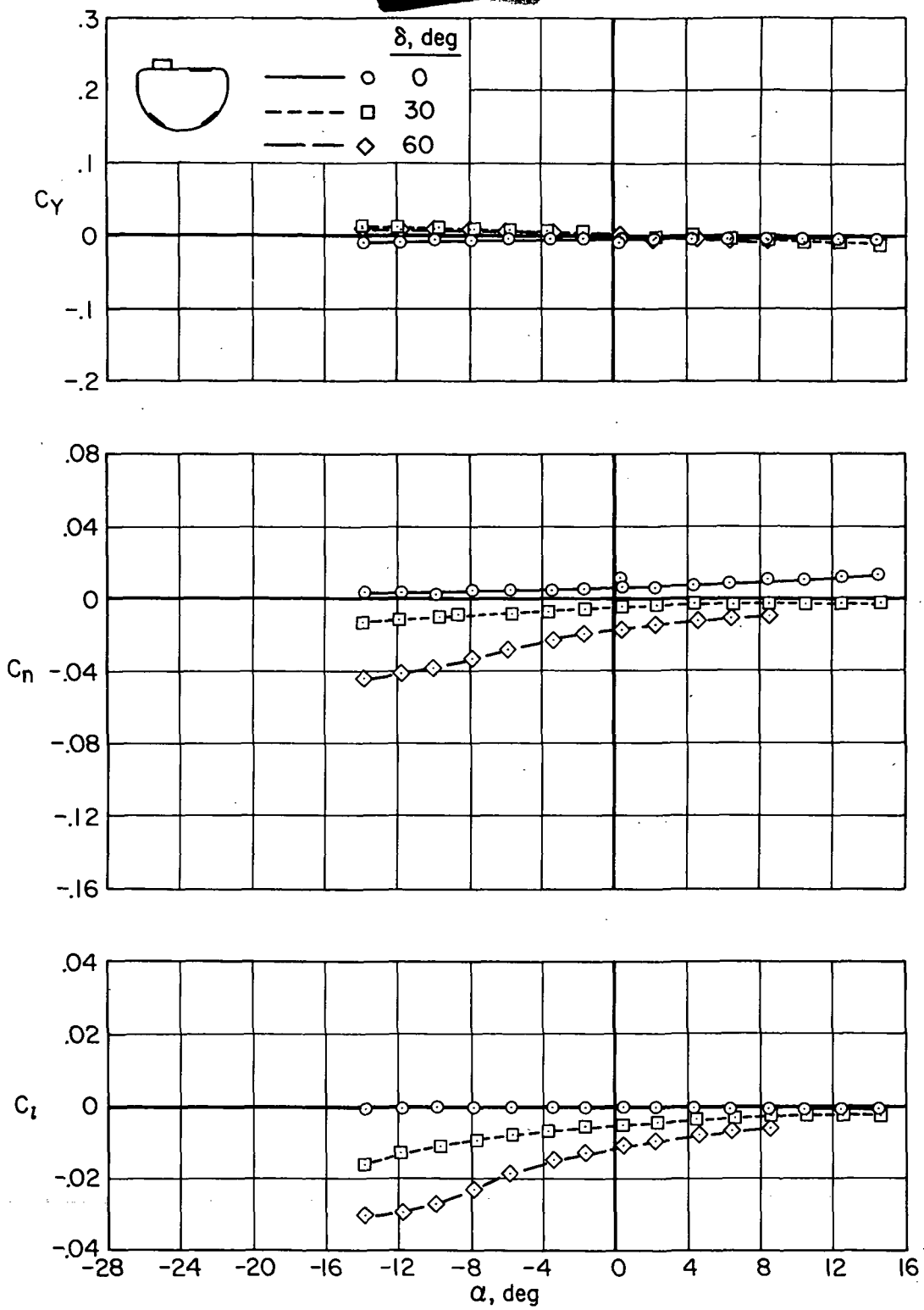

(c) C_Y, C_n, C_l

Figure 8.- Concluded.

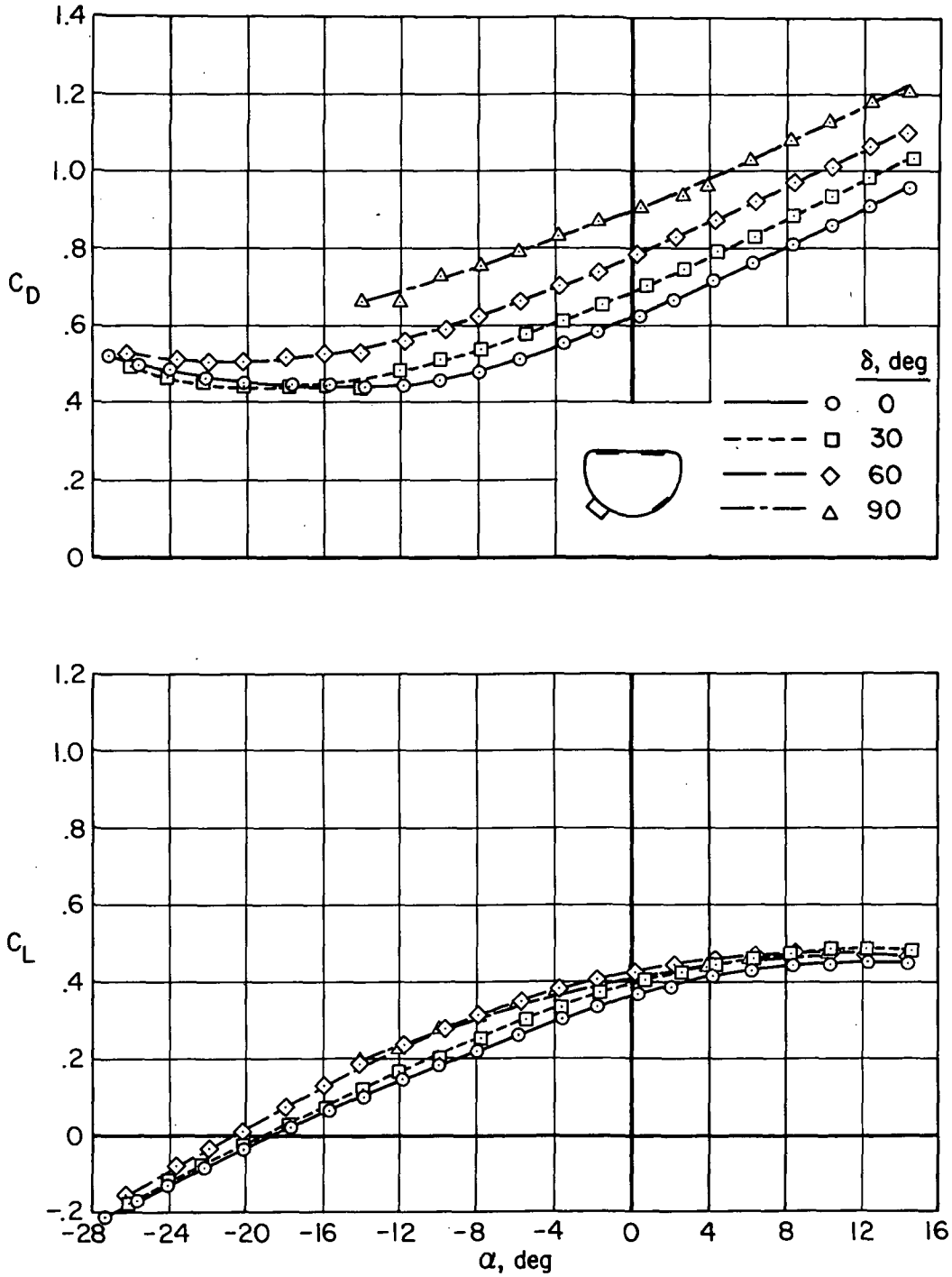

(a) C_D, C_L

Figure 9.- Variation of the longitudinal aerodynamic characteristics with angle of attack for one lower control of control set I deflected, M = 10.9.

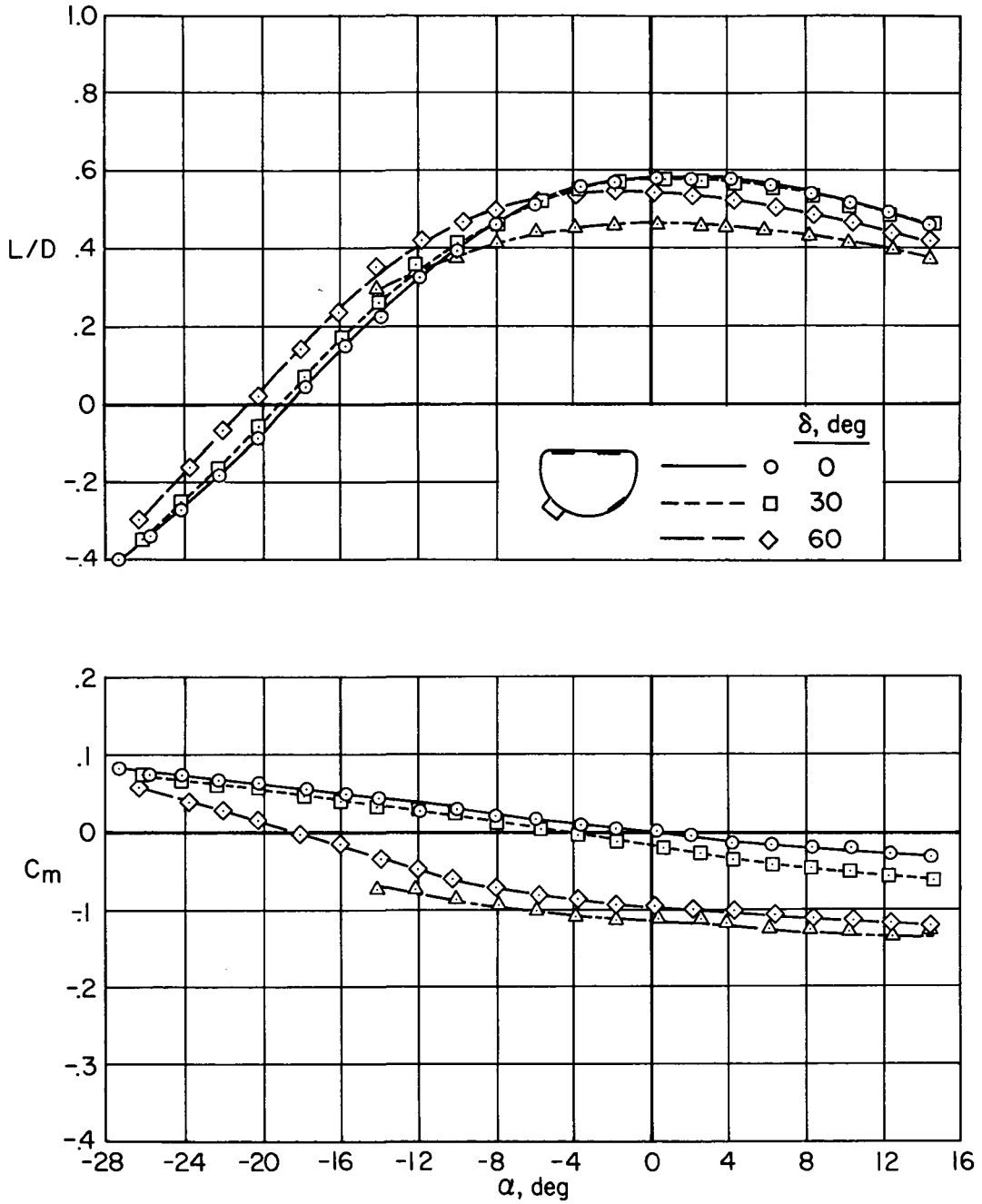

(b) L/D, C_m

Figure 9.- Continued.

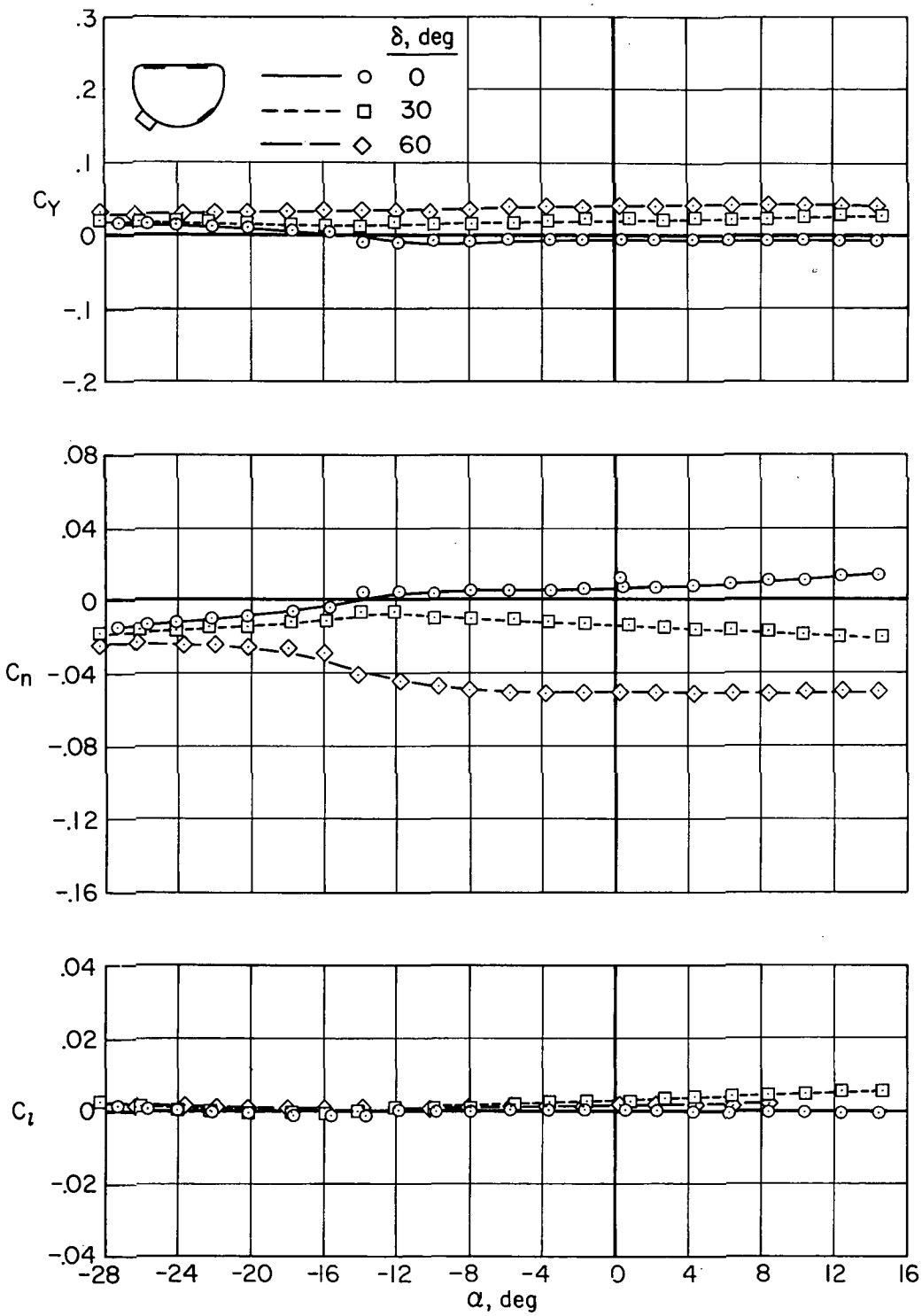

(c) C_Y, C_n, C_l

Figure 9.- Concluded.

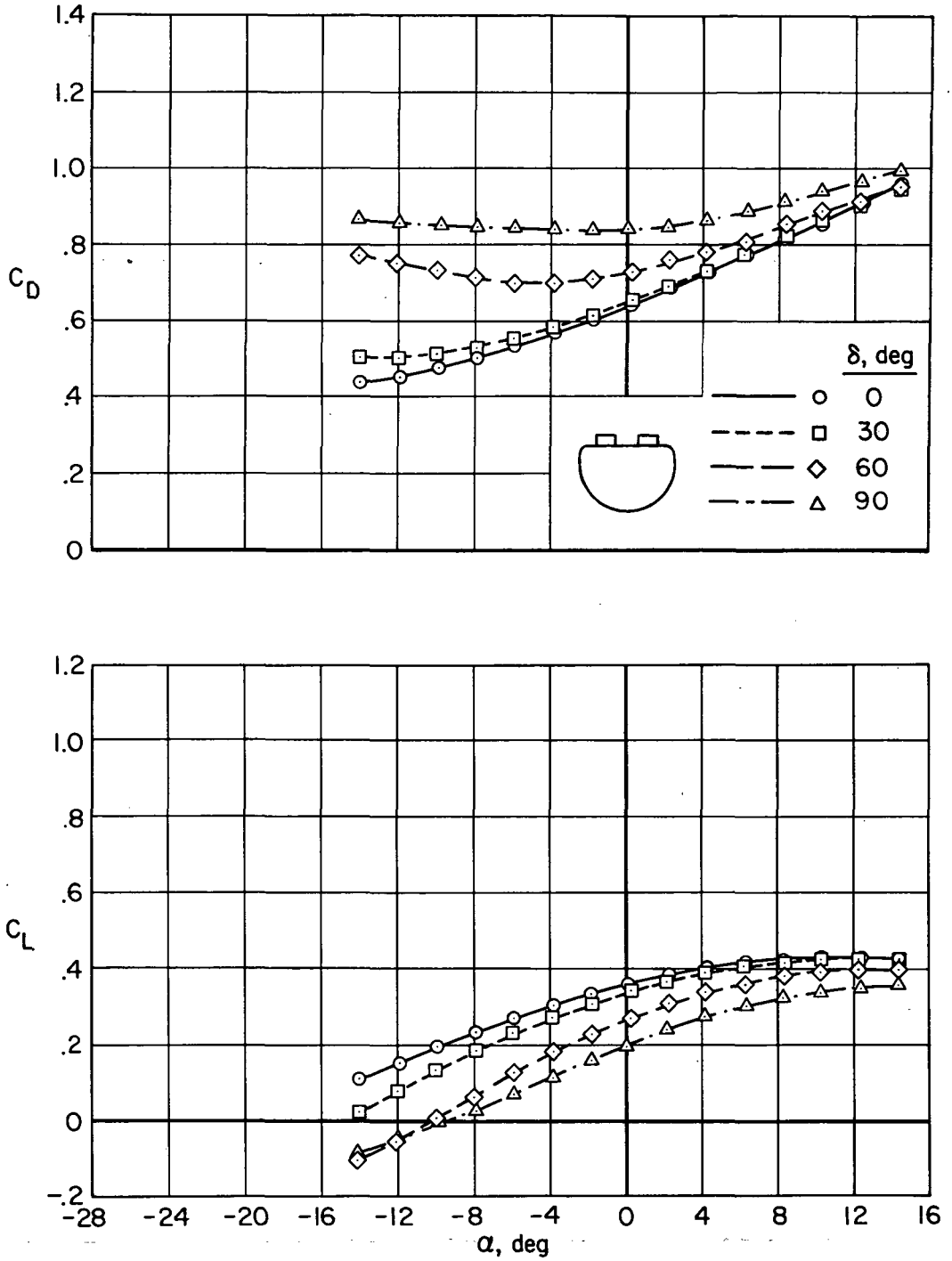

(a) C_D, C_L

Figure 10.- Variation of the longitudinal aerodynamic characteristics with angle of attack for two upper controls of control set I deflected, M = 10.9.

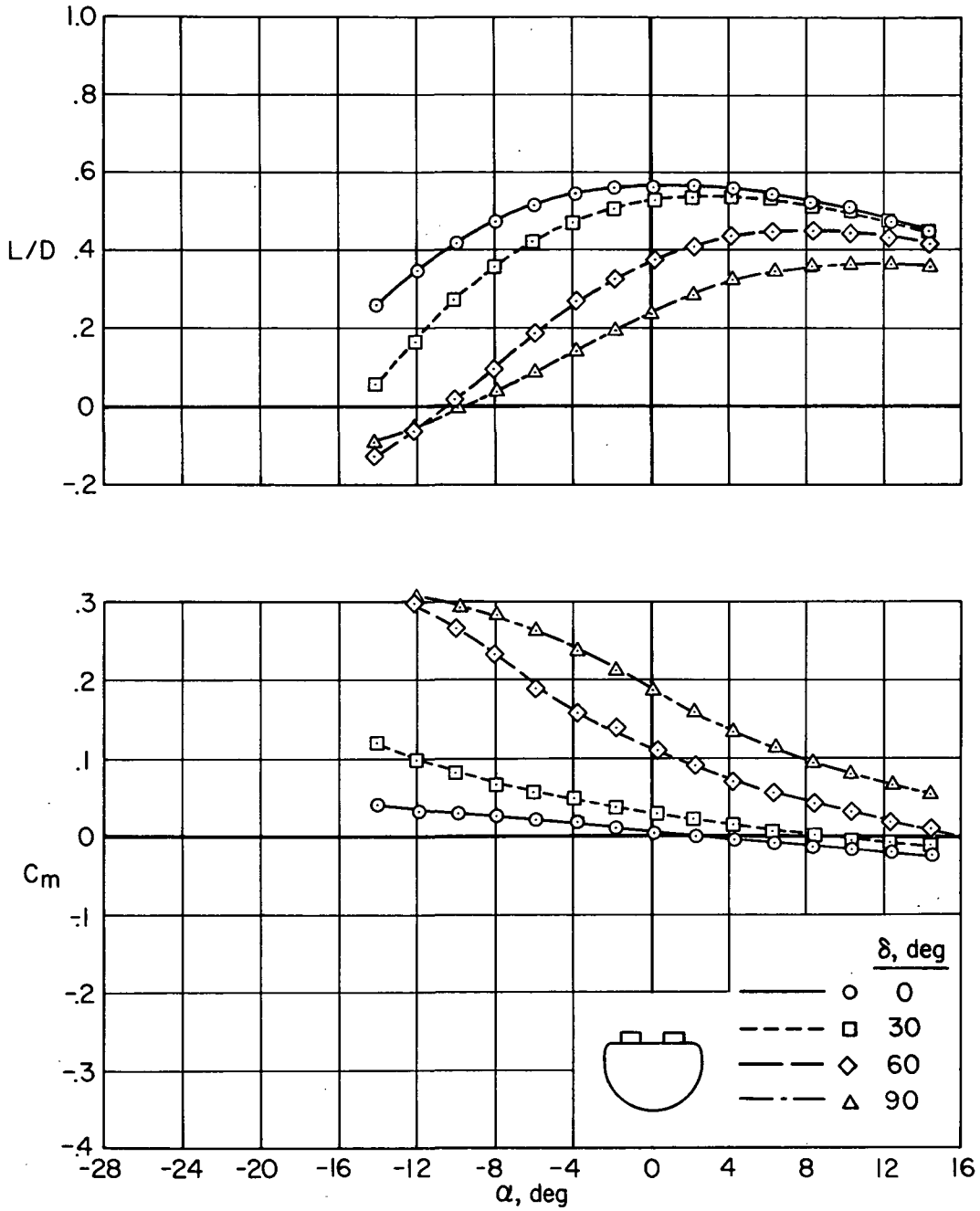

(b) L/D, C_m

Figure 10.- Concluded.

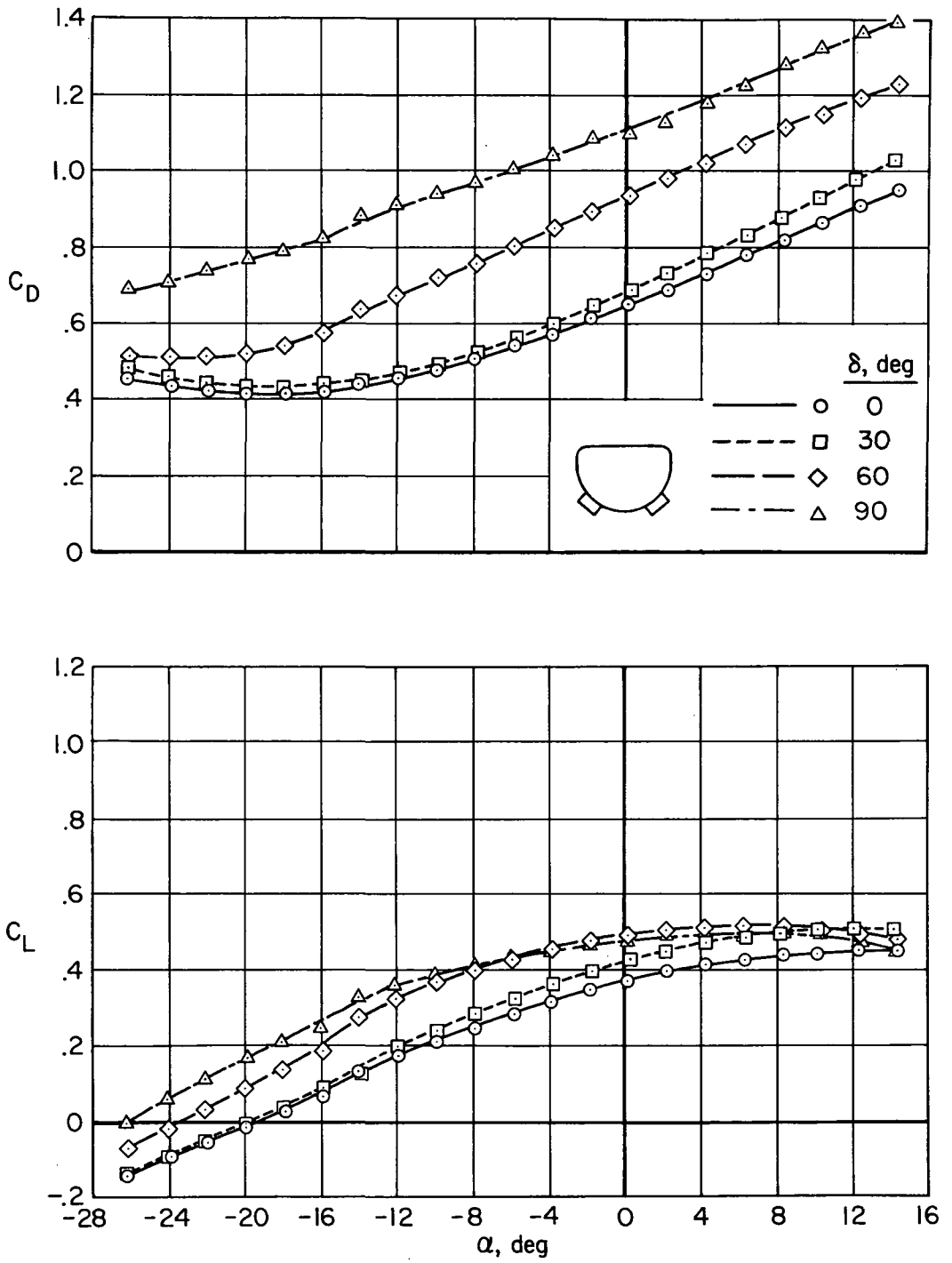

(a) C_D, C_L

Figure 11.- Variation of the longitudinal aerodynamic characteristics with angle of attack for two lower controls of control set I deflected, M = 10.9.

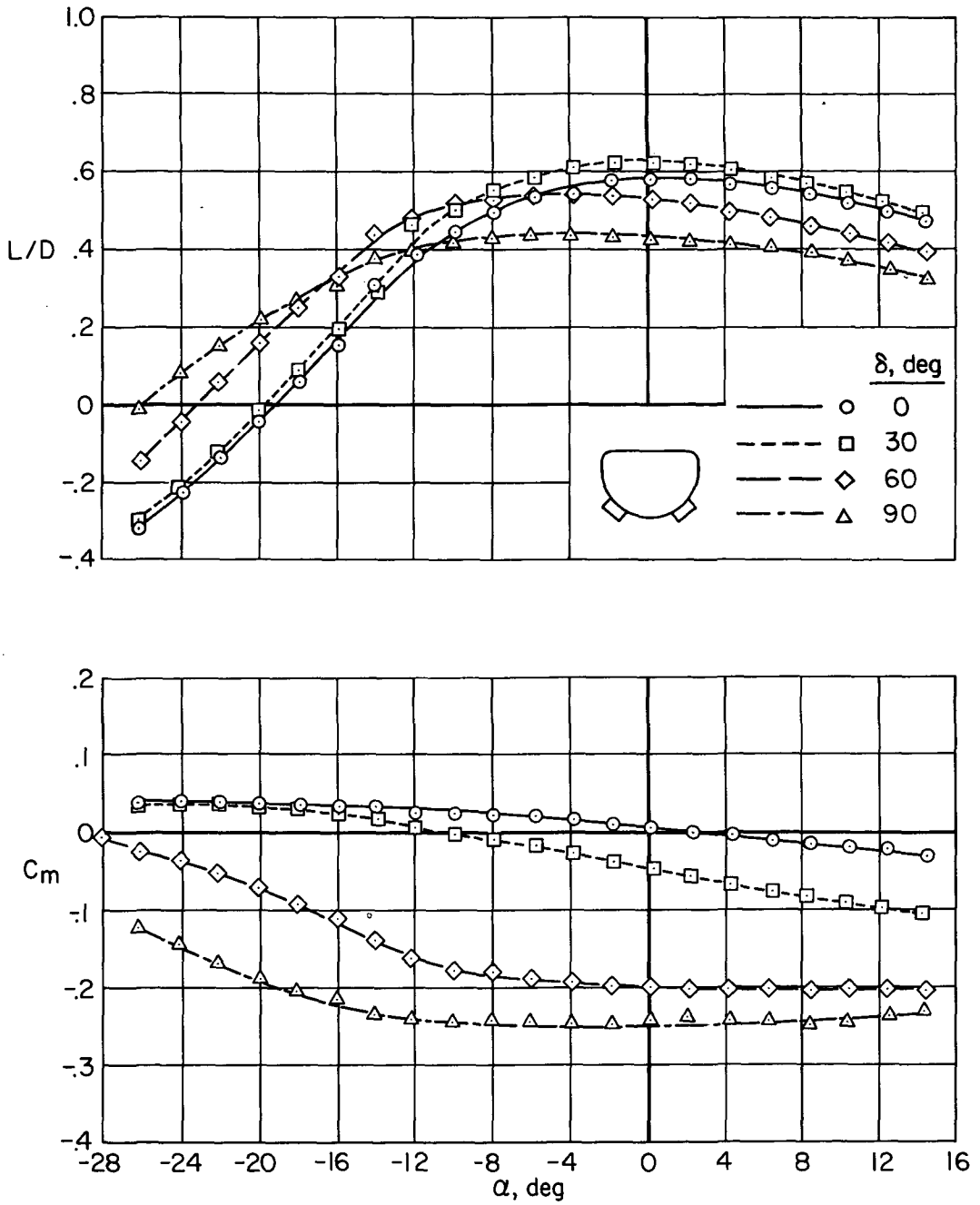

(b) L/D, C_m

Figure 11.- Concluded.

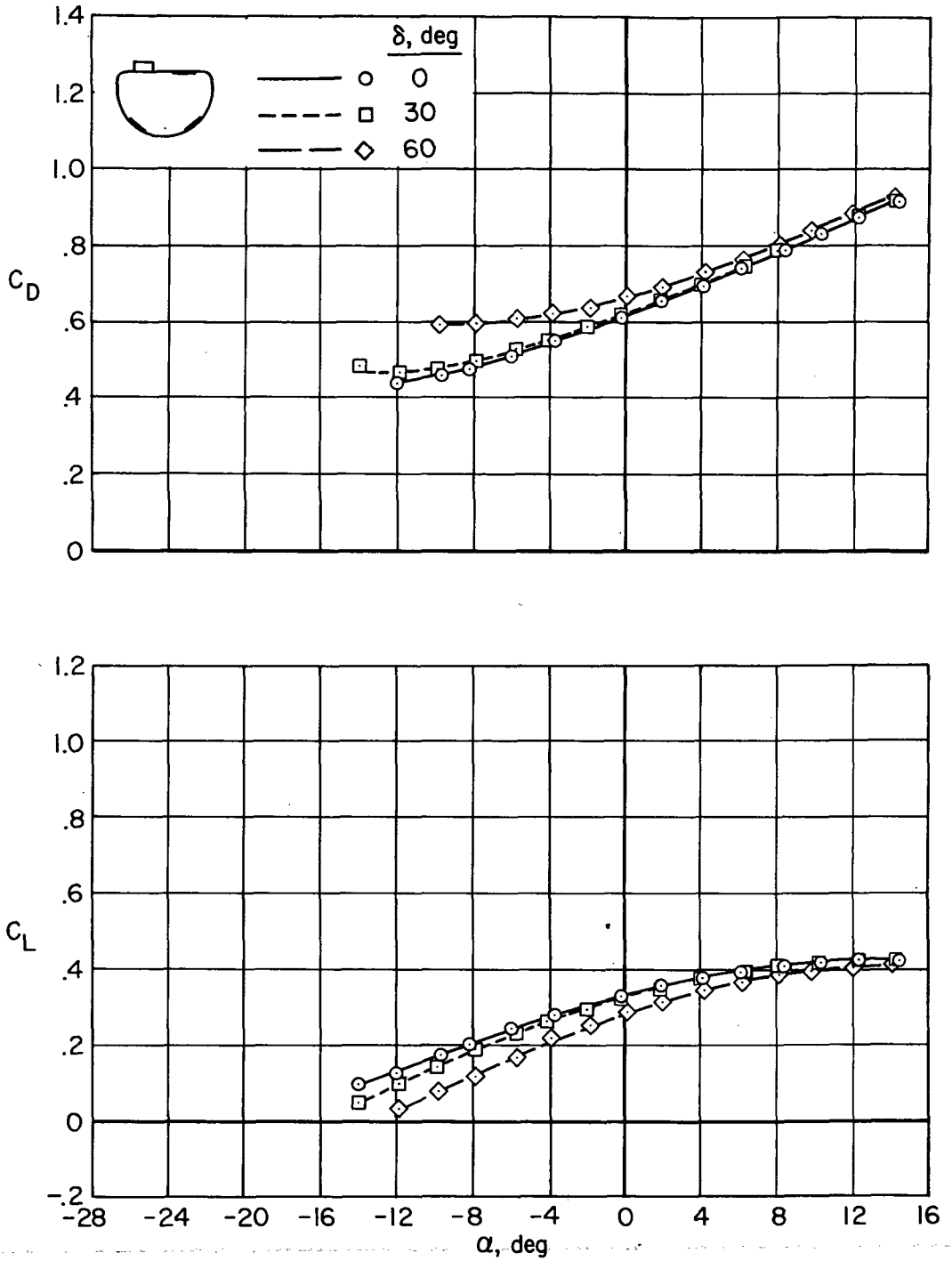

(a) C_D, C_L

Figure 12.- Variation of the longitudinal aerodynamic characteristics with angle of attack for one upper control of control set I deflected, M = 17.8.

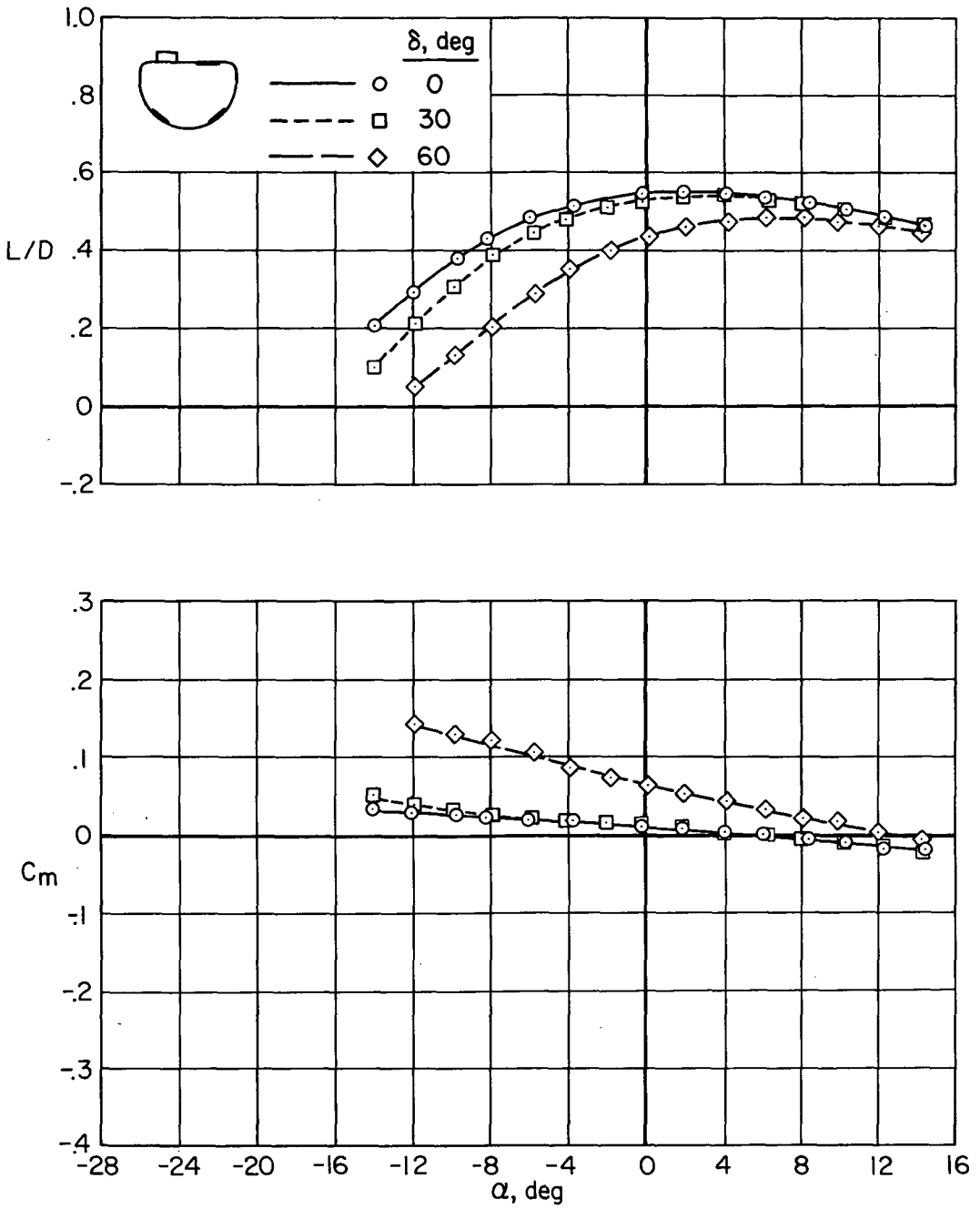

(b) L/D, C_m

Figure 12.- Continued.

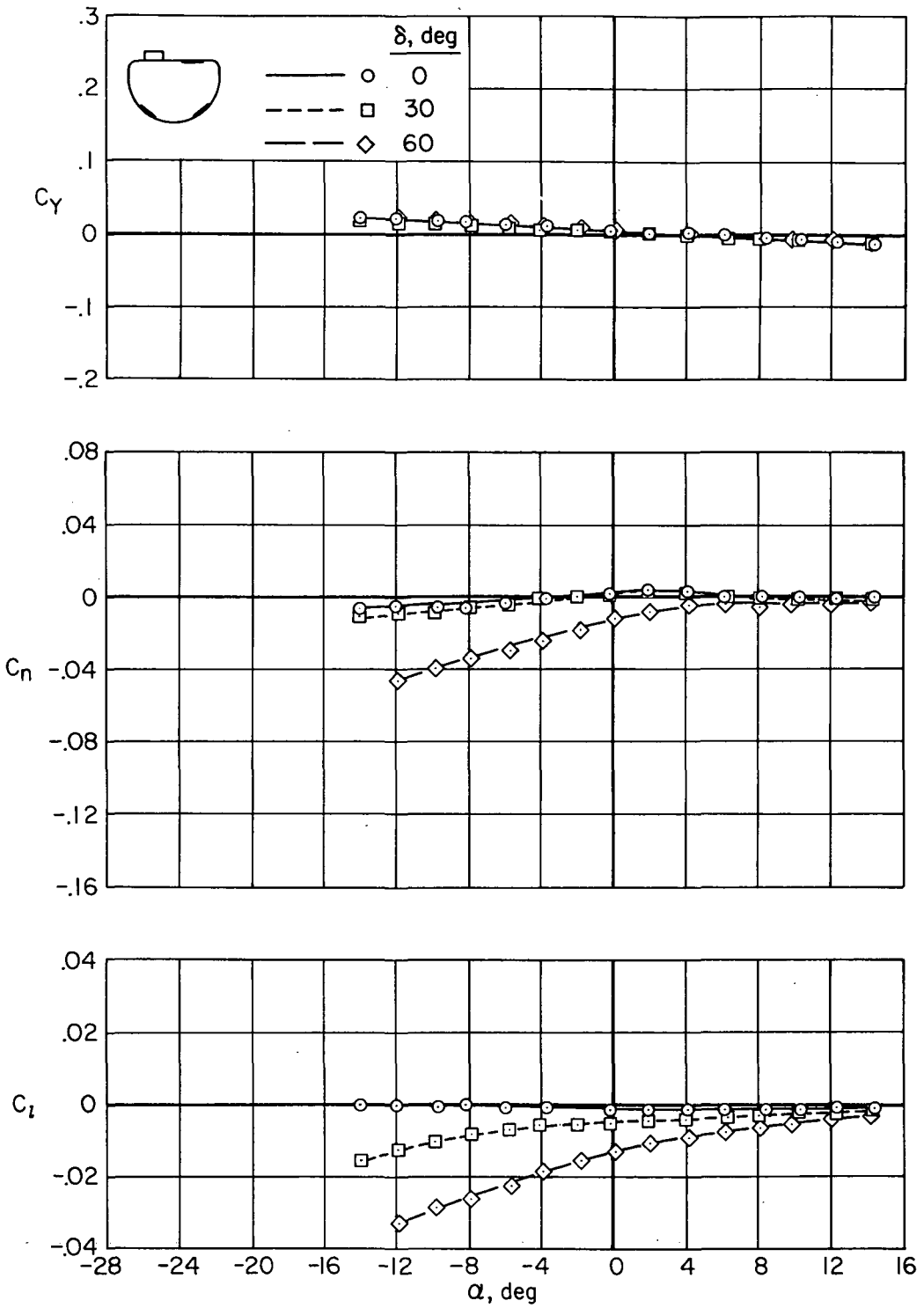

(c) C_Y, C_n, C_l

Figure 12.- Concluded.

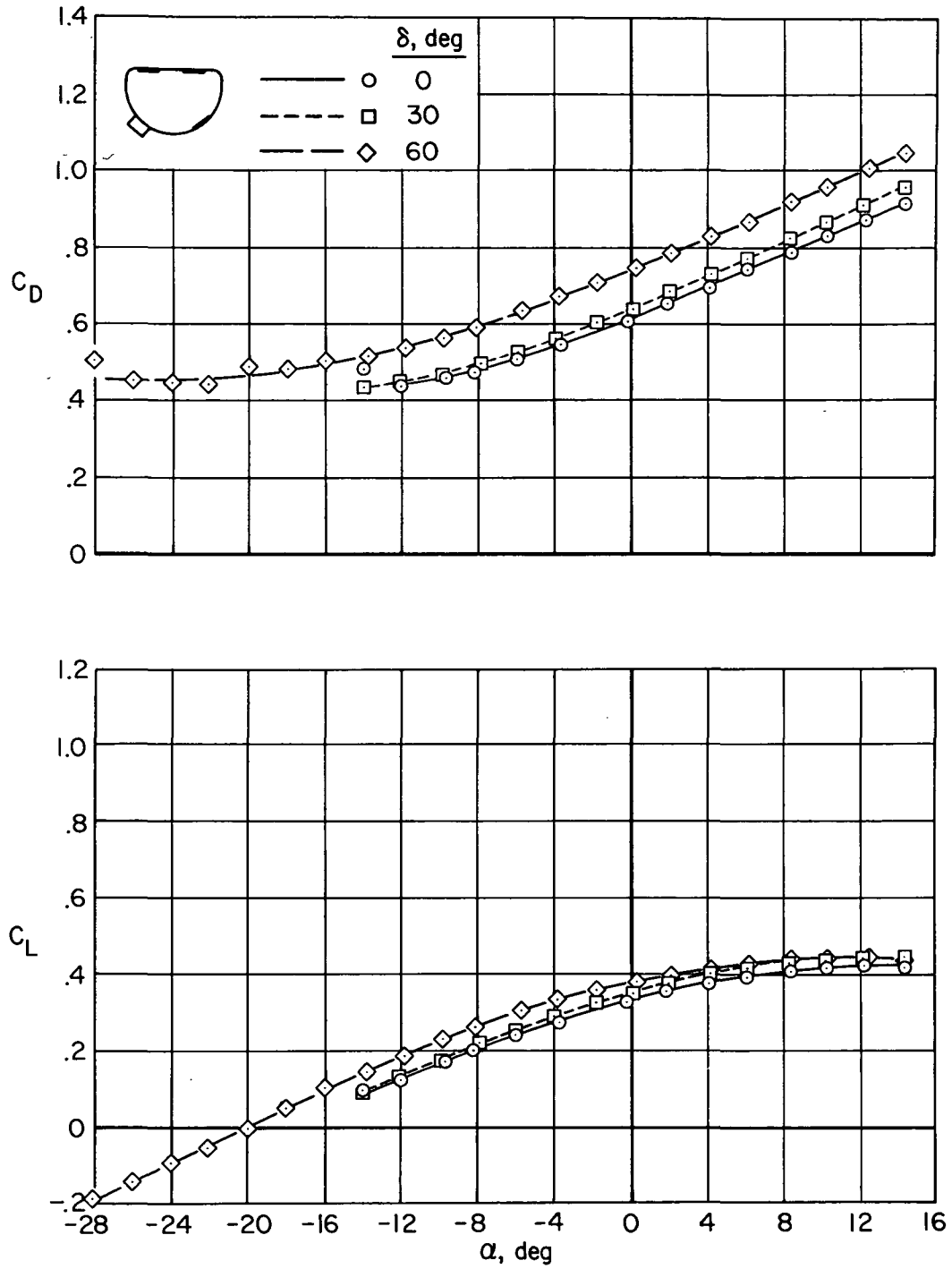

(a) C_D, C_L

Figure 13.- Variation of the longitudinal aerodynamic characteristics with angle of attack for one lower control of control set I deflected, M = 17.8.

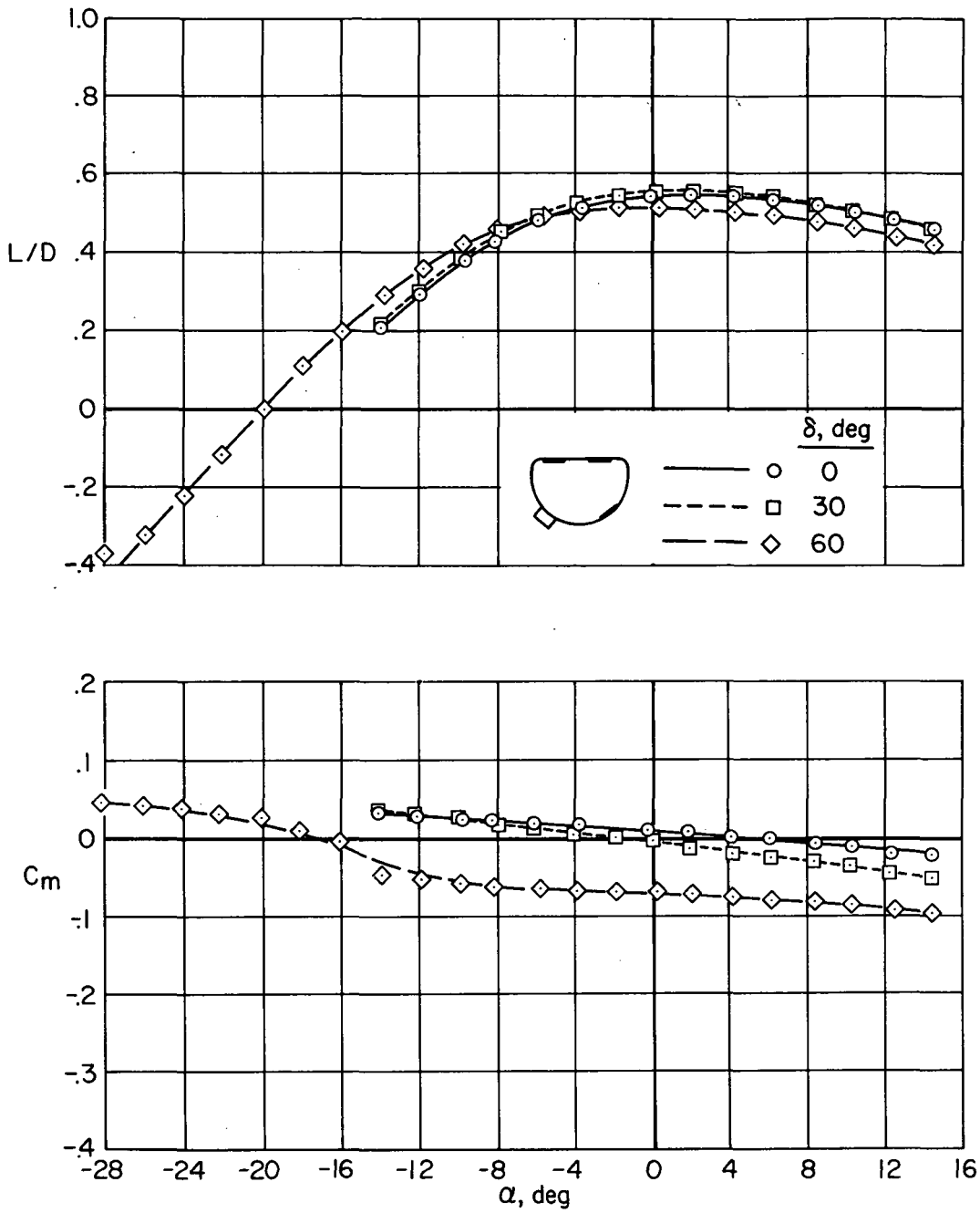

(b) L/D, C_m

Figure 13.- Continued.

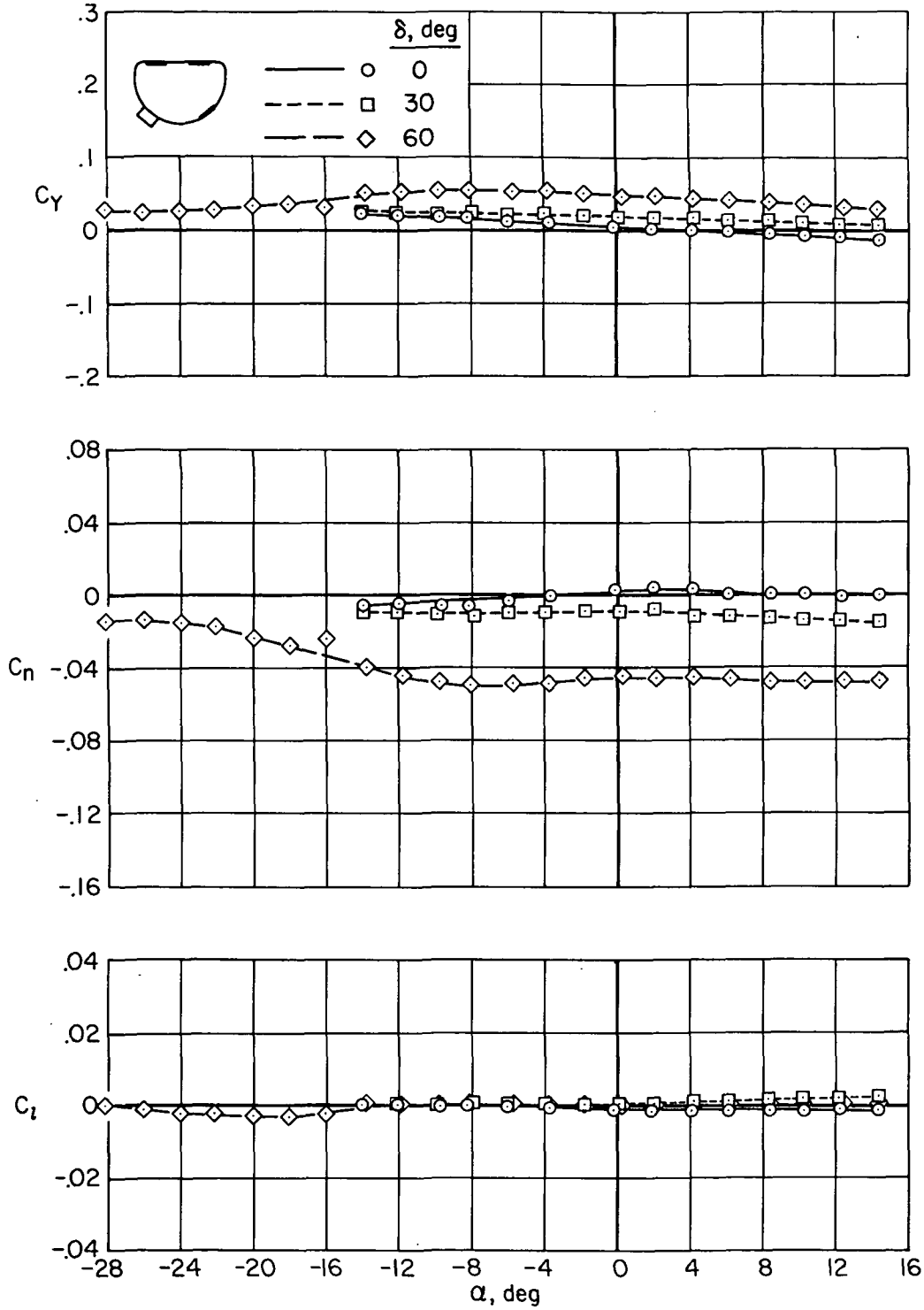

(c) C_Y, C_n, C_l

Figure 13.- Concluded.

CONFIDENTIAL

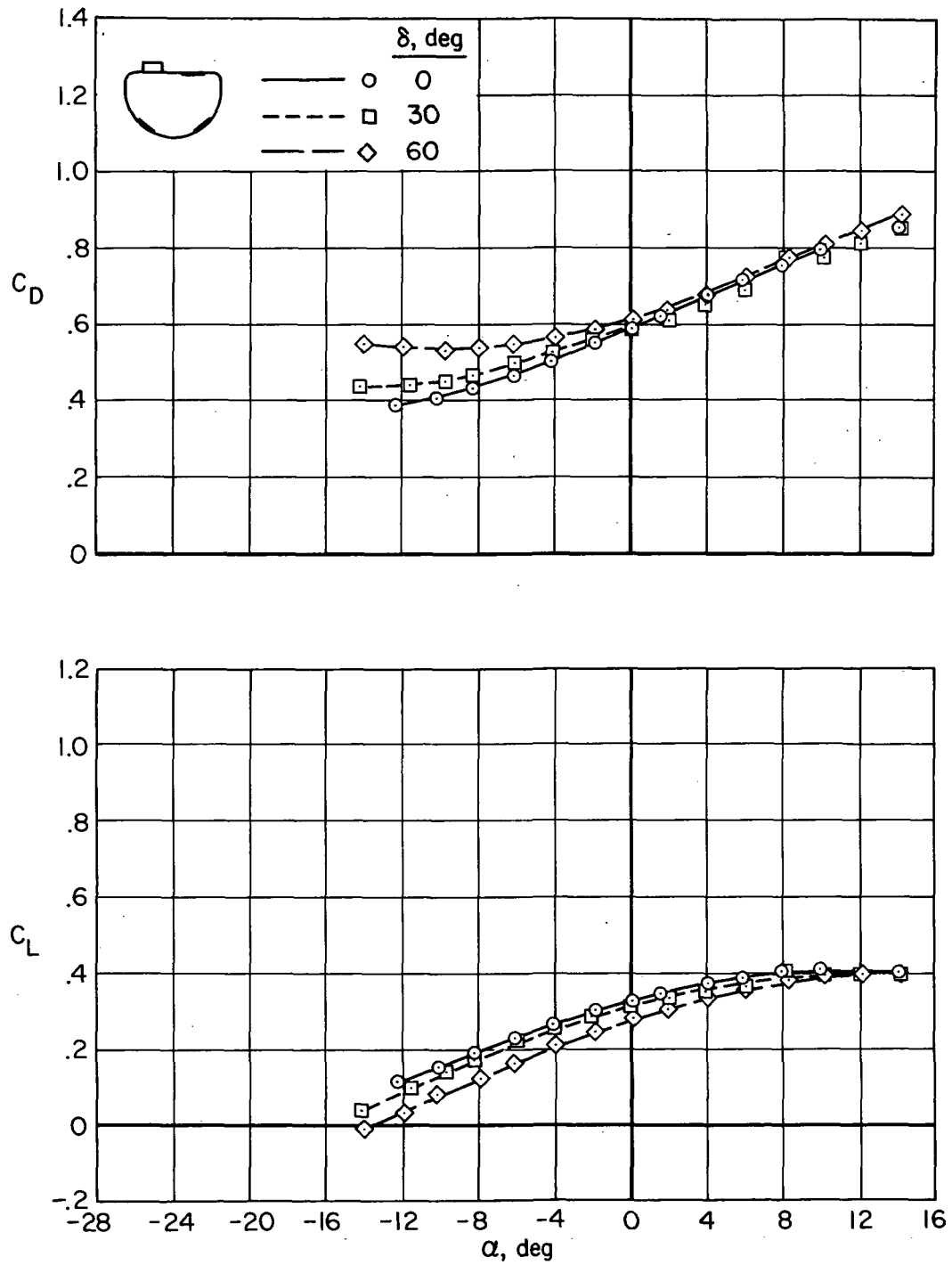

(a) C_D, C_L

Figure 14.- Variation of the longitudinal aerodynamic characteristics with angle of attack for one upper control of control set I deflected, M = 21.2.

[redacted]

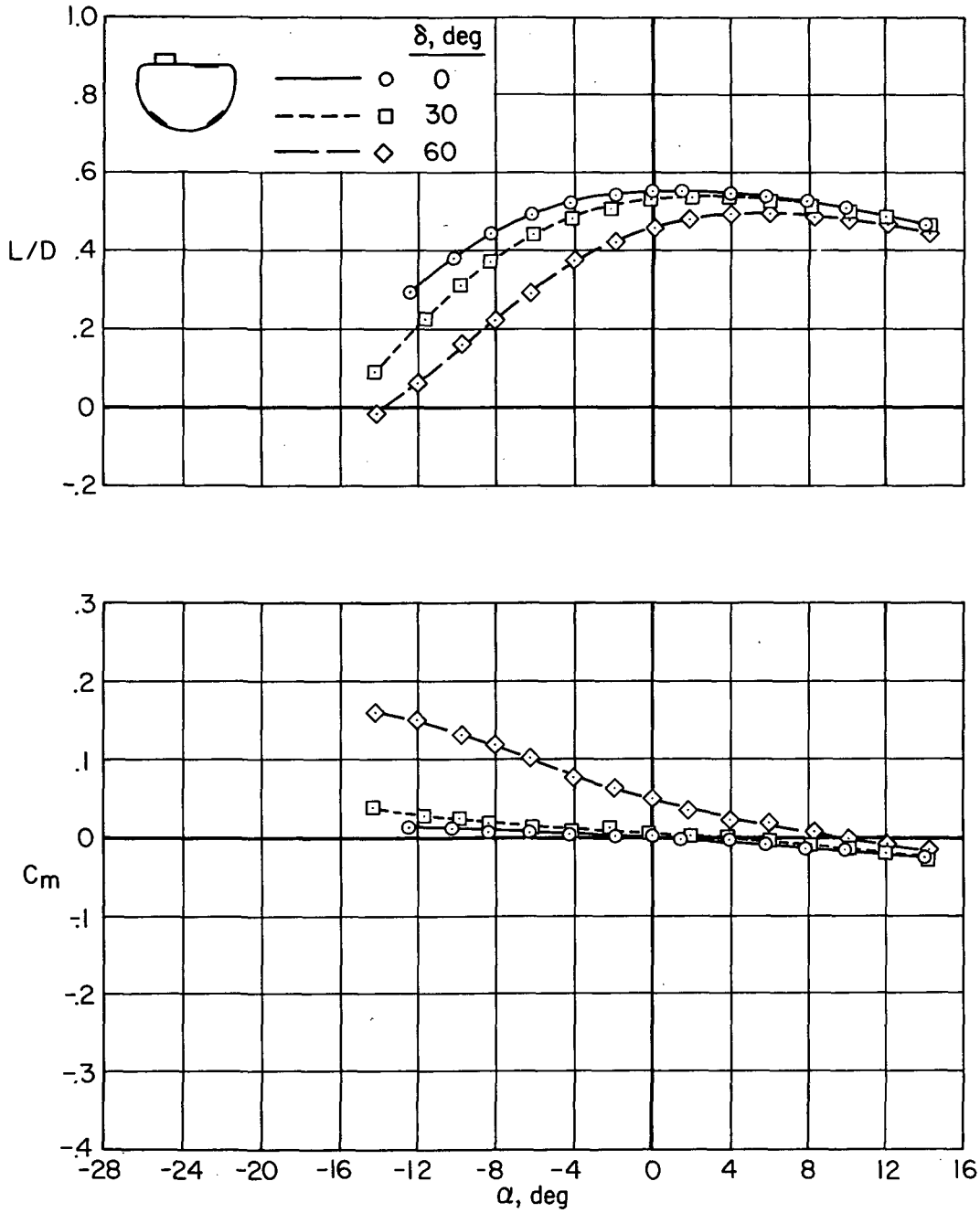

(b) L/D, C_m

Figure 14.- Continued.

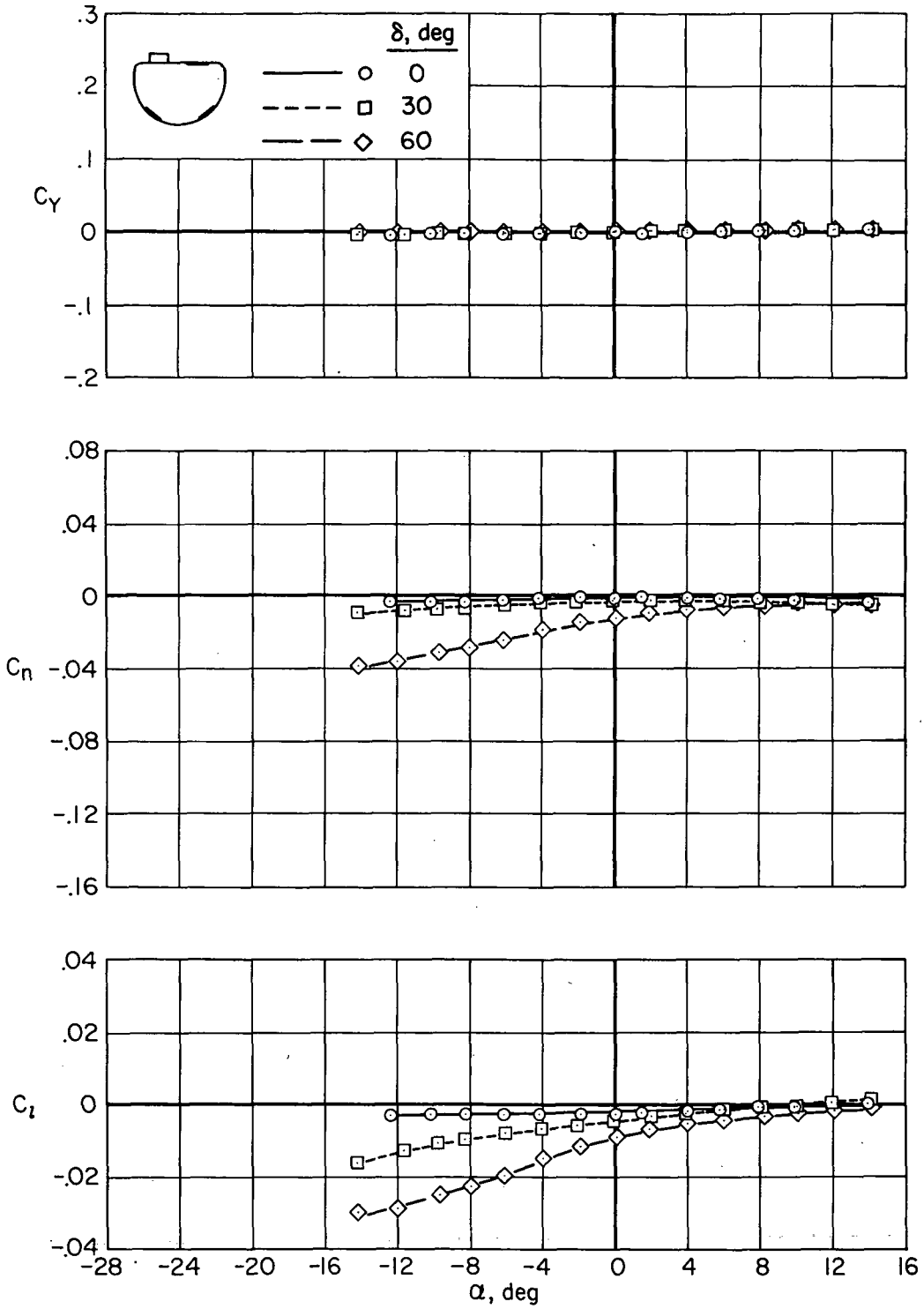

(c) C_Y, C_n, C_l

Figure 14.- Concluded.

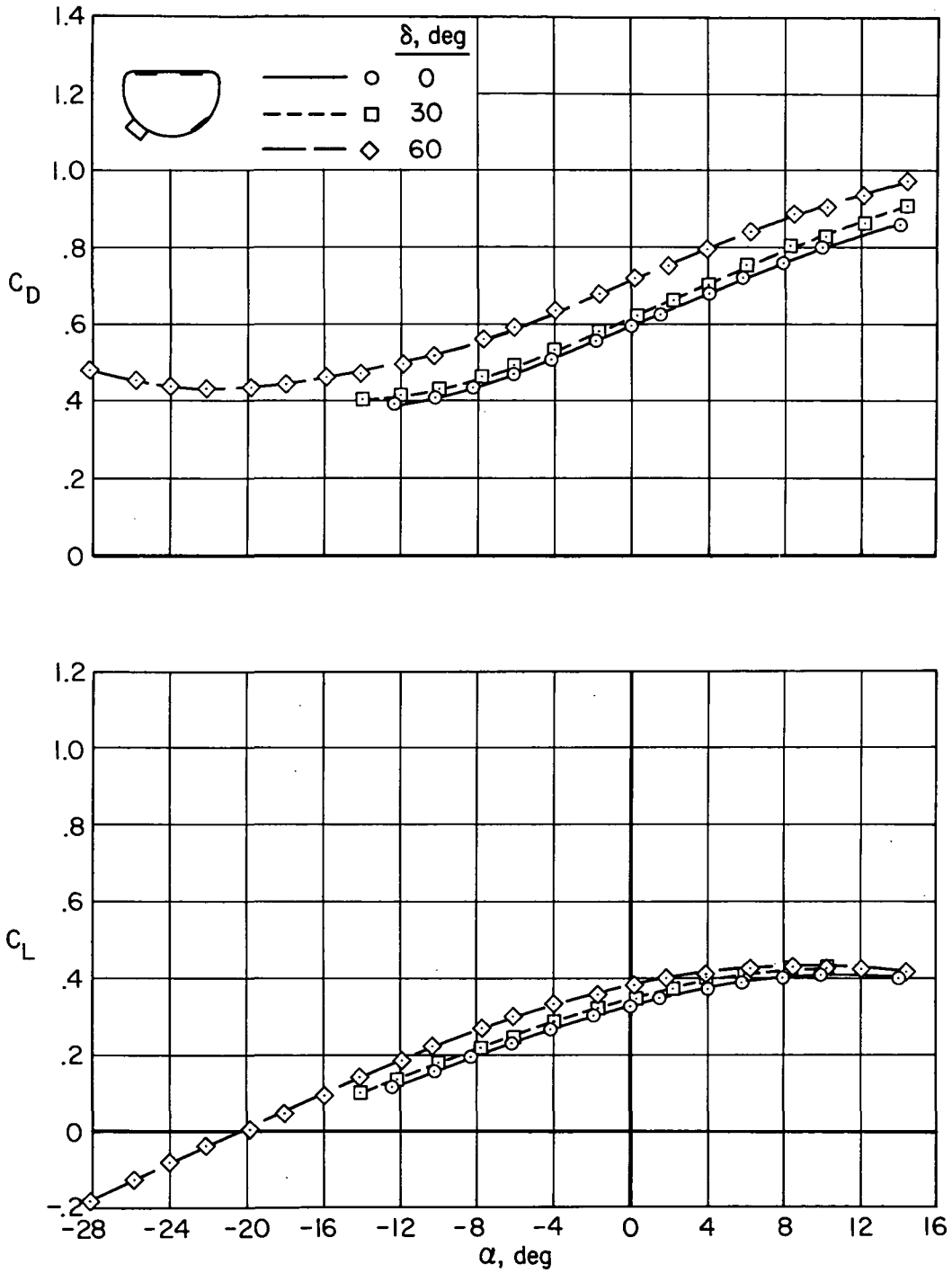

(a) C_D, C_L

Figure 15.- Variation of the longitudinal aerodynamic characteristics with angle of attack for one lower control of control set I deflected, M = 21.2.

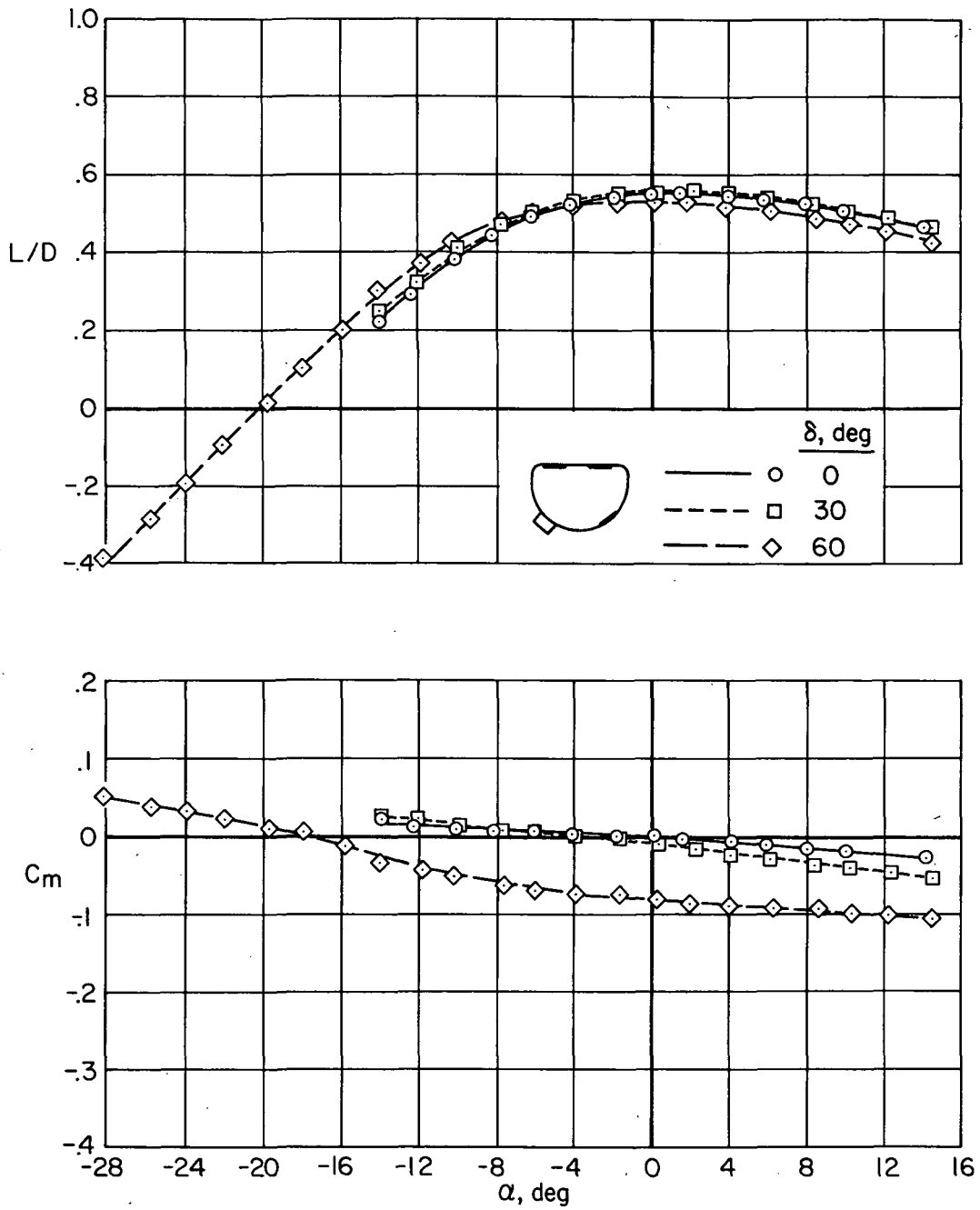

(b) L/D, C_m

Figure 15.- Continued.

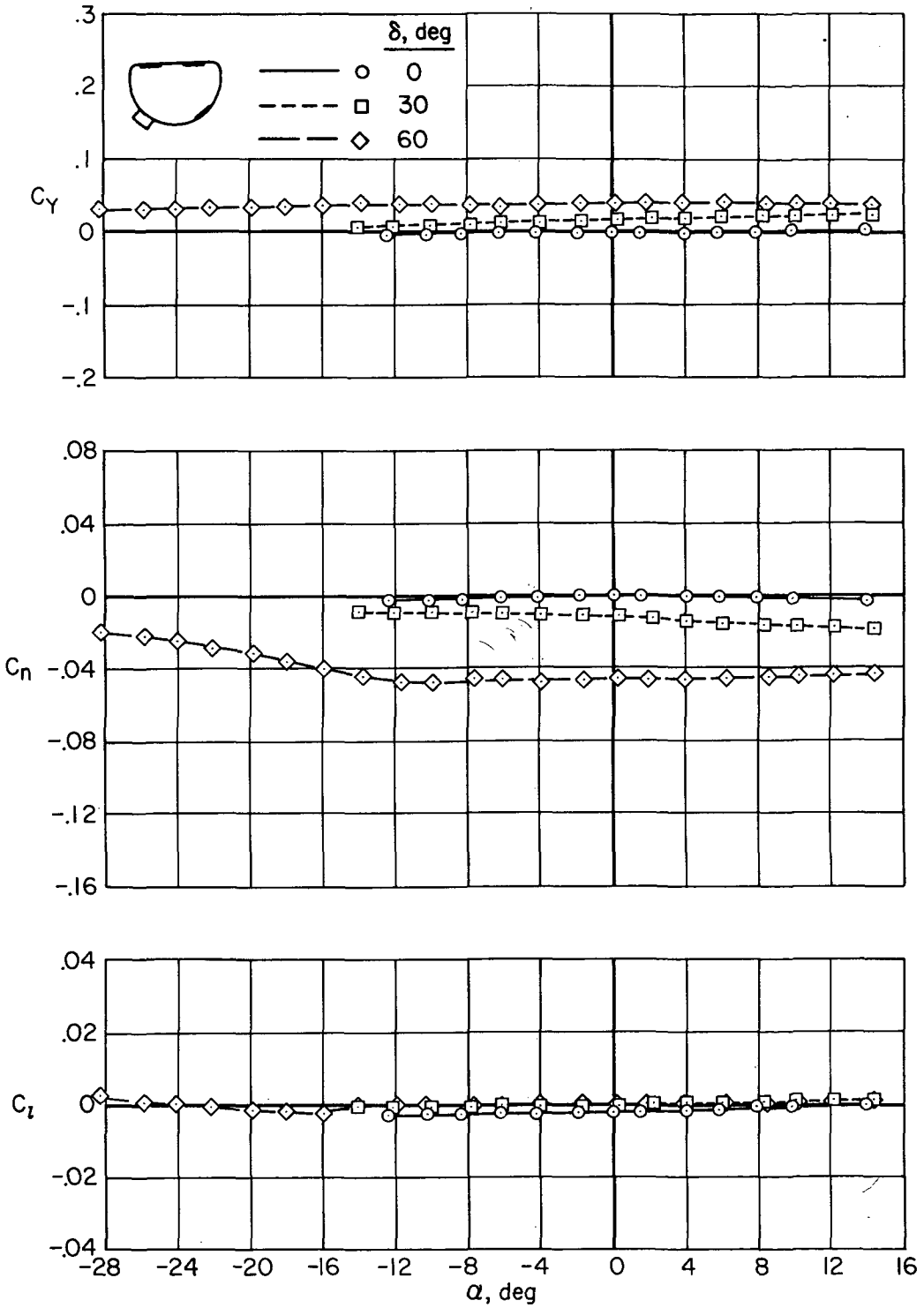

(c) C_Y, C_n, C_l

Figure 15.- Concluded.

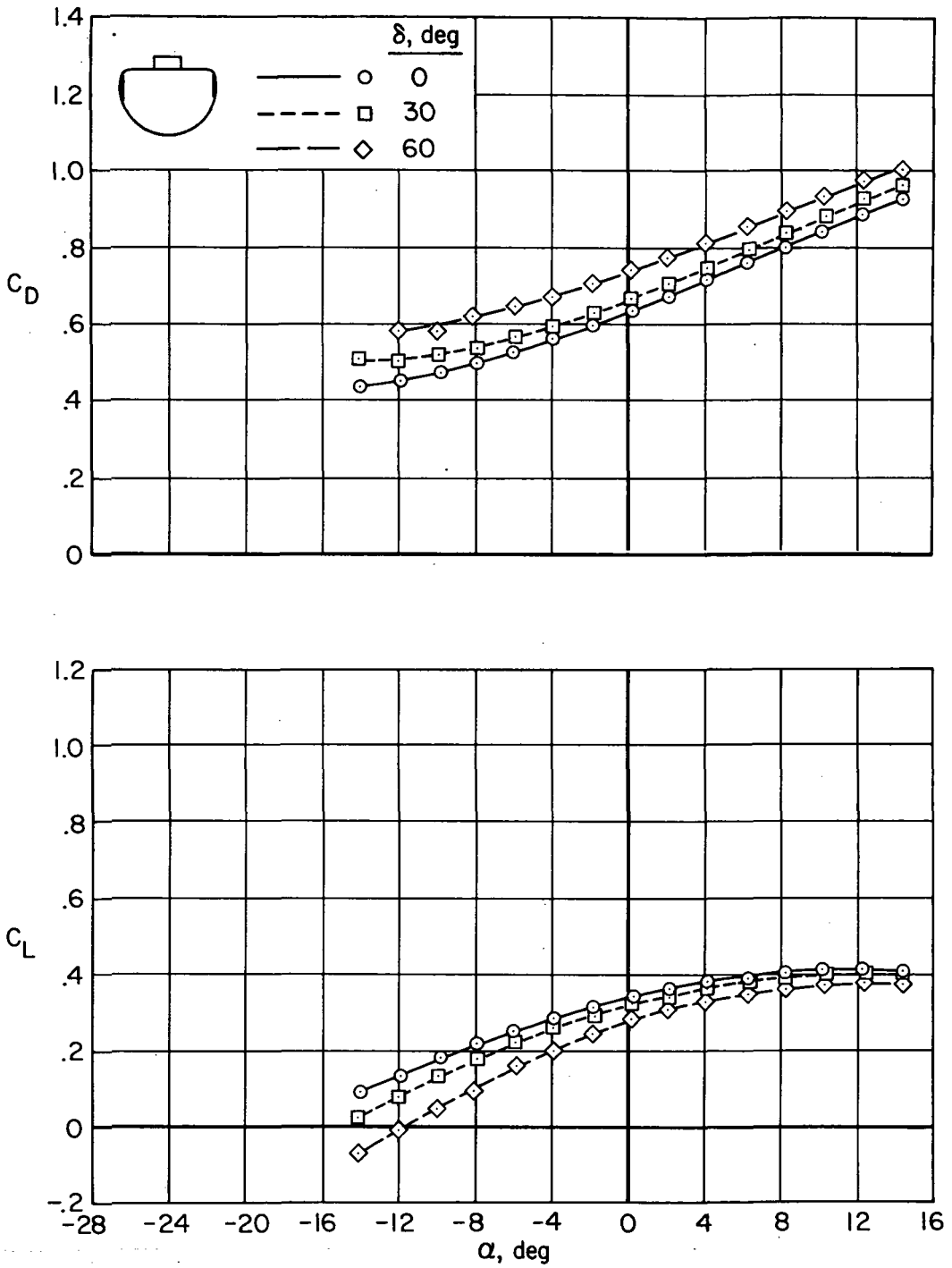

(a) C_D, C_L

Figure 16.- Variation of the longitudinal aerodynamic characteristics with angle of attack for the upper control of control set II deflected, M = 10.9.

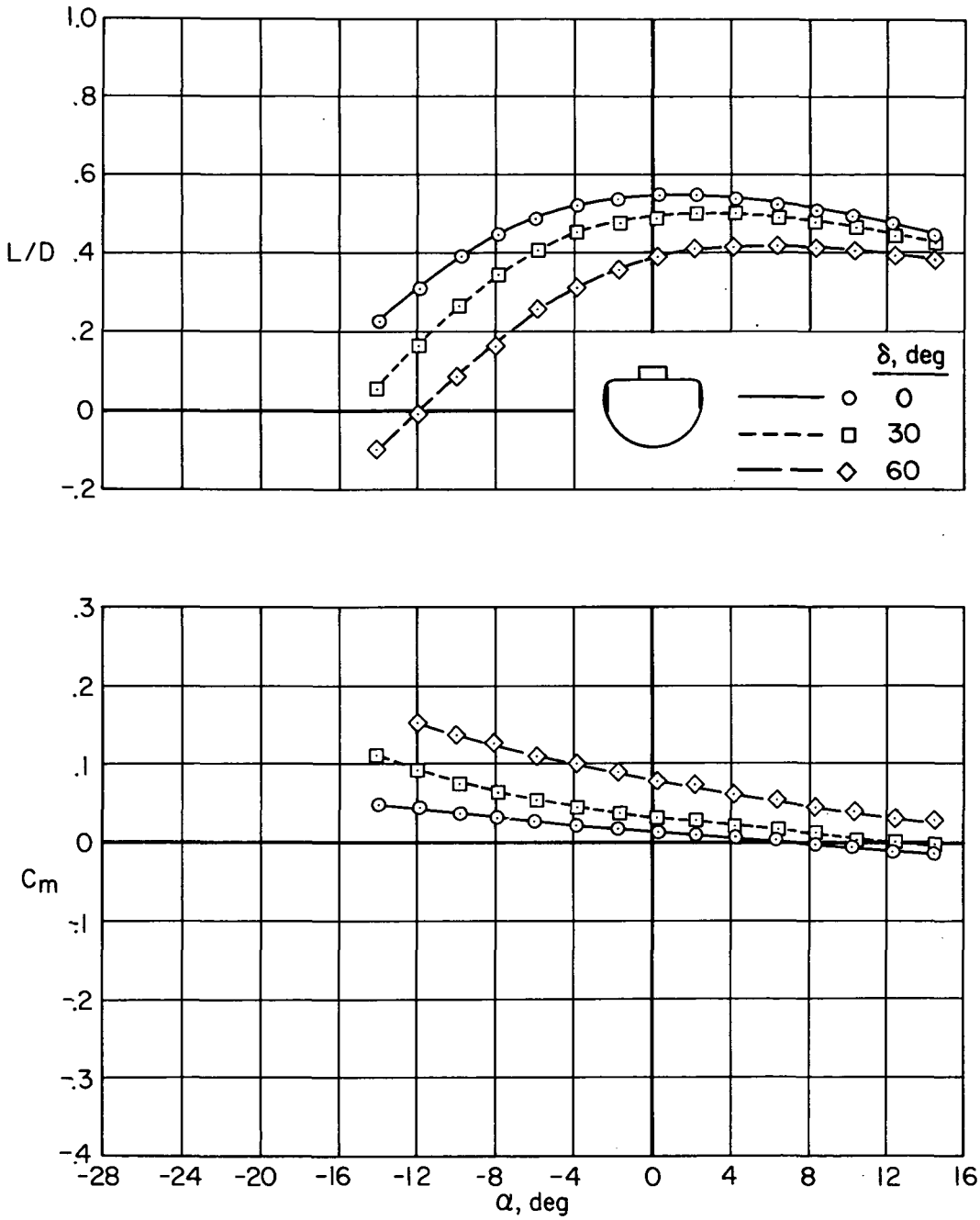

(b) L/D, C_m

Figure 16.- Concluded.

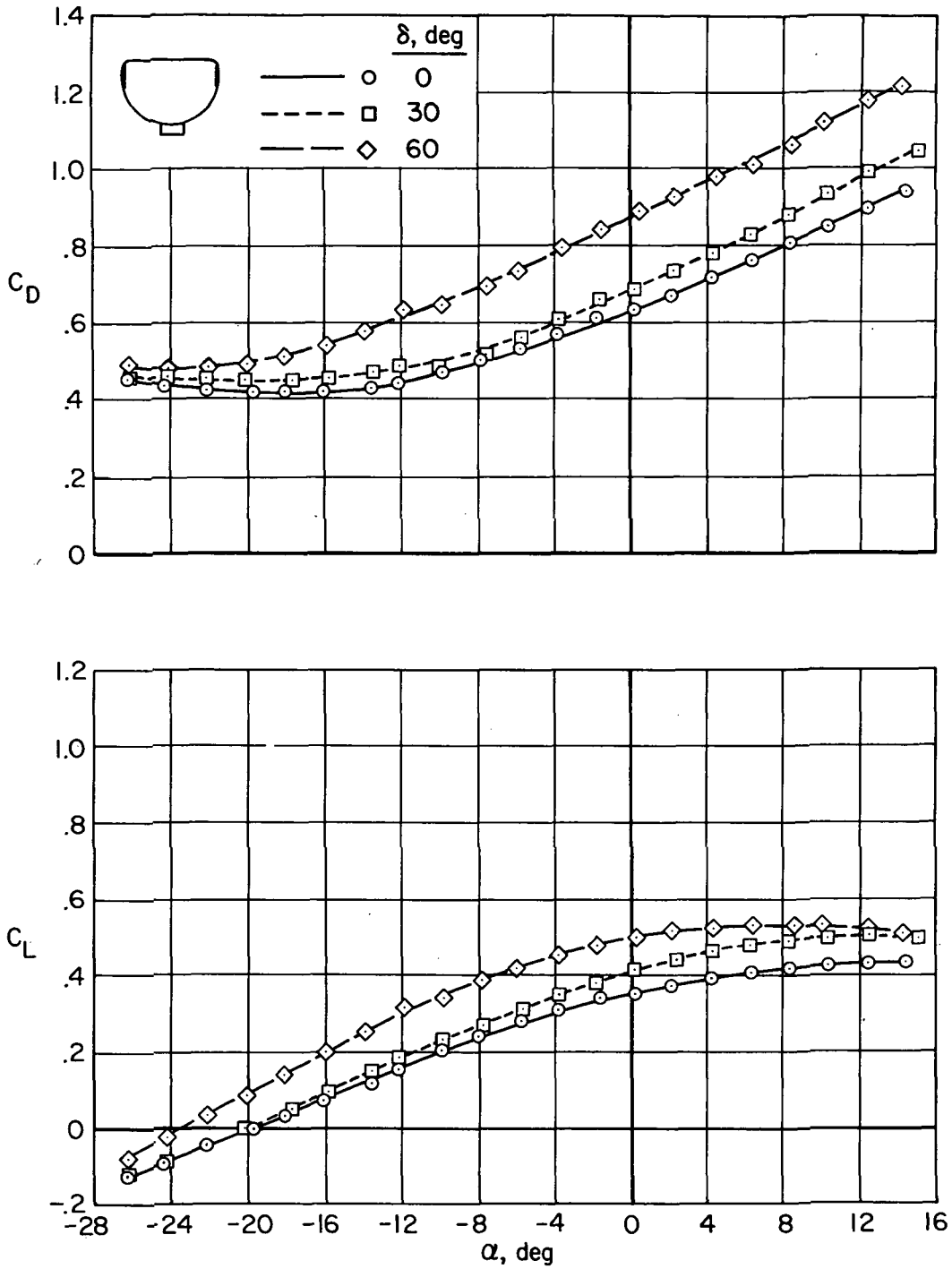

(a) C_D, C_L

Figure 17.- Variation of the longitudinal aerodynamic characteristics with angle of attack for the lower control of control set II deflected, M = 10.9.

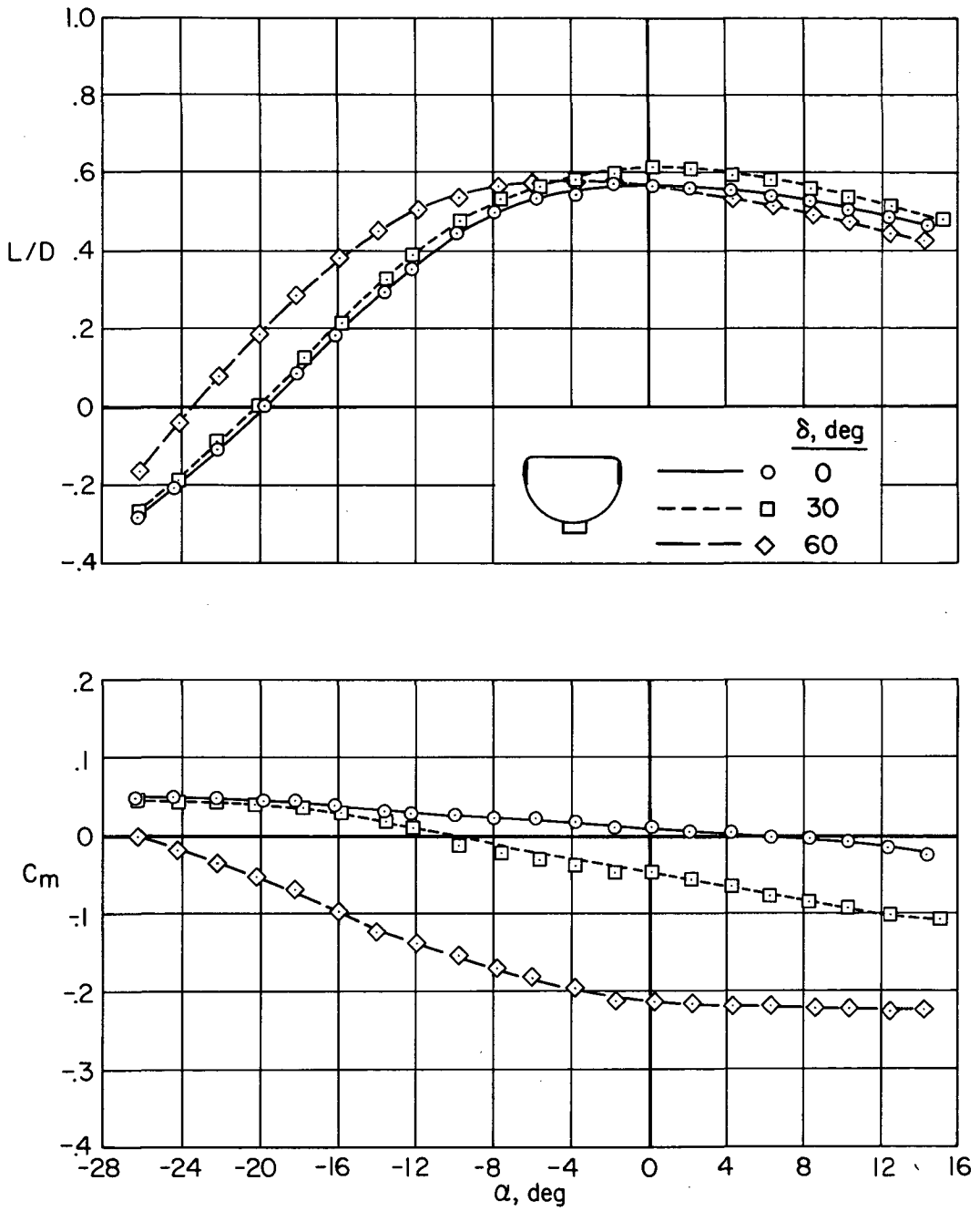

(b) L/D, C_m

Figure 17.- Concluded.

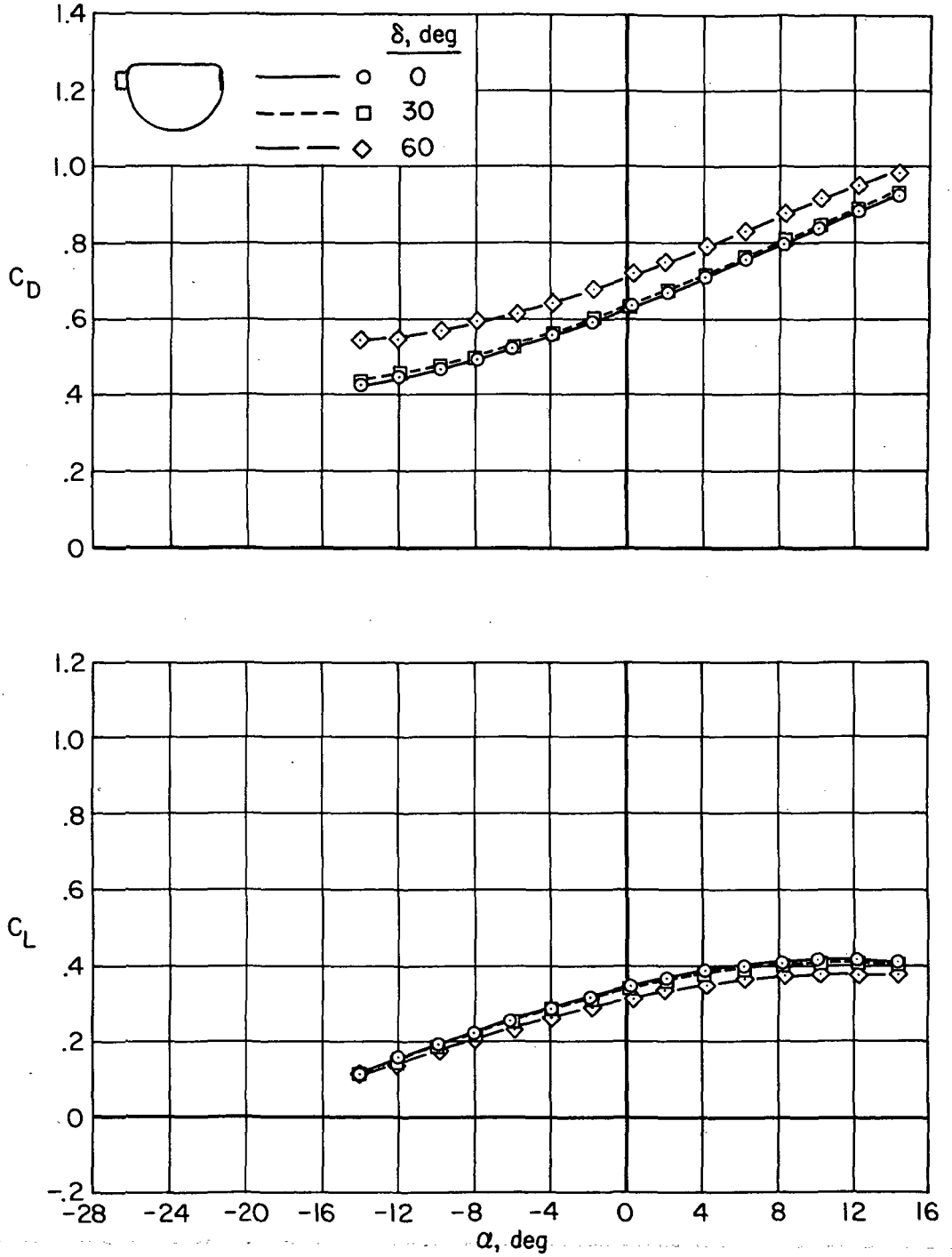

(a) C_D, C_L

Figure 18.- Variation of the longitudinal aerodynamic characteristics with angle of attack for a side control of control set II deflected, M = 10.9.

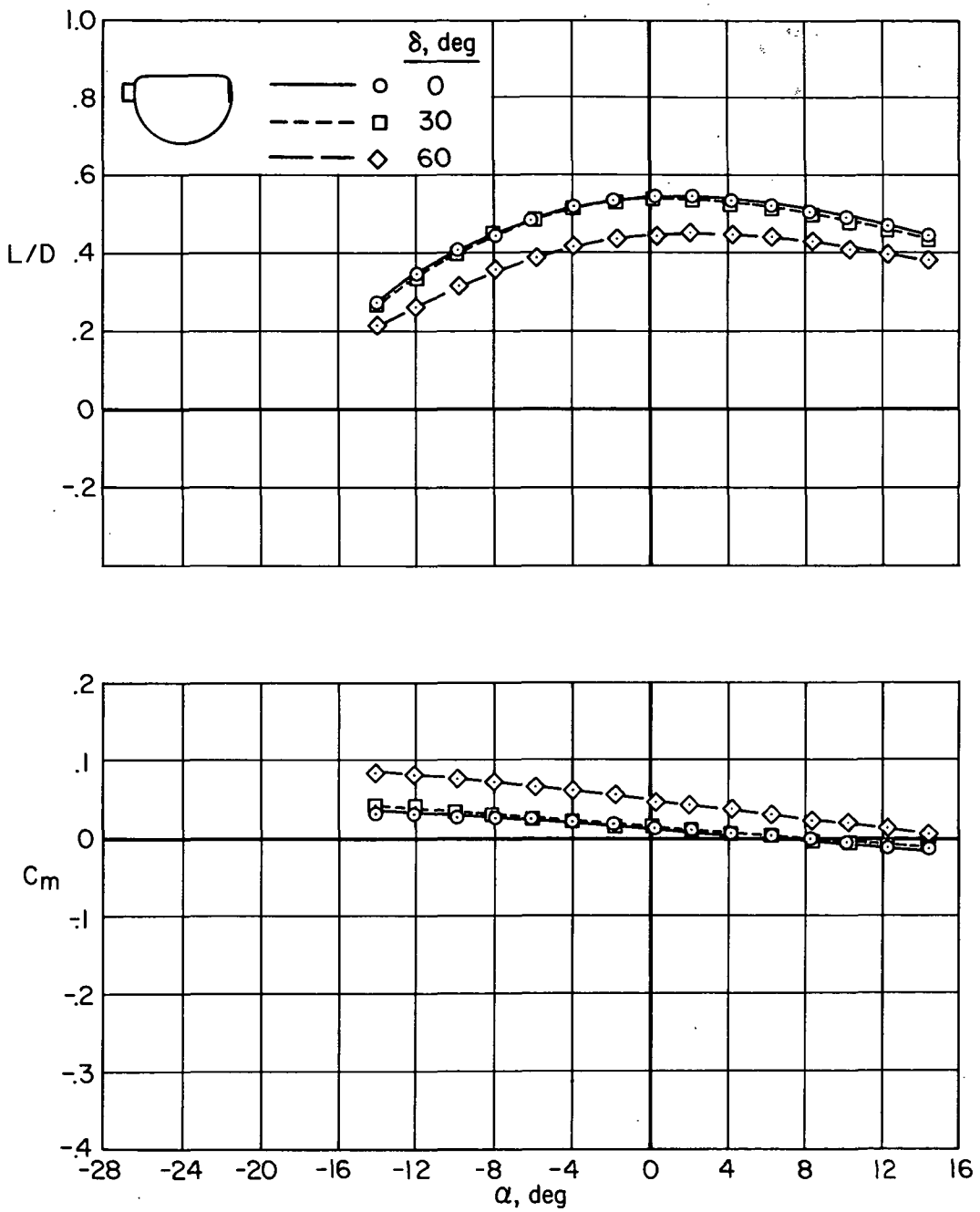

(b) L/D, C_m

Figure 18.- Continued.

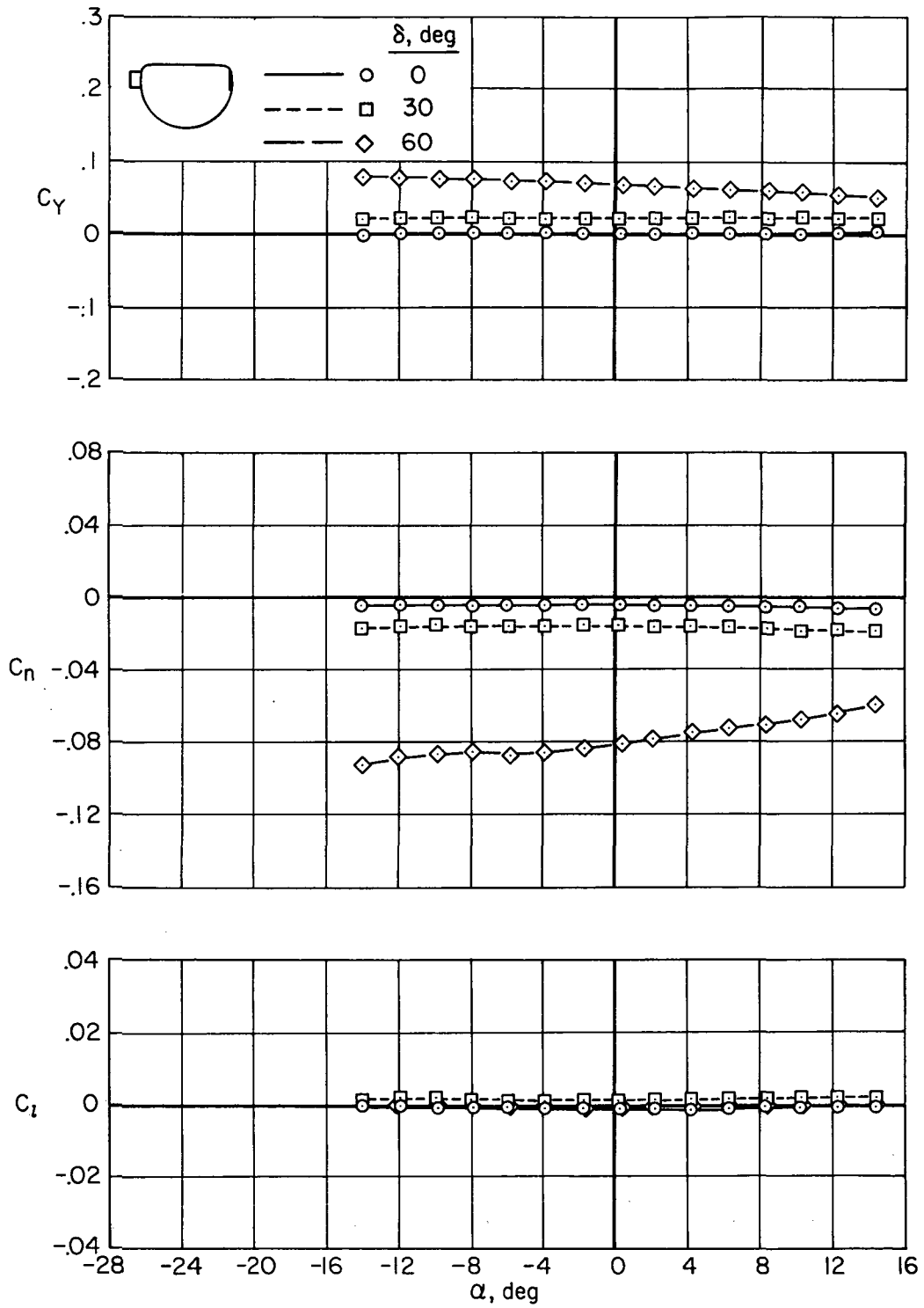

(c) C_Y, C_n, C_l

Figure 18.- Concluded.

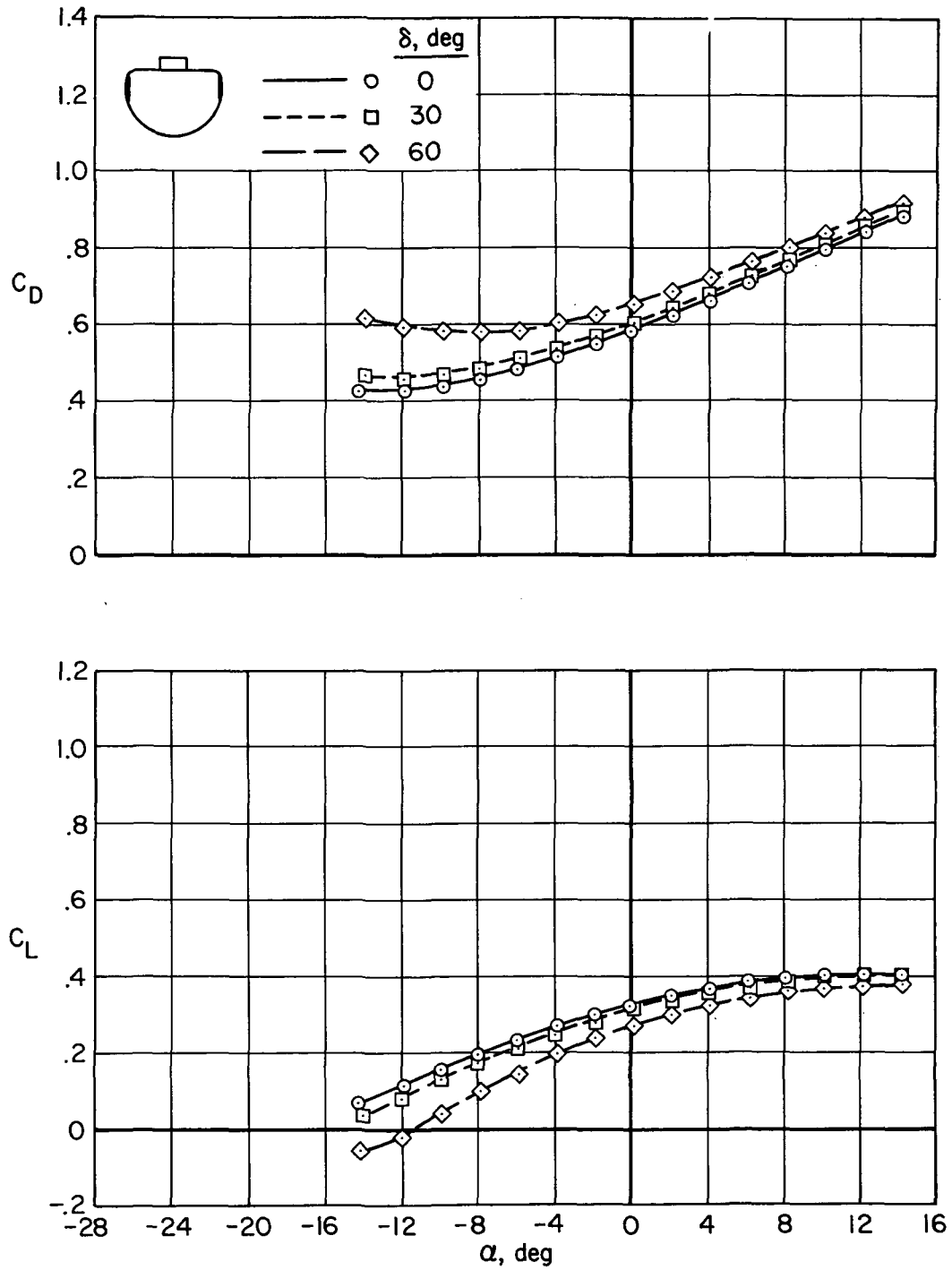

(a) C_D, C_L

Figure 19.- Variation of the longitudinal aerodynamic characteristics with angle of attack for the upper control of control set II deflected, M = 17.8.

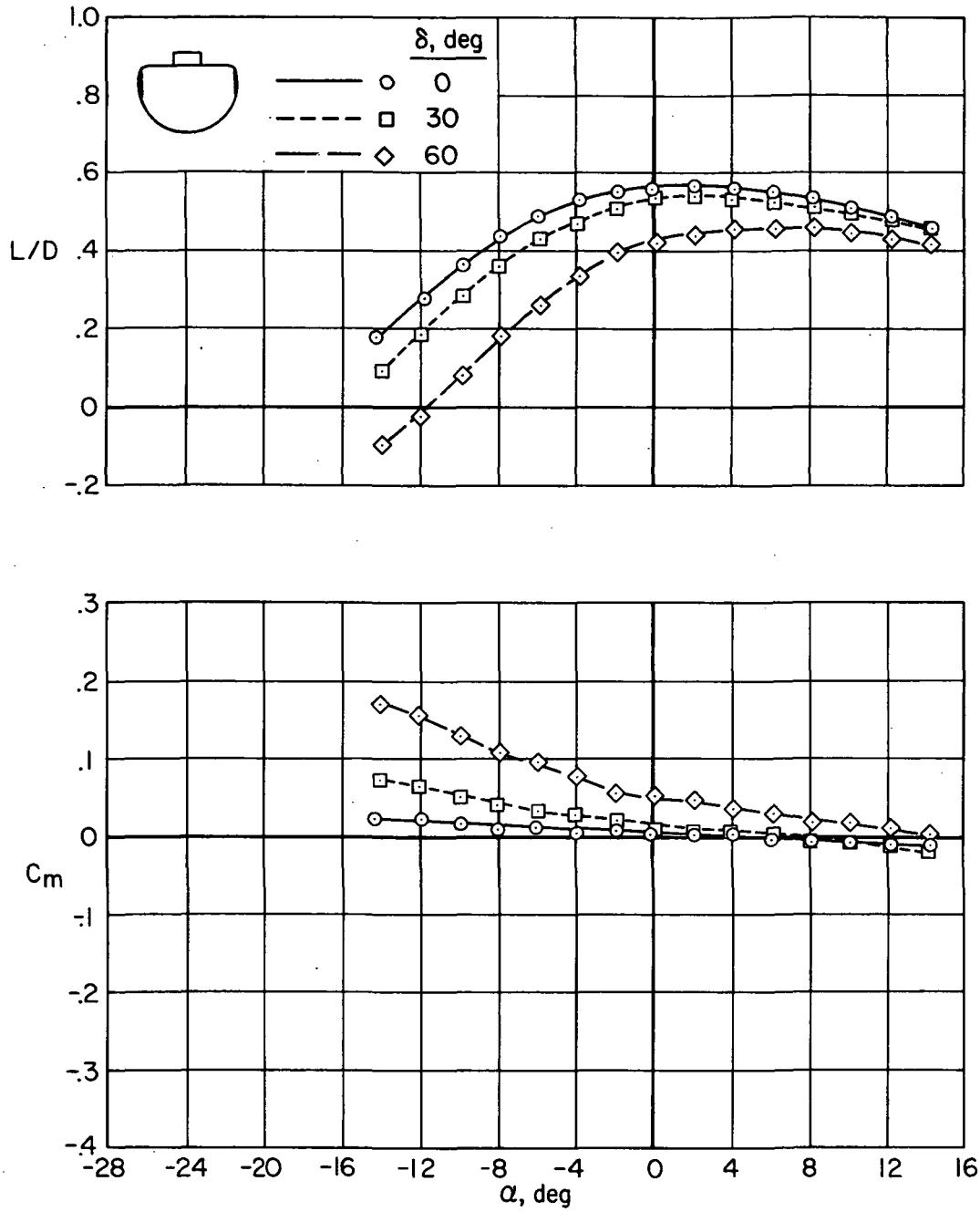

(b) L/D, C_m

Figure 19.- Concluded.

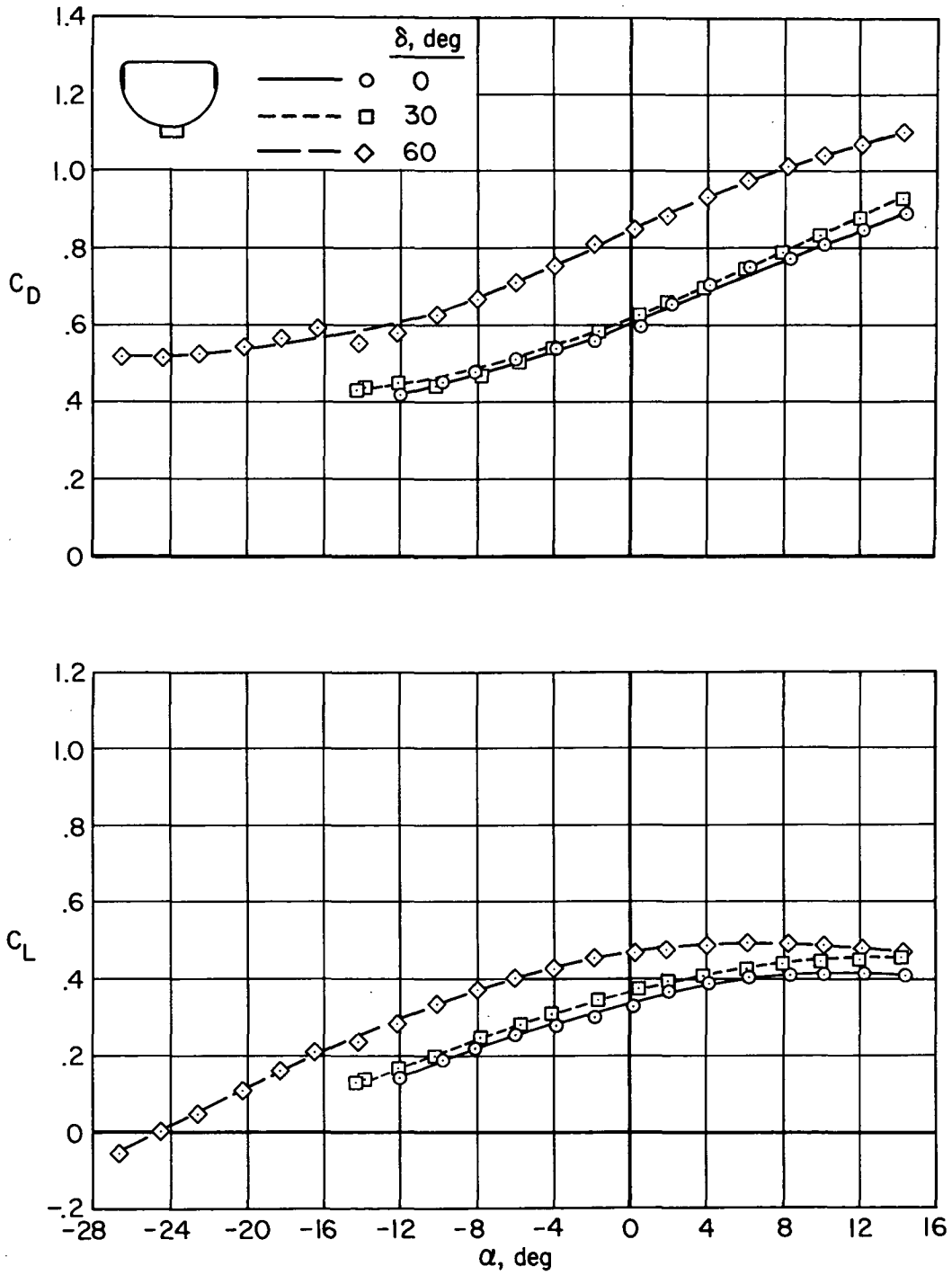

(a) C_D, C_L

Figure 20.- Variation of the longitudinal aerodynamic characteristics with angle of attack for the lower control of control set II deflected, M = 17.8.

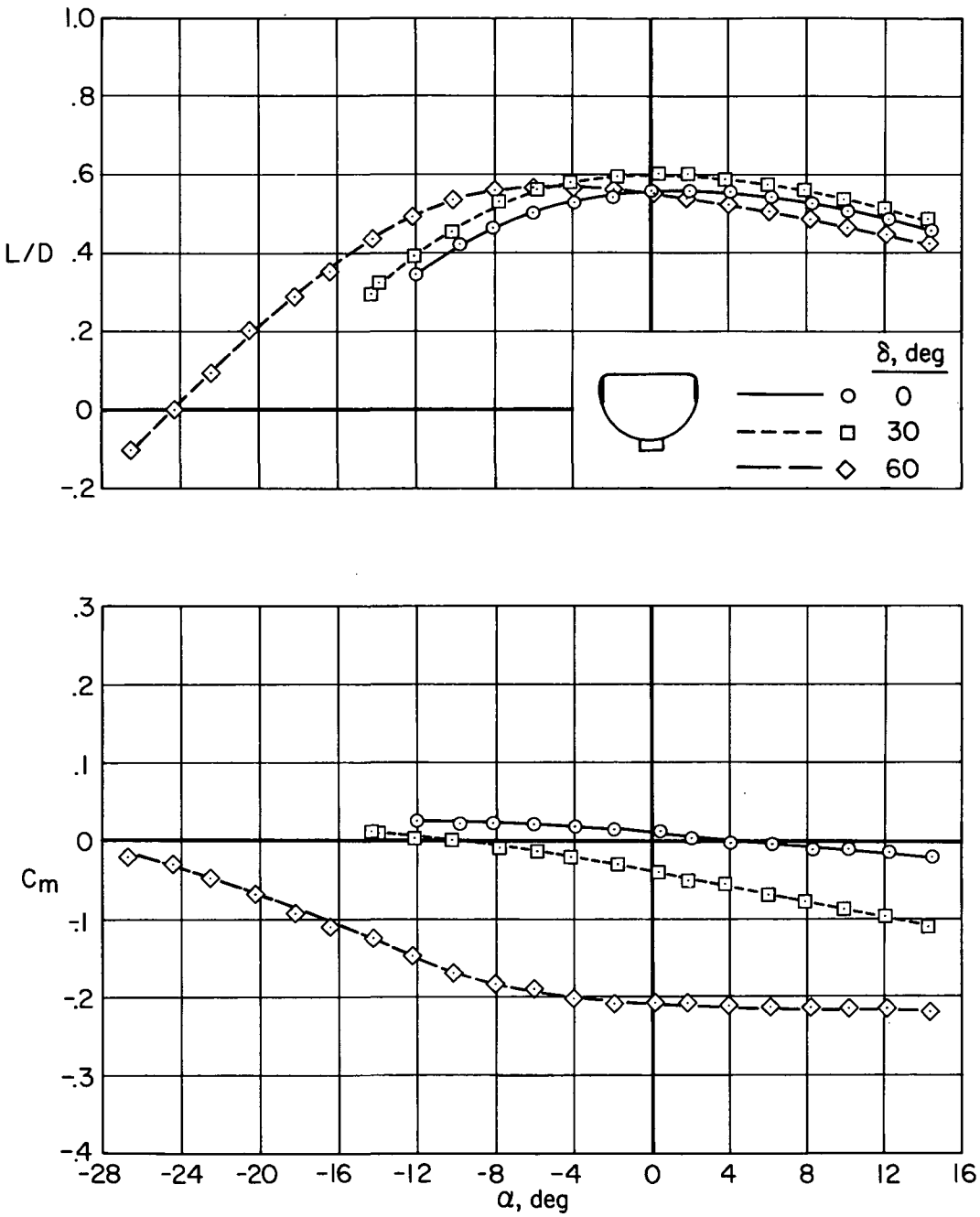

(b) L/D, C_m

Figure 20.- Concluded.

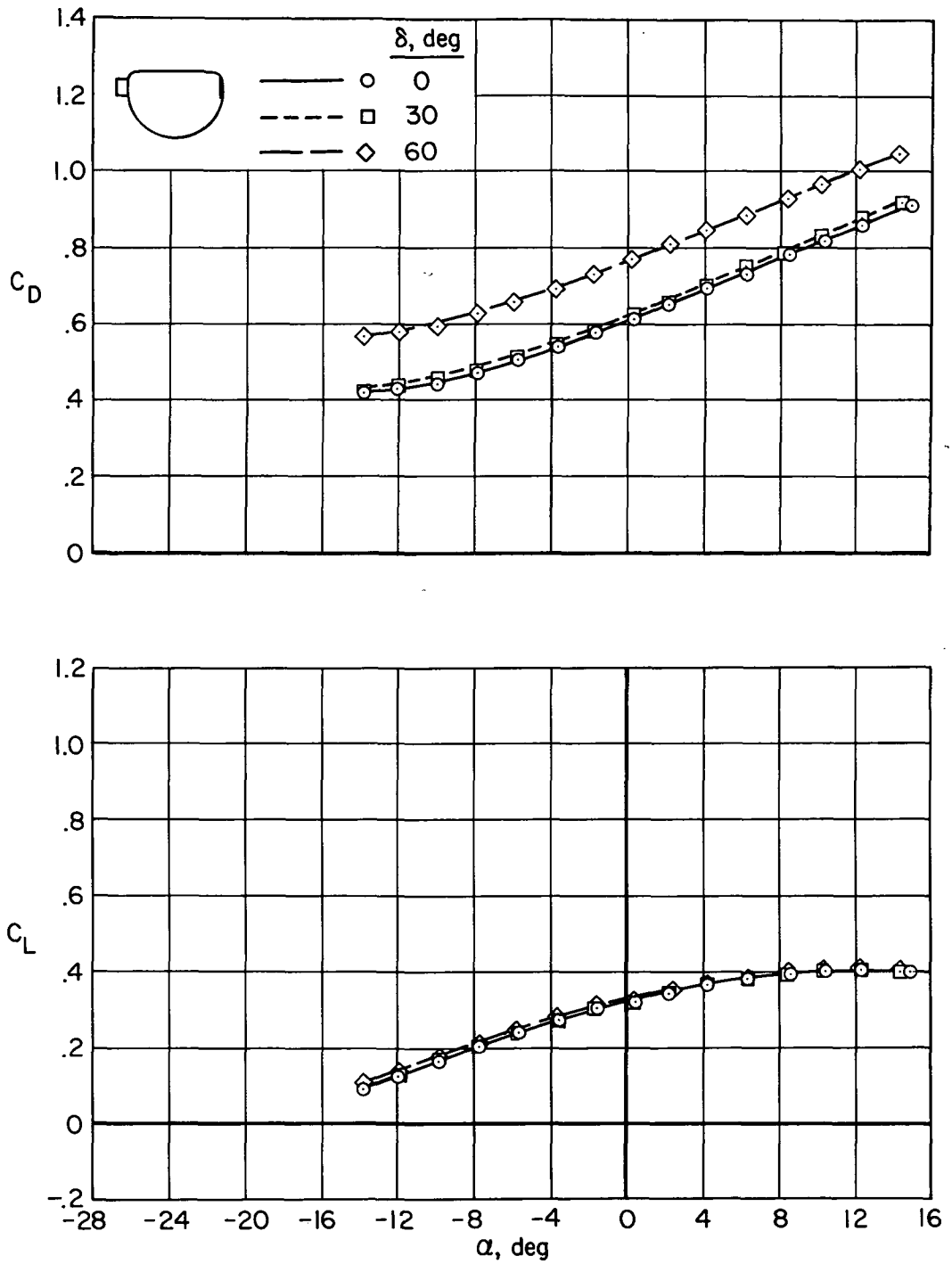

(a) C_D, C_L

Figure 21.- Variation of the longitudinal aerodynamic characteristics with angle of attack for a side control of control set II deflected, M = 17.8.

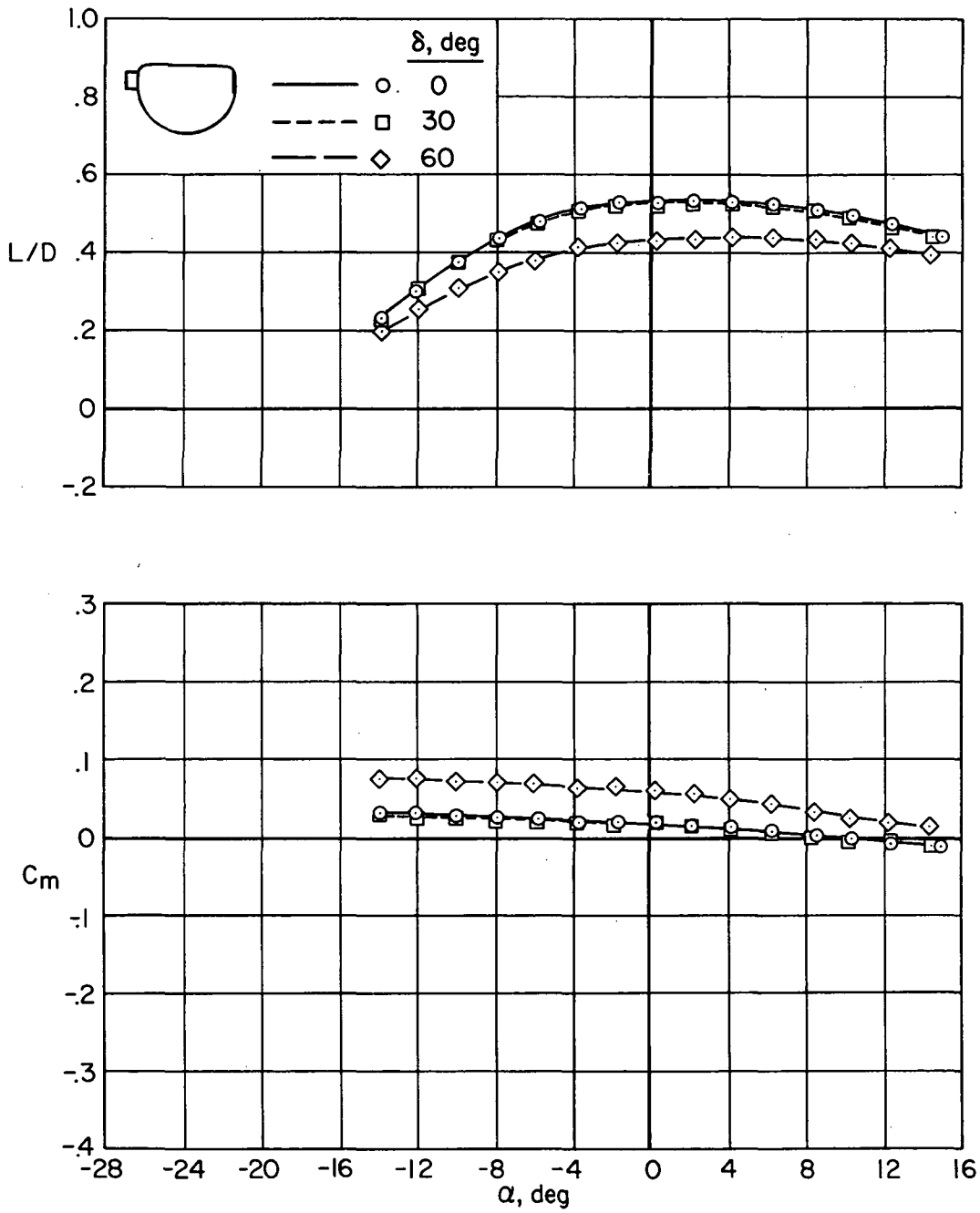

(b) L/D, C_m

Figure 21.- Continued.

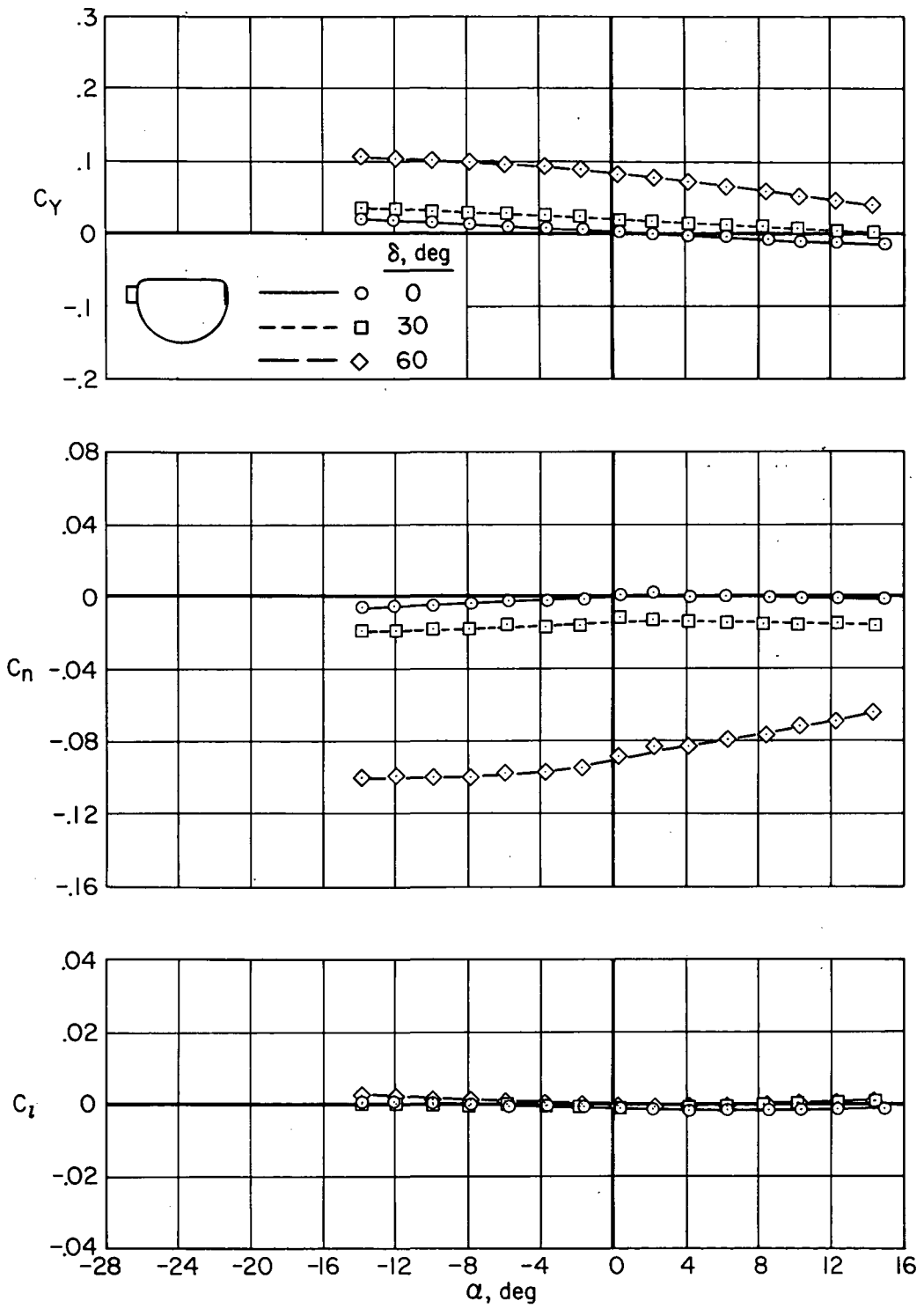

(c) C_Y, C_n, C_l

Figure 21-. Concluded.

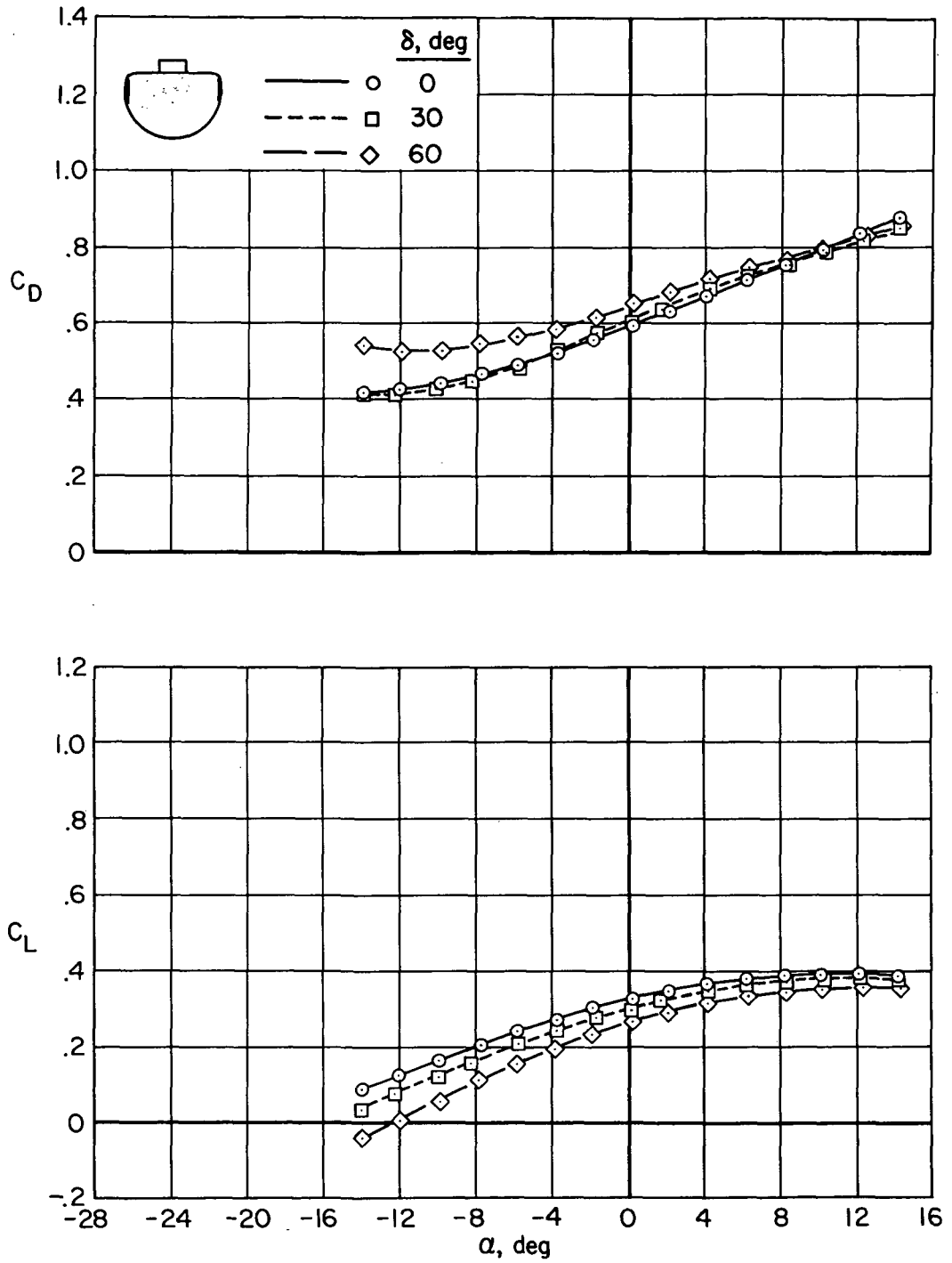

(a) C_D, C_L

Figure 22.- Variation of the longitudinal aerodynamic characteristics with angle of attack for the upper control of control set II deflected, M = 21.2.

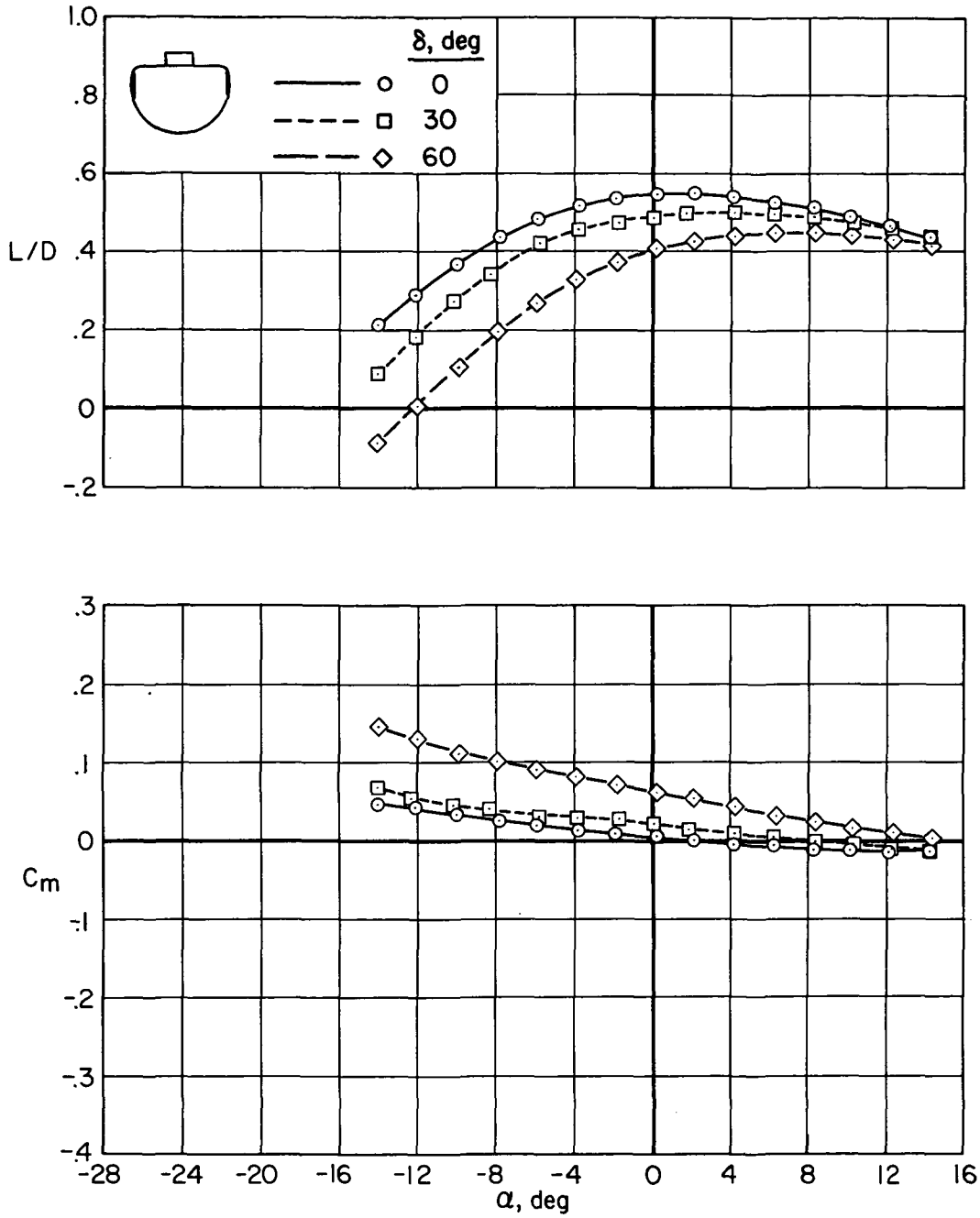

(b) L/D, C_m

Figure 22.- Concluded.

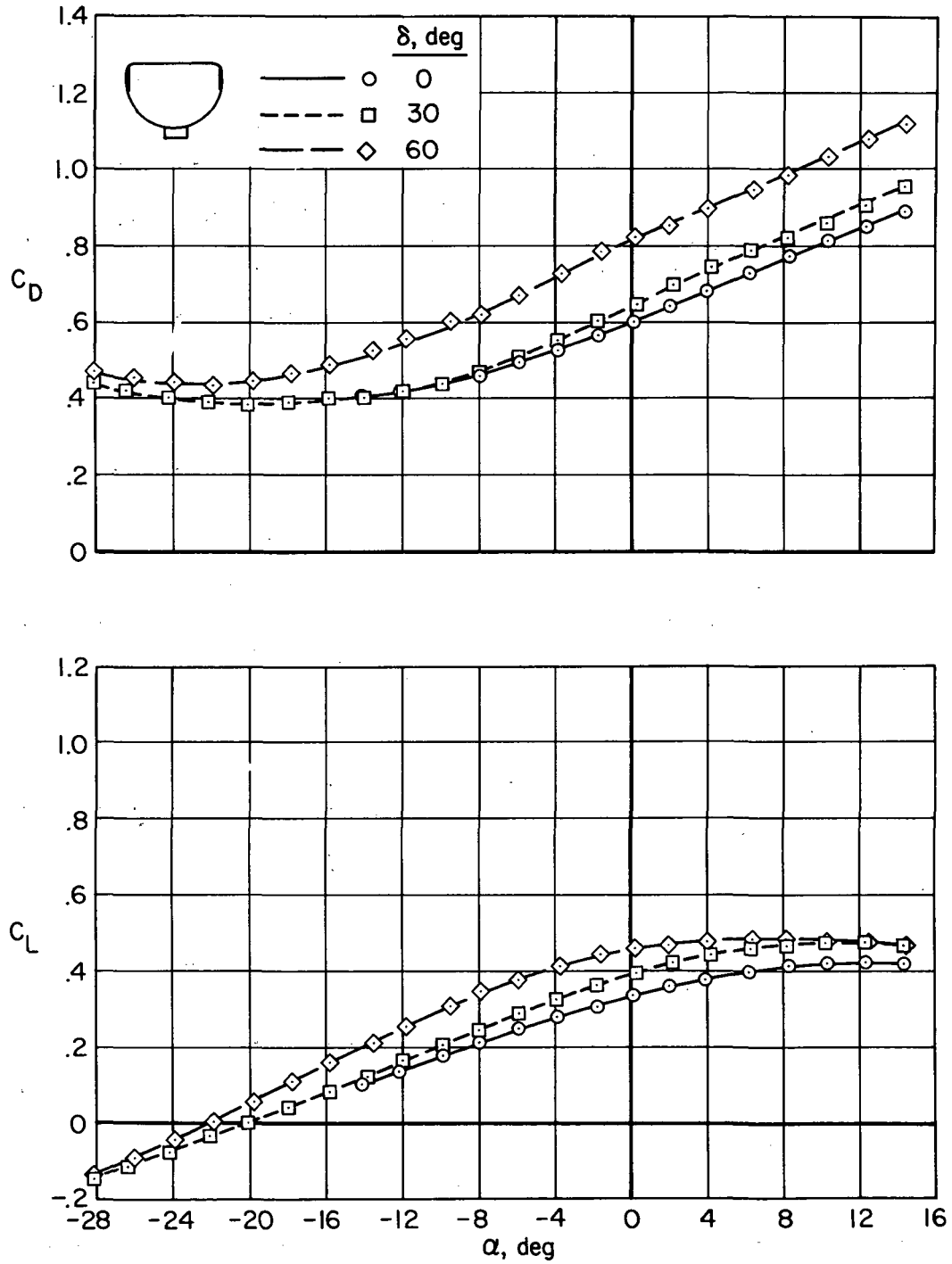

(a) C_D, C_L

Figure 23.- Variation of the longitudinal aerodynamic characteristics with angle of attack for the lower control of control set II deflected, M = 21.2.

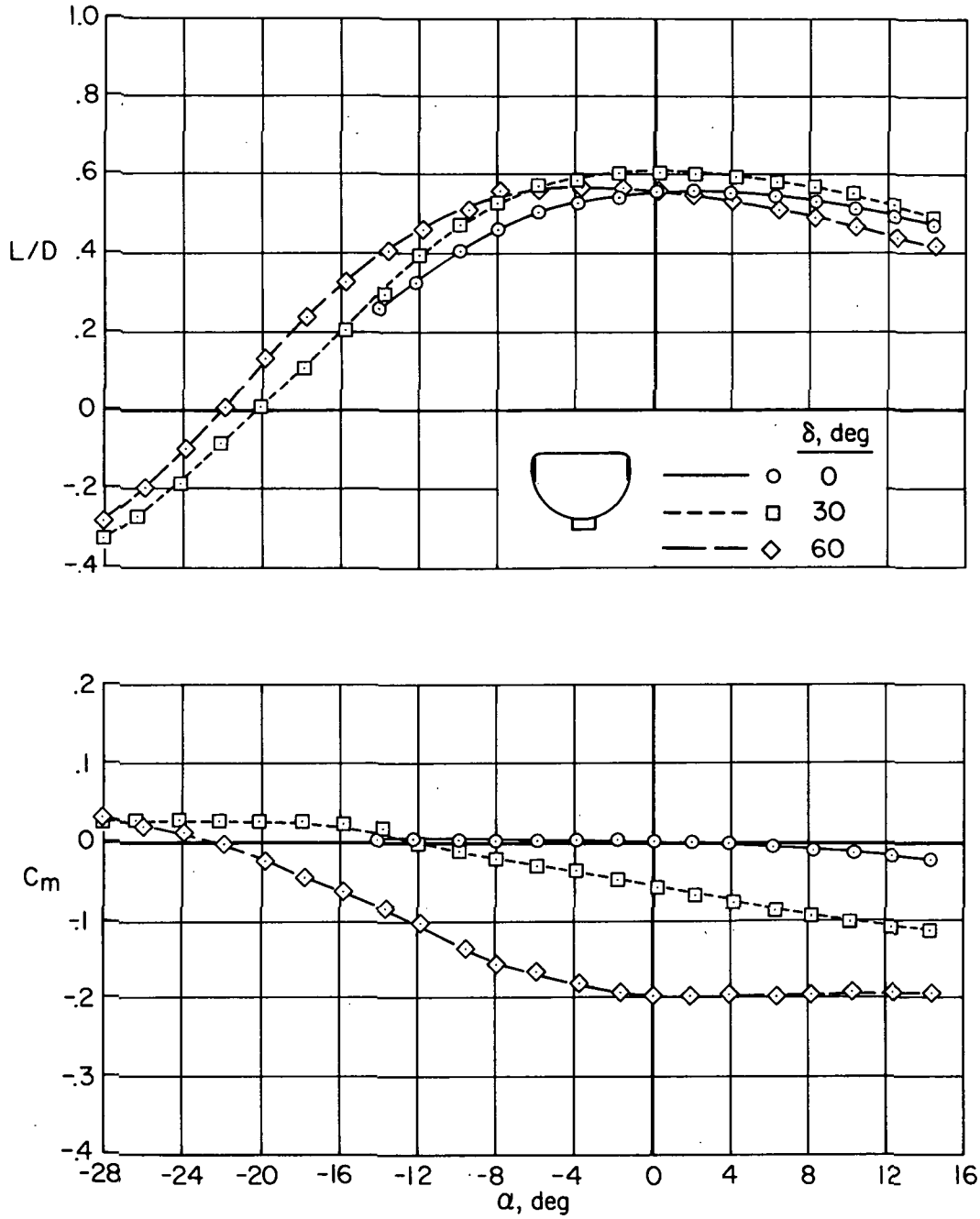

(b) L/D, C_m

Figure 23.- Concluded.

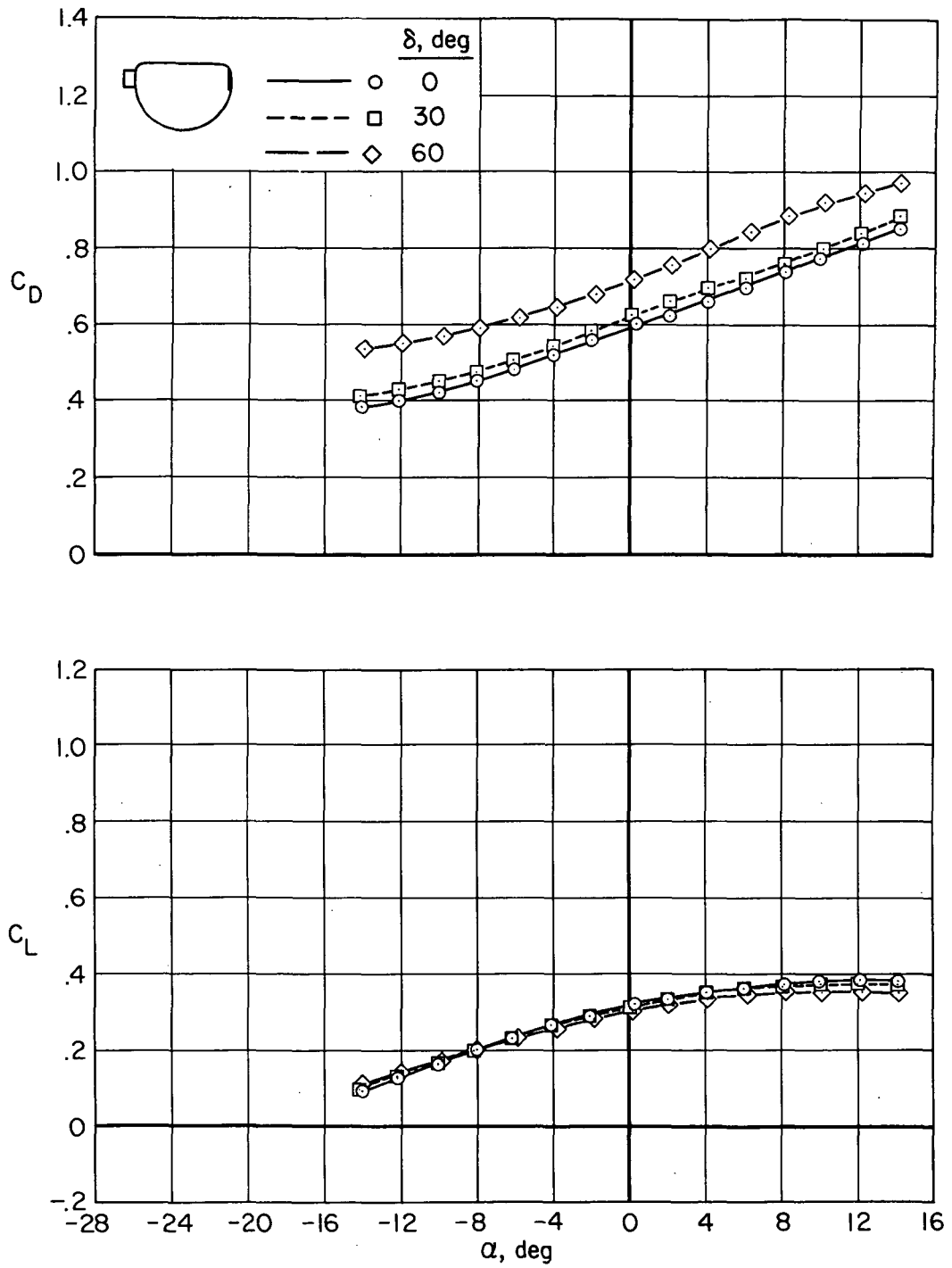

(a) C_D, C_L

Figure 24.- Variation of the longitudinal aerodynamic characteristics with angle of attack for a side control of control set II deflected, M = 21.2.

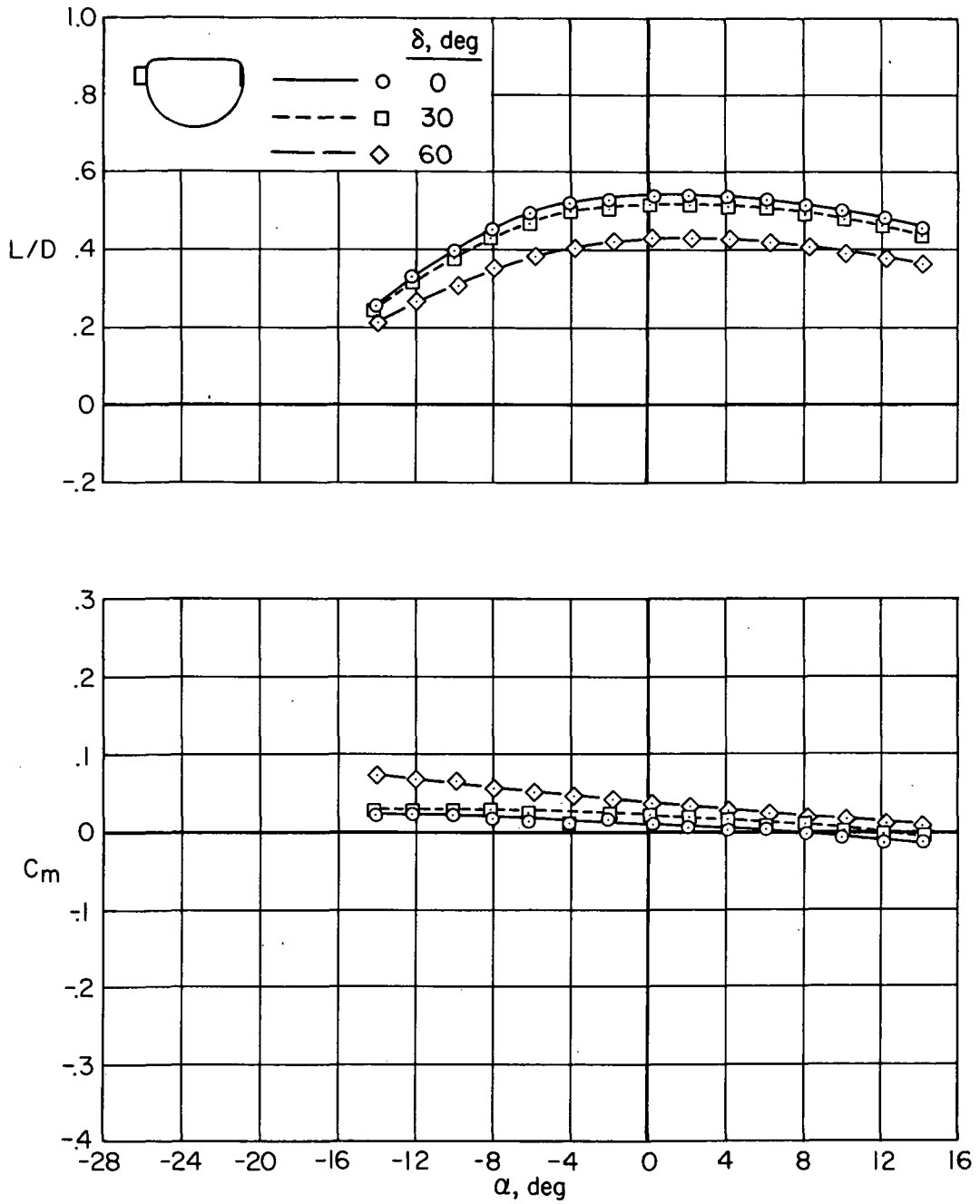

(b) L/D, C_m

Figure 24.- Continued.

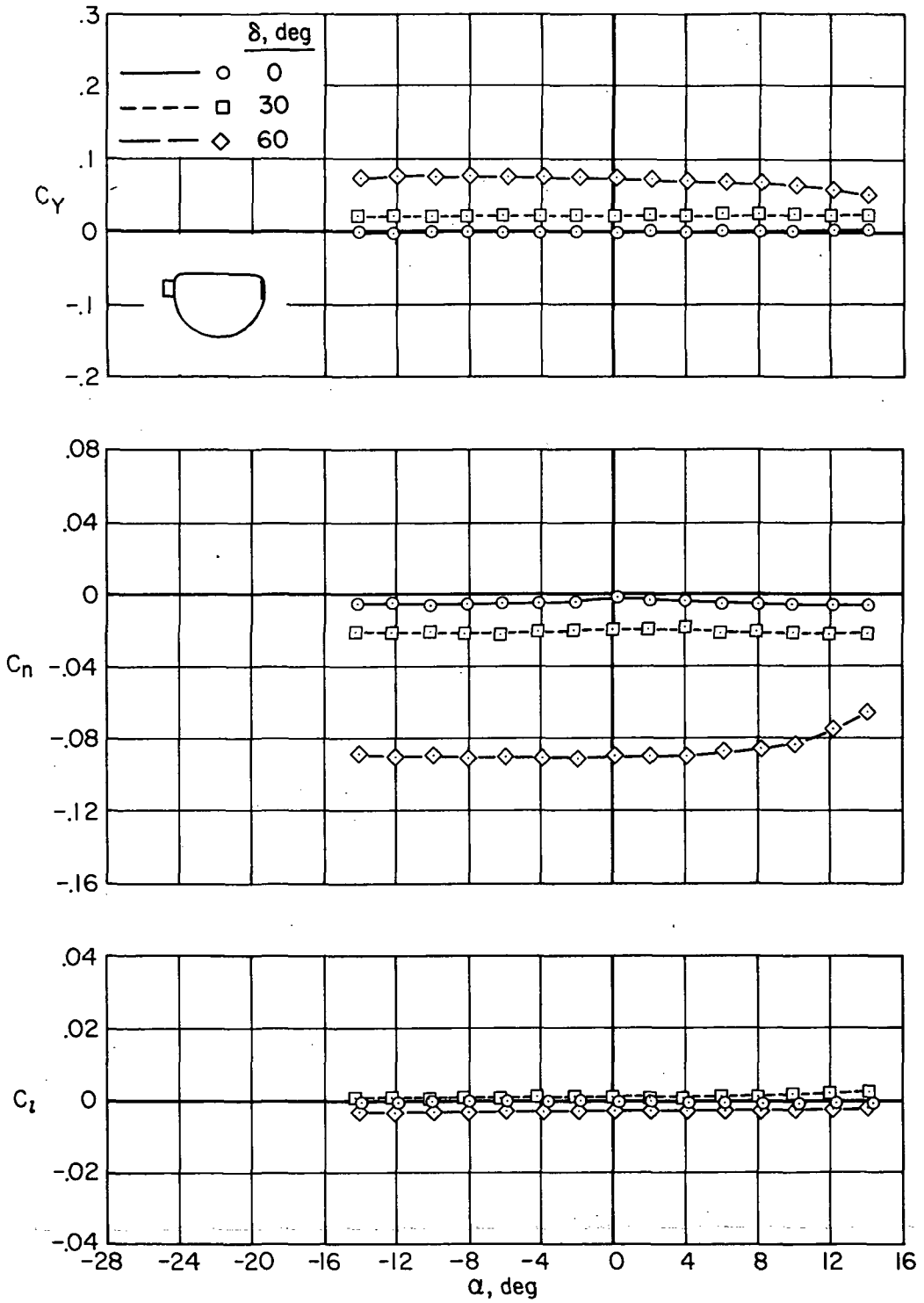

(c) C_Y, C_n, C_l

Figure 24.- Concluded.

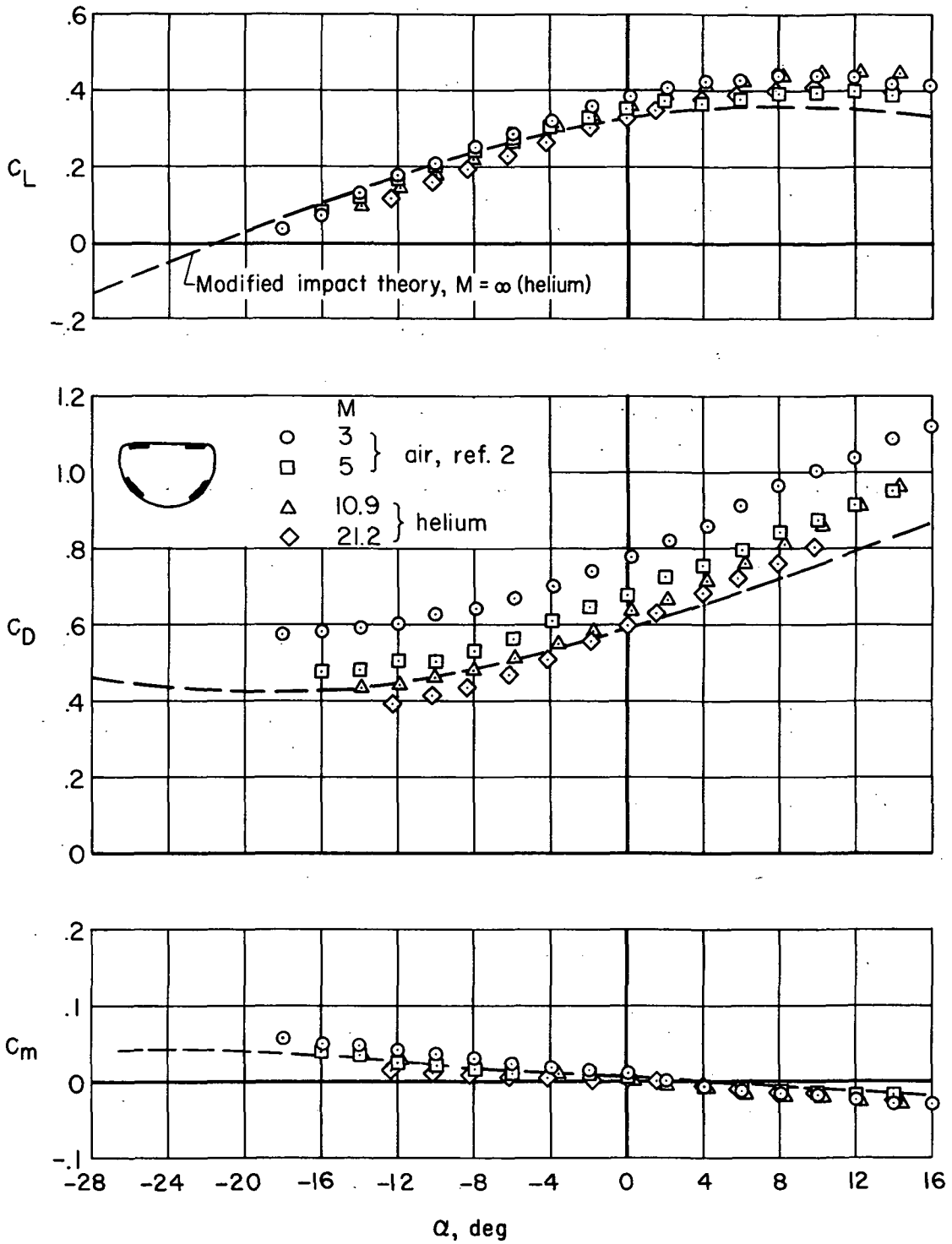

Figure 25.- Variation of the longitudinal aerodynamic characteristics with angle of attack at several Mach numbers for control set I undeflected.

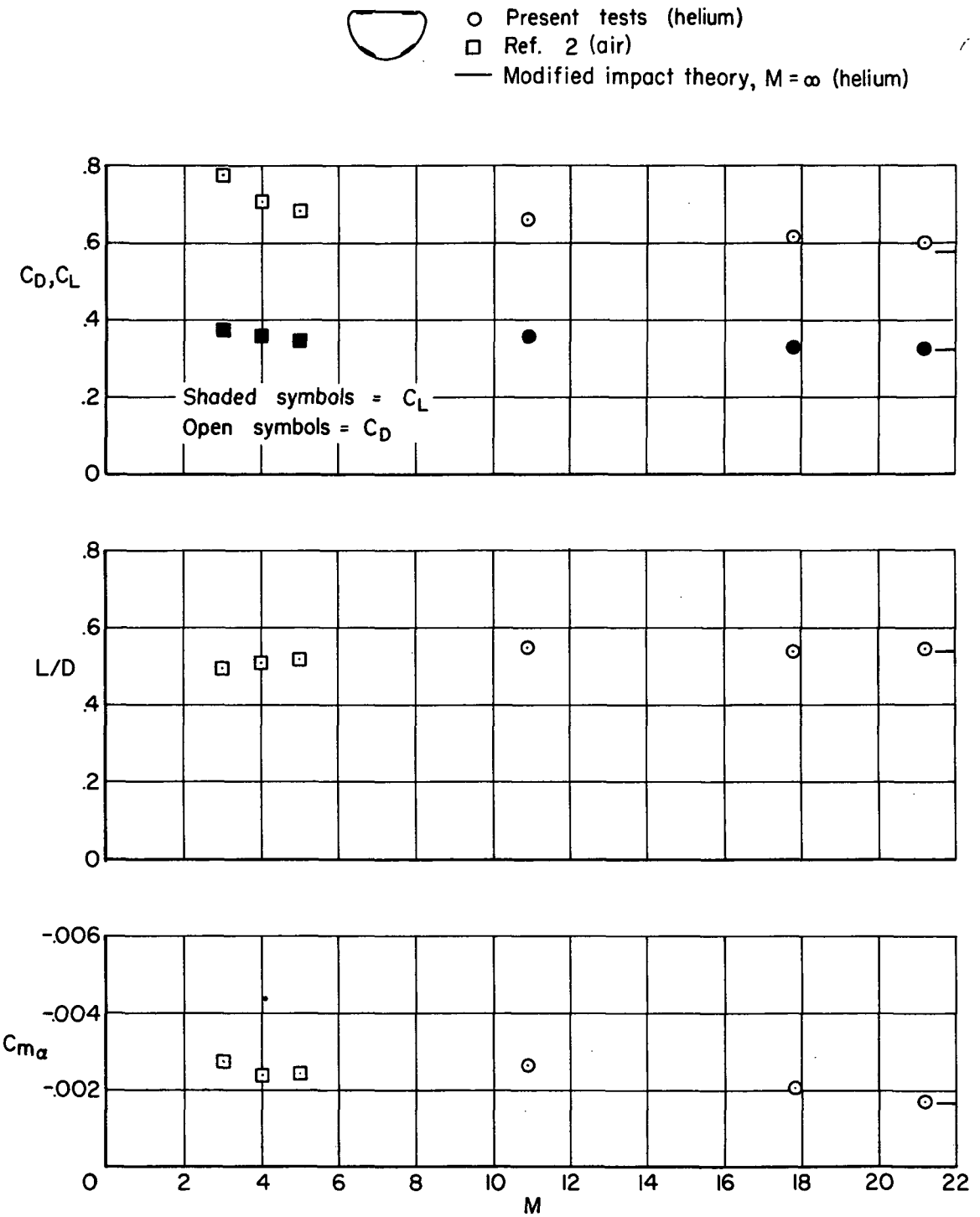

Figure 26.- Variation of the longitudinal aerodynamic characteristics with Mach number for control set I undeflected, $\alpha = 0^\circ$.

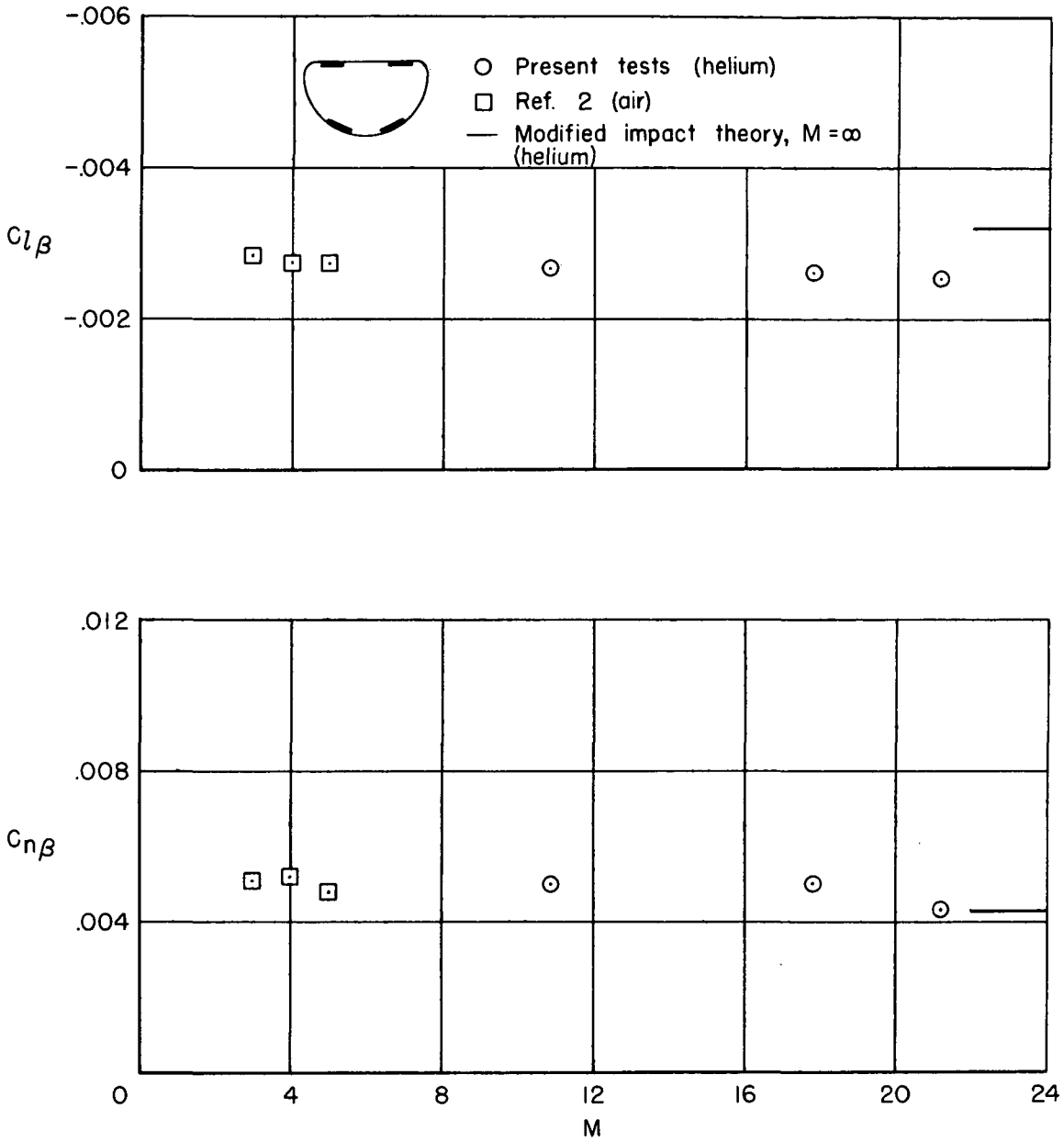

Figure 27.- Variation of lateral-stability derivatives with Mach number for control set I undeflected, $\alpha = 0^{\circ}$.

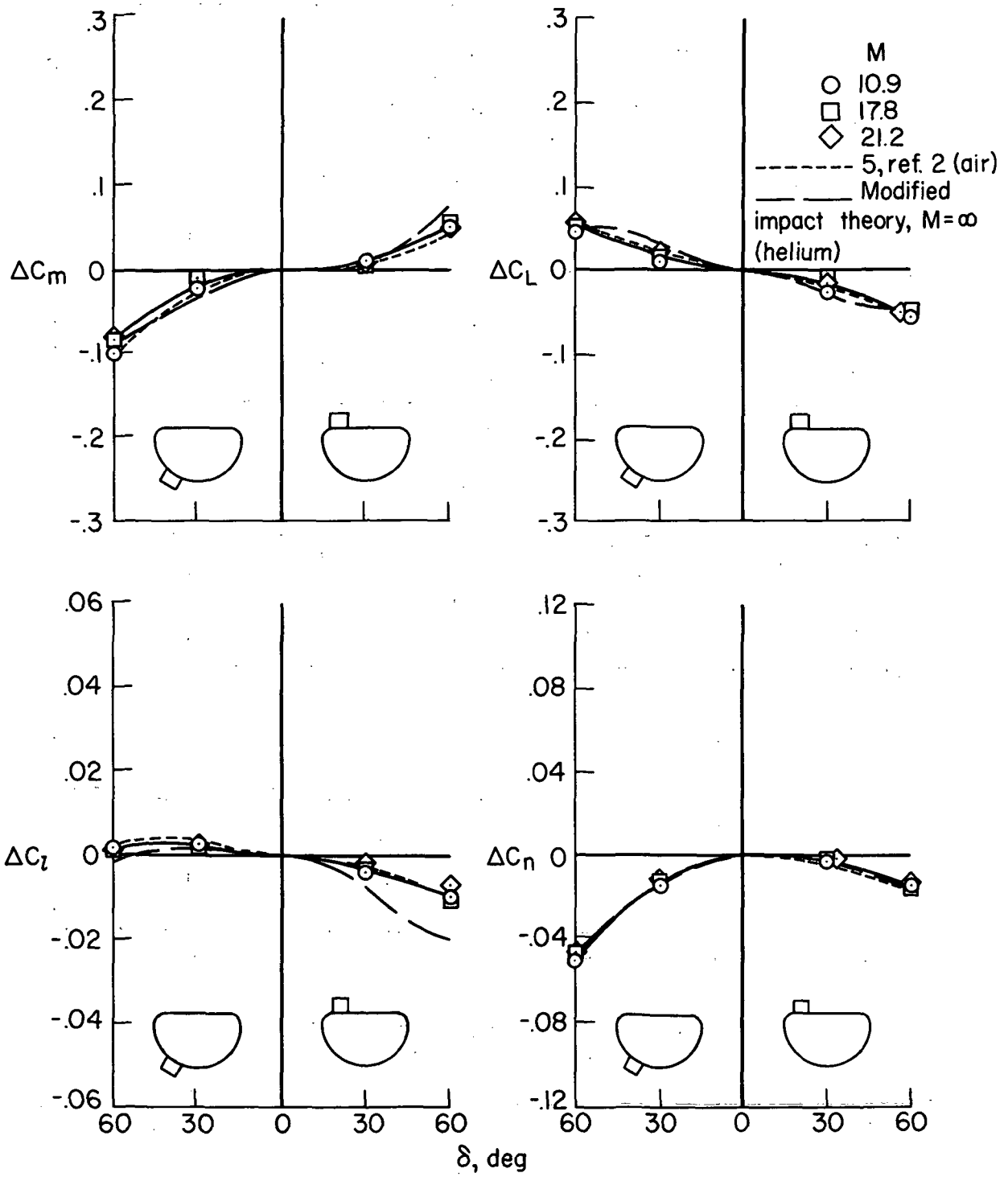

Figure 28.- Variation of incremental changes of moment and lift coefficient with flap deflection for control set I at $\alpha = 0^{o}$.

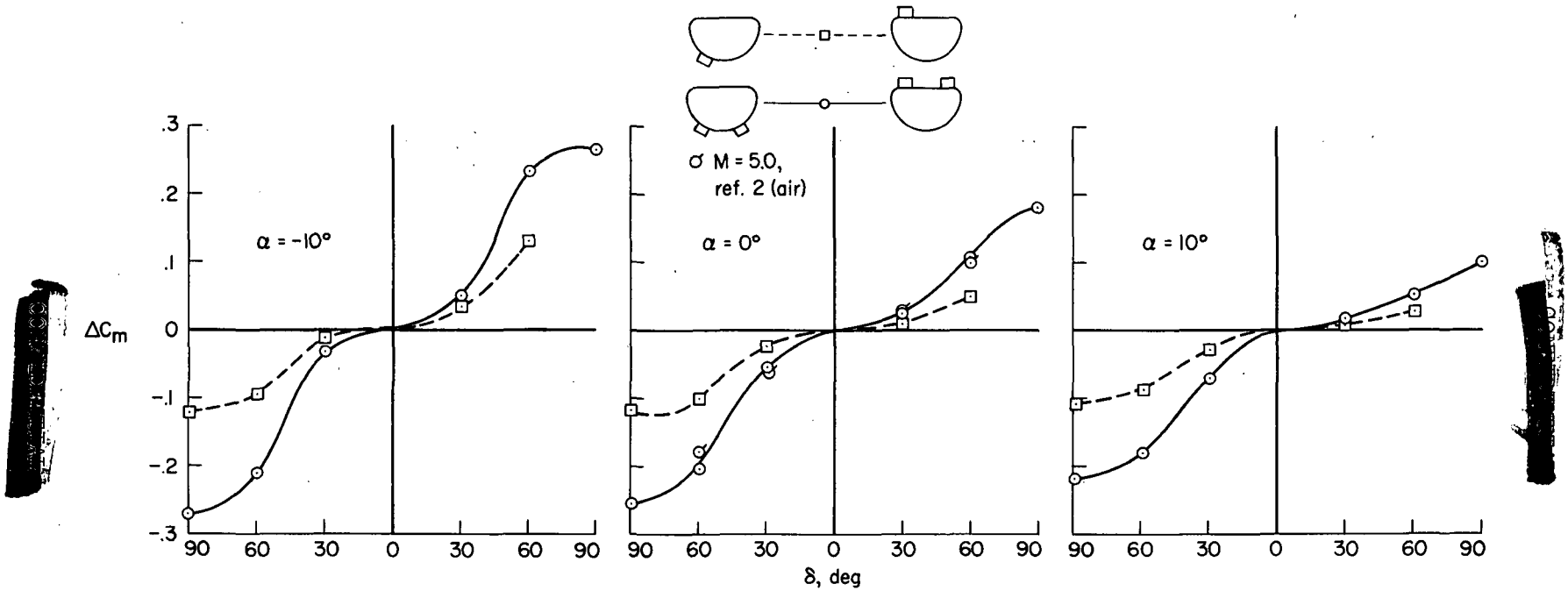

(a) ΔC_m

Figure 29.- Comparison of incremental changes of pitching-moment and force coefficients with flap deflection for single and double flaps of control set I, M = 10.9.

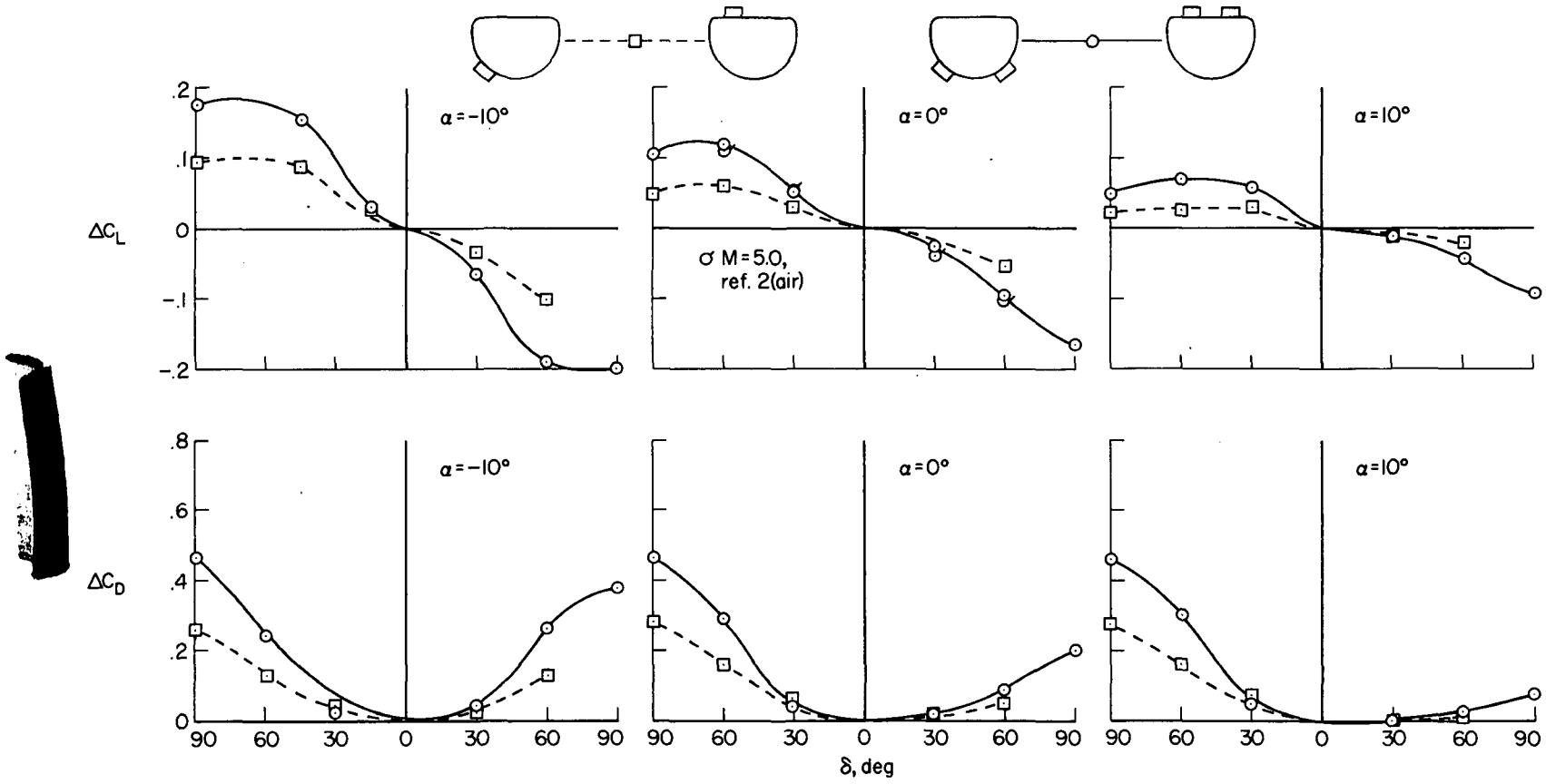

(b) ΔC_L, ΔC_D

Figure 29.- Concluded.

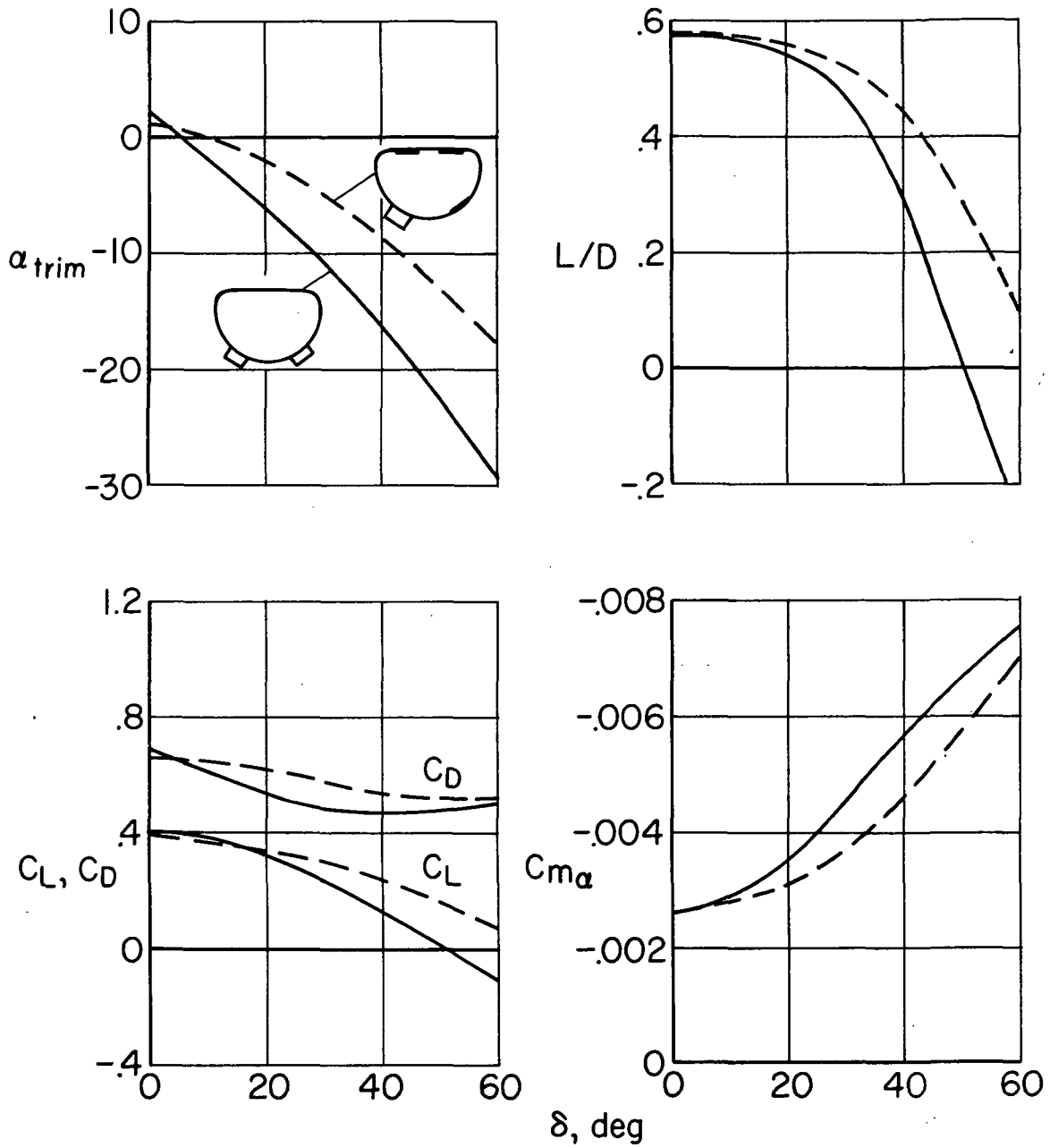

(a) Lower controls.

Figure 30.- Longitudinal aerodynamic characteristics at trim for control set I, M = 10.9.

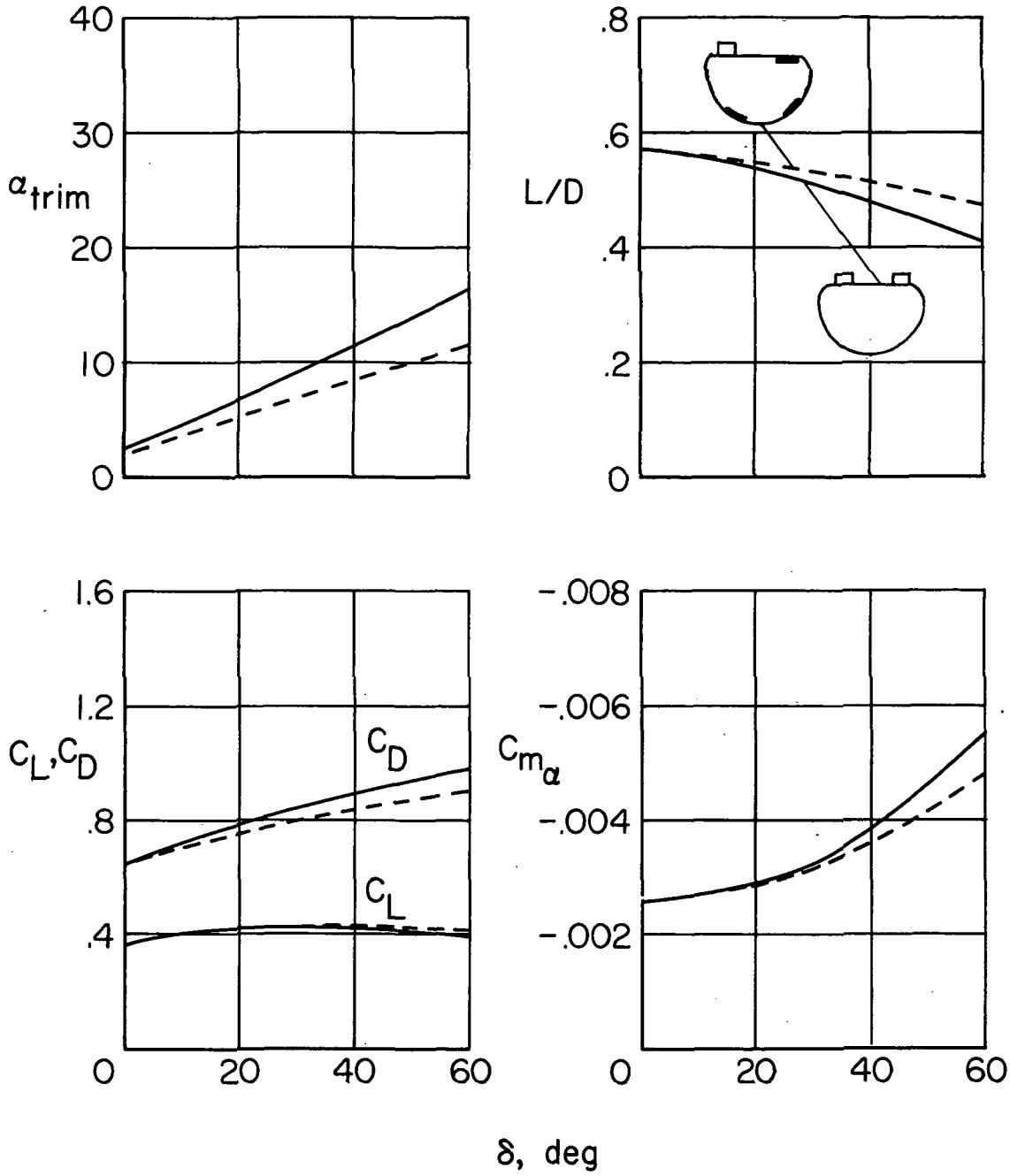

(b) Upper controls.

Figure 30.- Concluded.

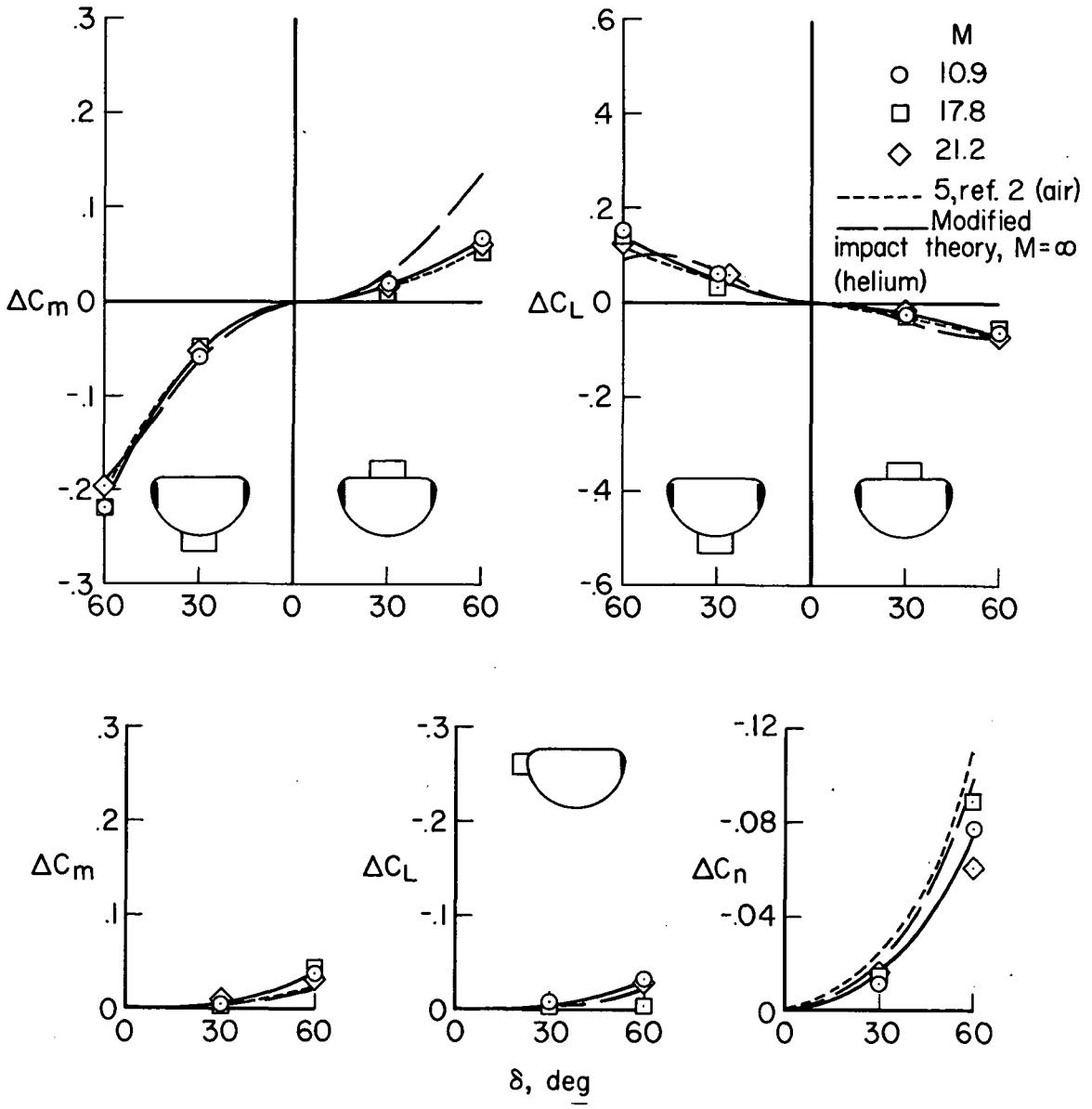

Figure 31.- Variation of incremental changes of moment and lift coefficients with flap deflection for control set II at $\alpha = 0^{\circ}$.

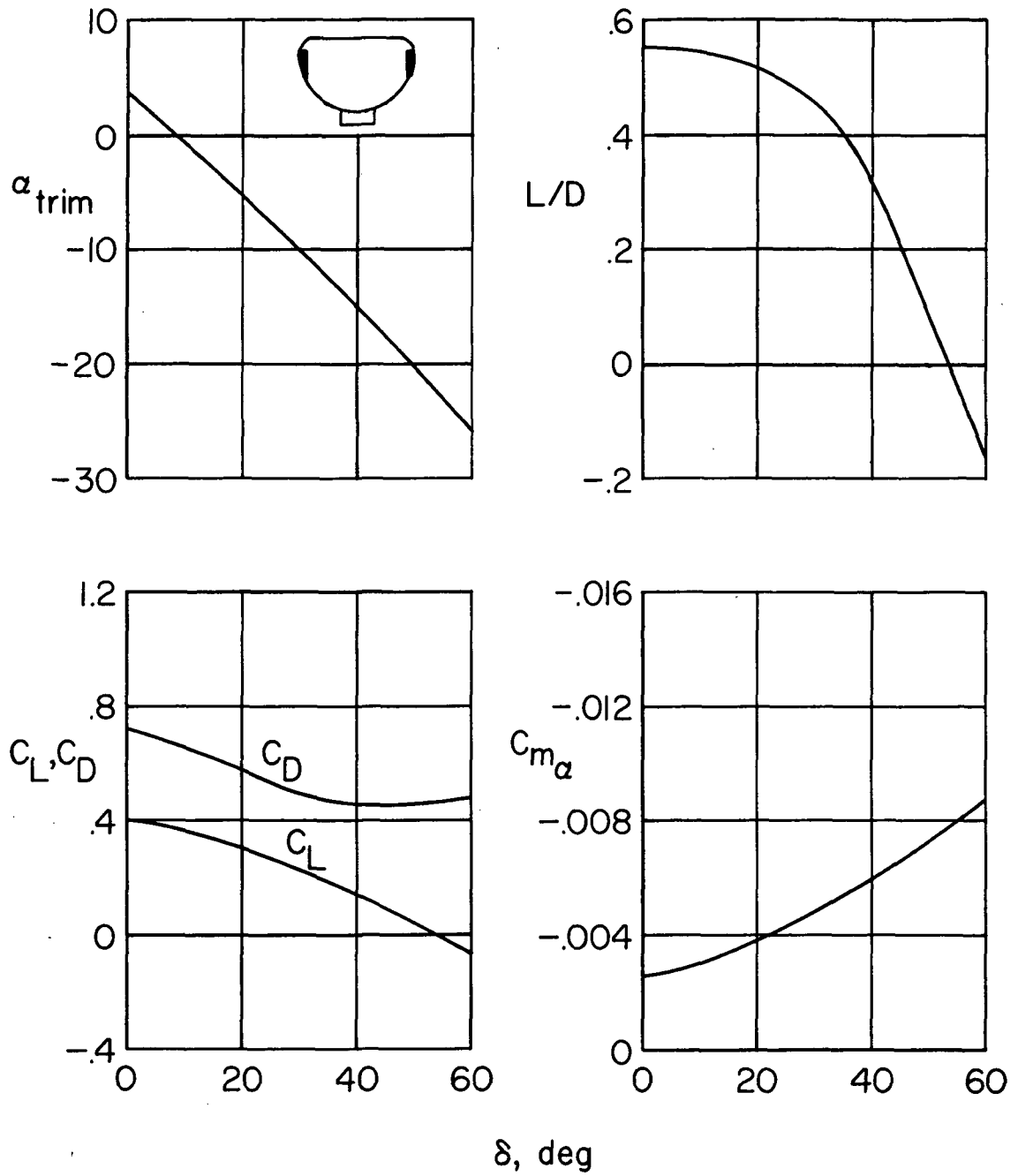

(a) Lower control.

Figure 32.- Longitudinal aerodynamic characteristics at trim for control set II, M = 10.9.

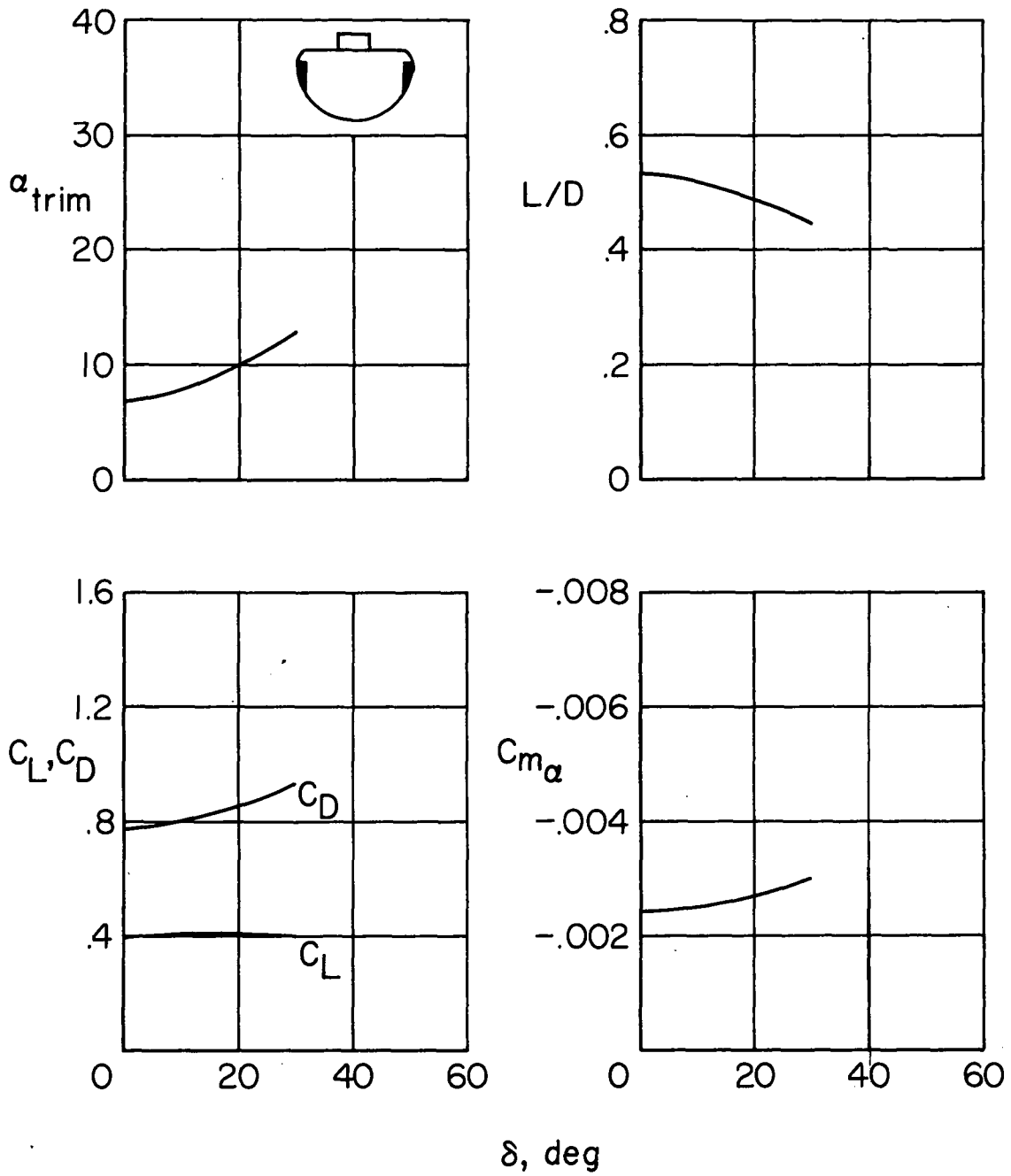

(b) Upper control.

Figure 32.- Concluded.

CONFIDENTIAL

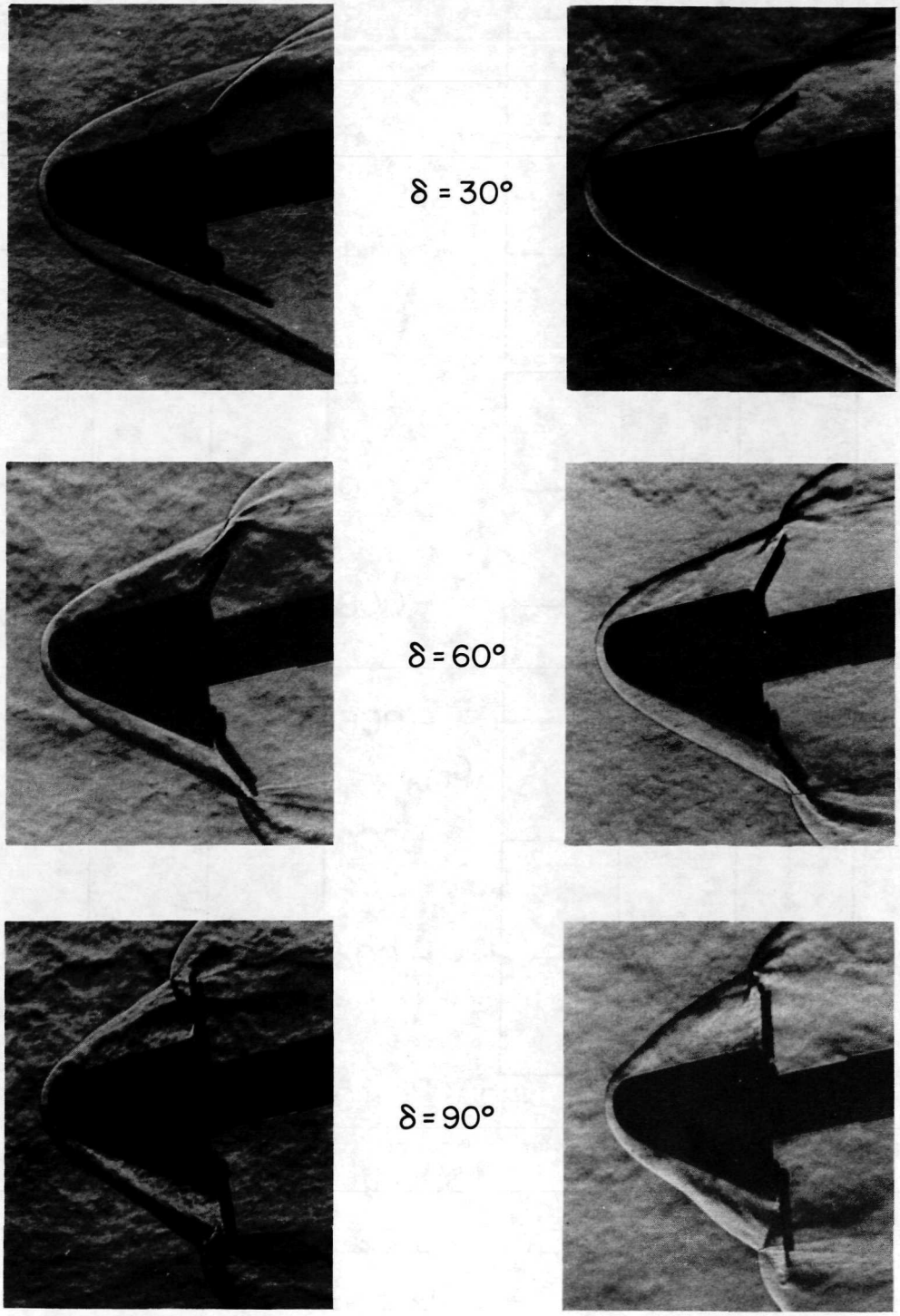

(a) $\alpha = -12^{\circ}$

Figure 33.- Schlieren photographs of model with upper and lower controls of set II, M = 10.9.

CONFIDENTIAL

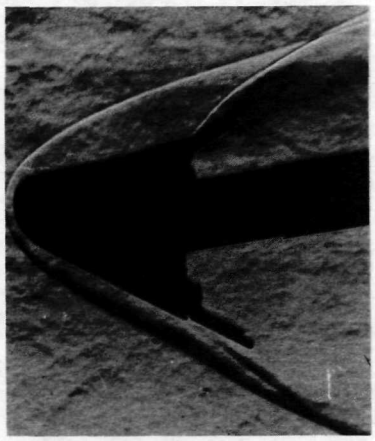

δ = 30°

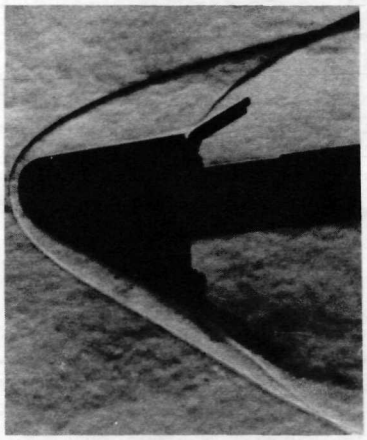

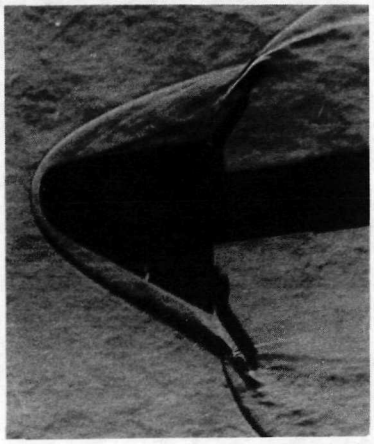

δ = 60°

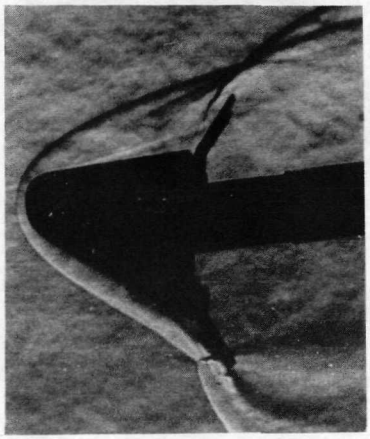

δ = 90°

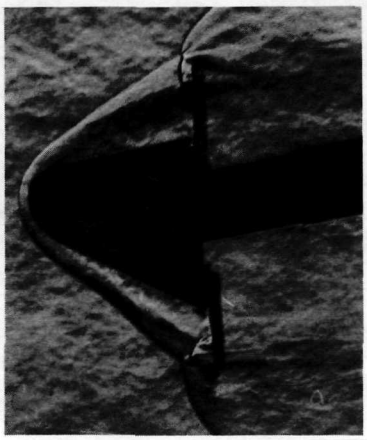

(b) $\alpha = -8^{\circ}$

Figure 33.- Continued.

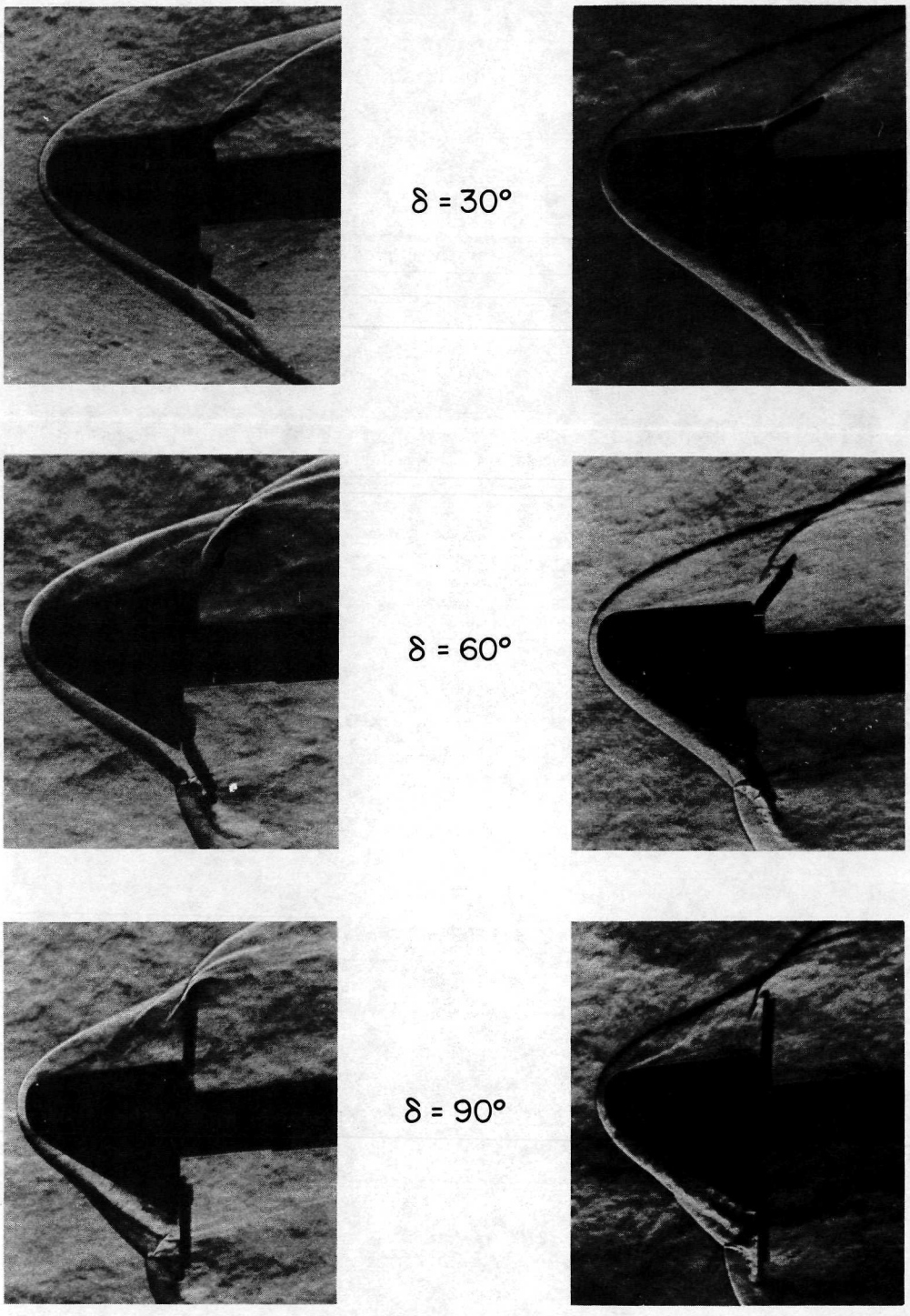

(c) $\alpha = -4^{\circ}$

Figure 33.- Continued.

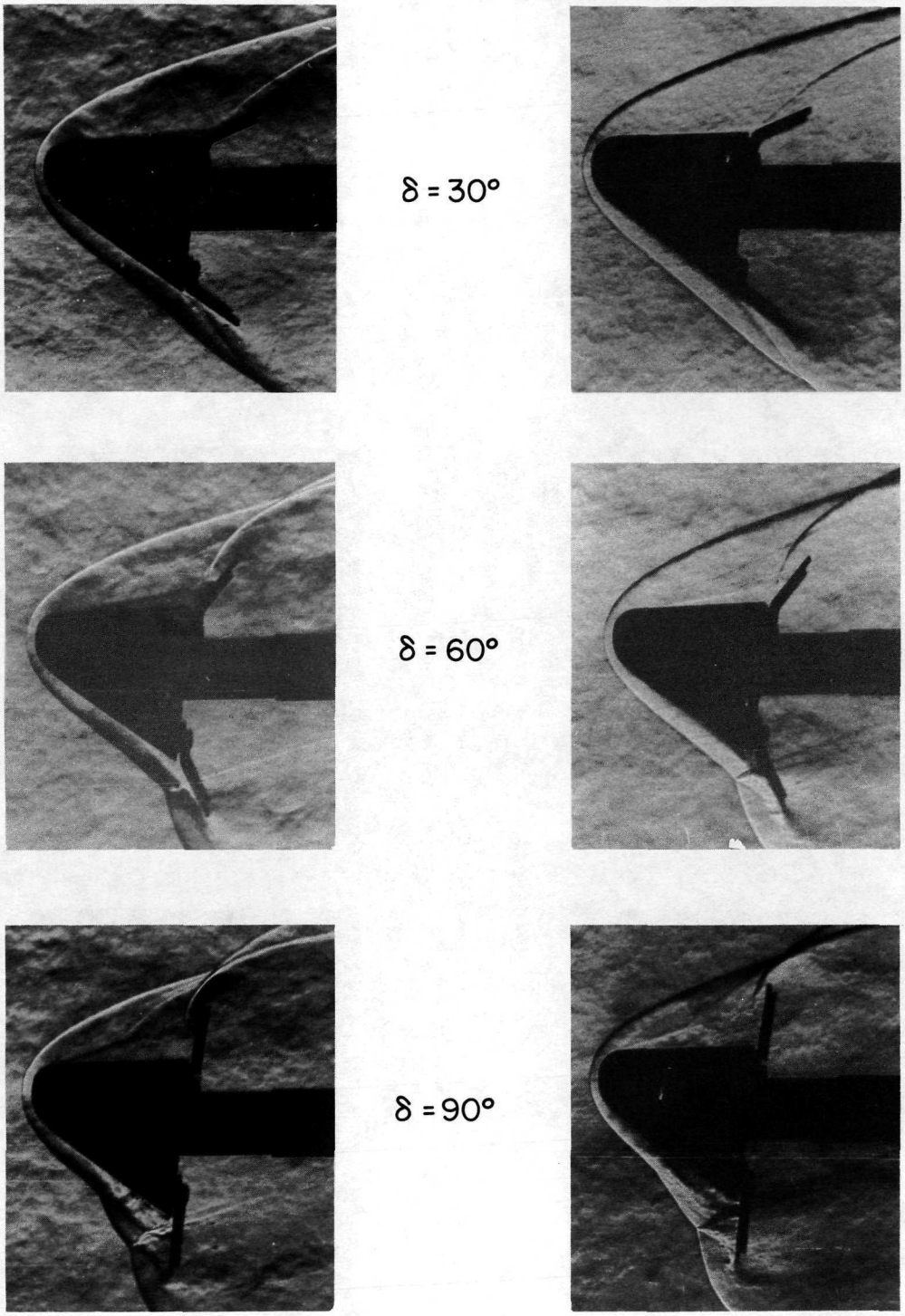

(d) $\alpha = 0^{\circ}$

Figure 33.- Continued.

CONFIDENTIAL

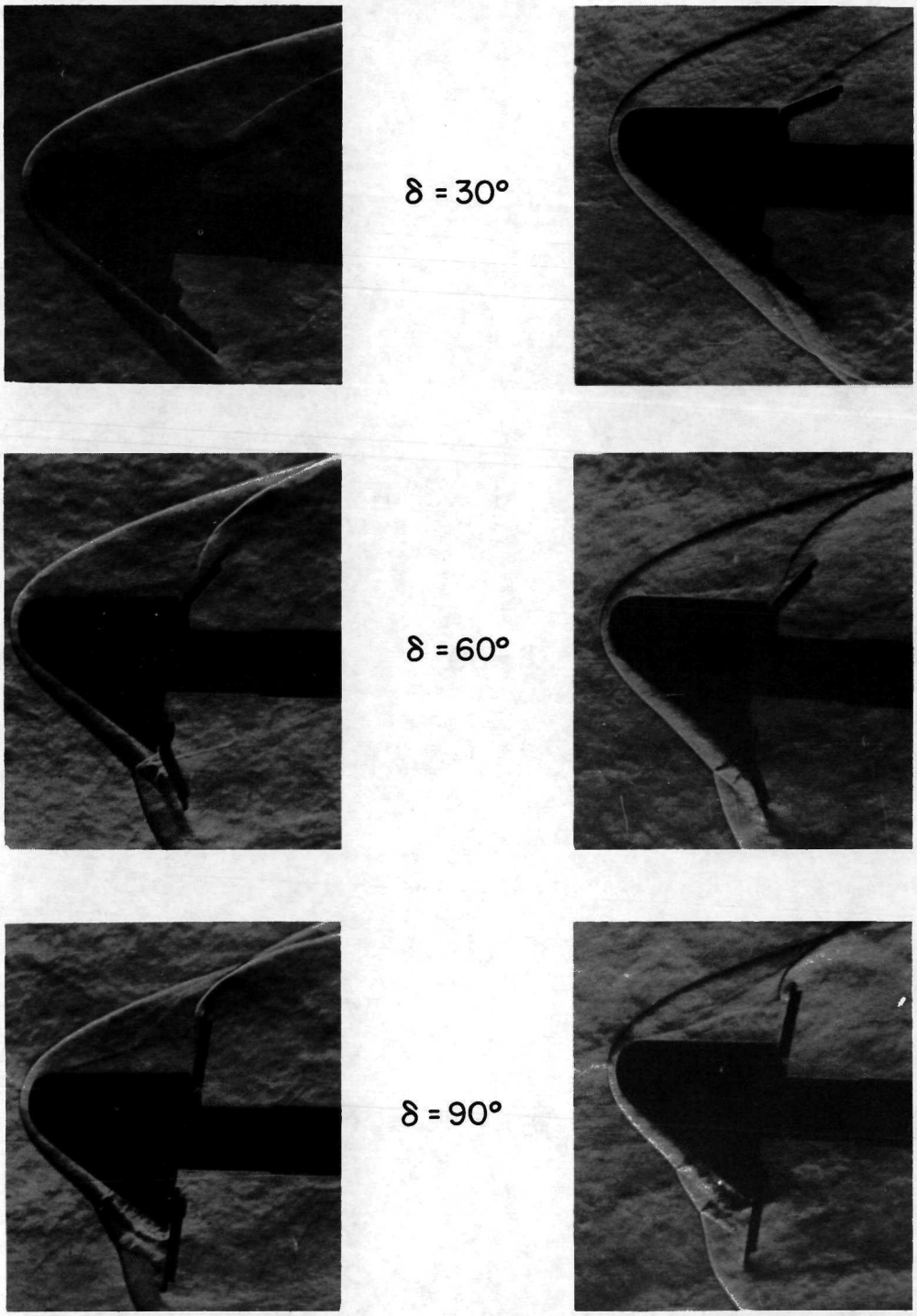

(e) $\alpha = 4^{\circ}$

Figure 33.- Continued.

CONFIDENTIAL

δ = 30°

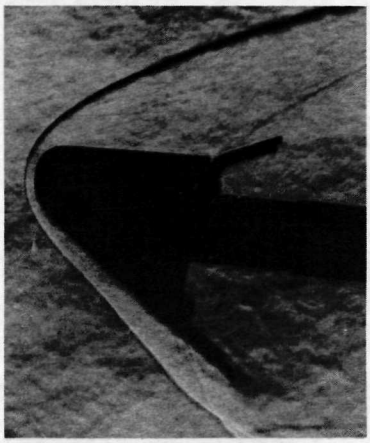

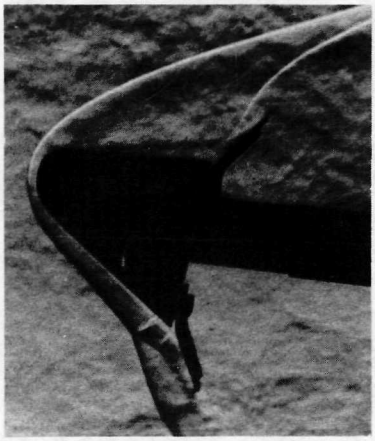

δ = 60°

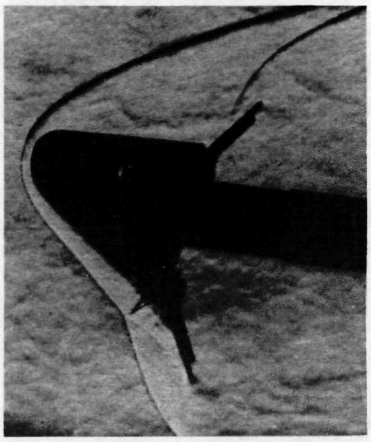

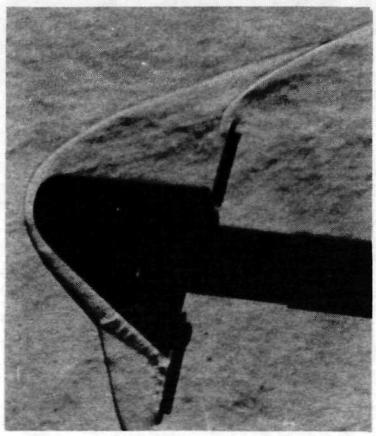

δ = 90°

(f) $\alpha = 8^{\circ}$

Figure 33.- Continued.

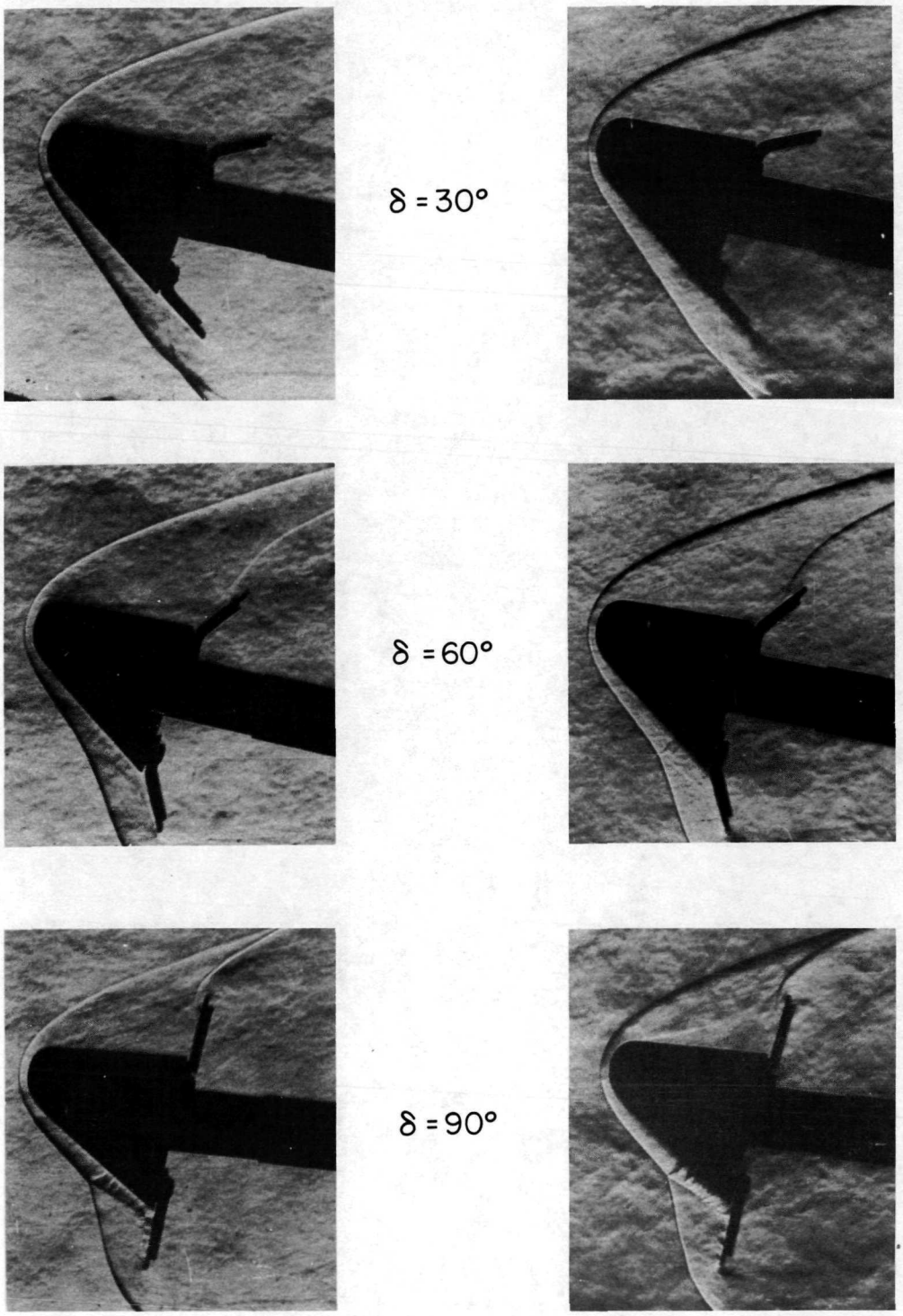

(g) $\alpha = 12^{\circ}$

Figure 33.- Concluded.

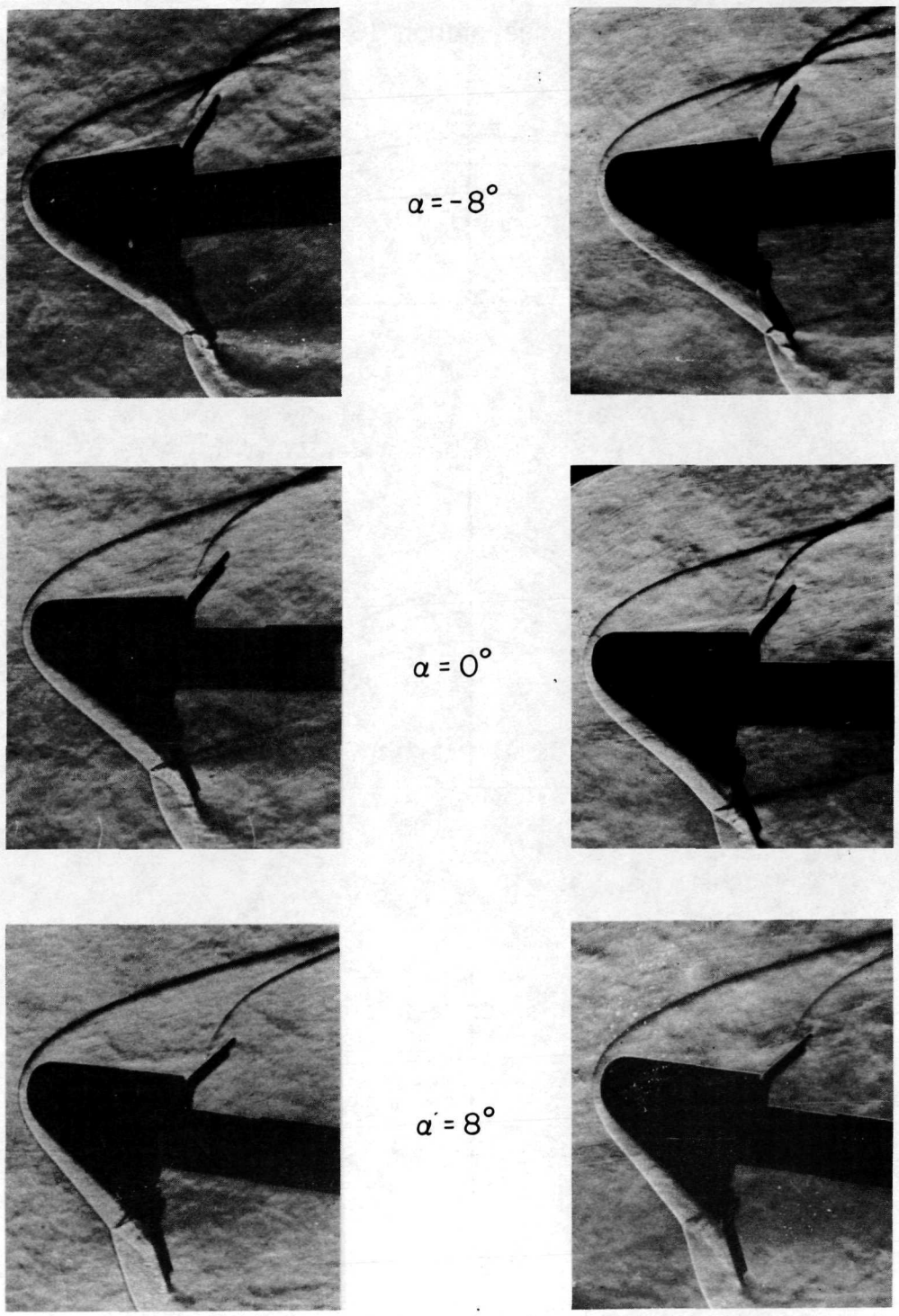

Figure 34.- Comparison of schlieren photographs at Mach numbers of 10.9 and 21.2 for the model with upper and lower controls of control set II deflected 60°.

CONFIDENTIAL

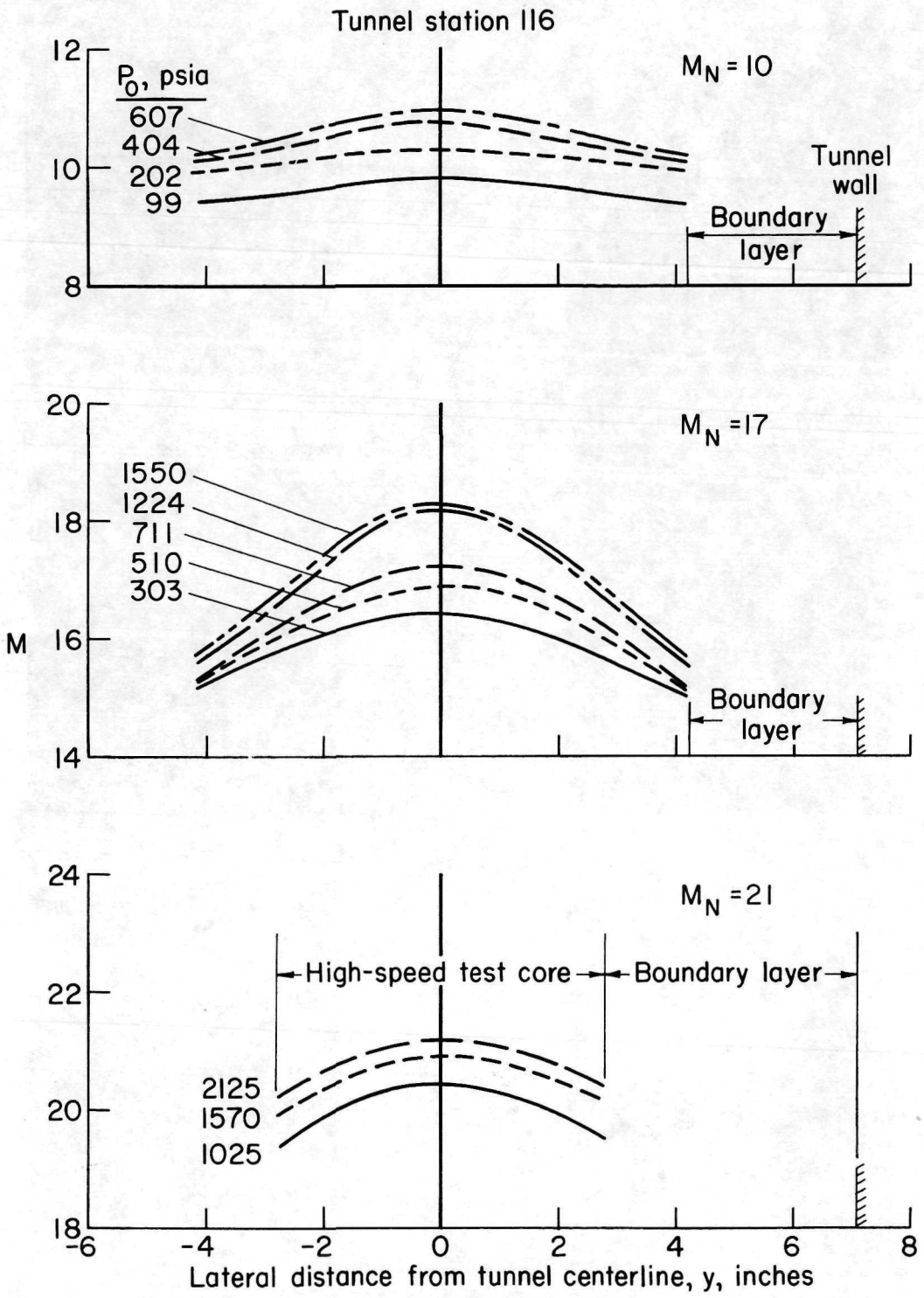

Figure 35.- Lateral Mach number distributions in the model testing area for various values of helium supply pressure.

CONFIDENTIAL

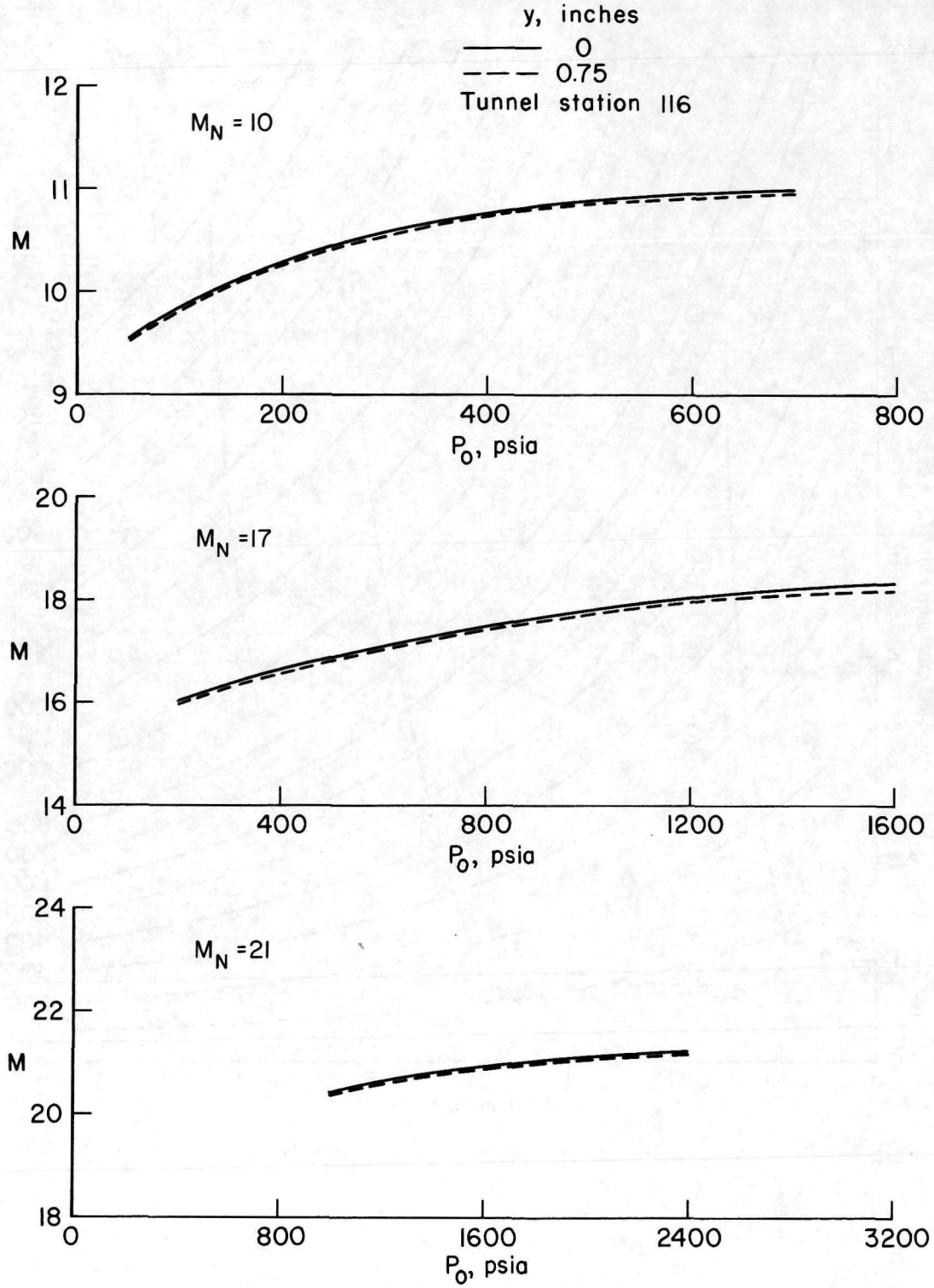

Figure 36.- Variation of Mach number with helium supply pressure.

CONFIDENTIAL

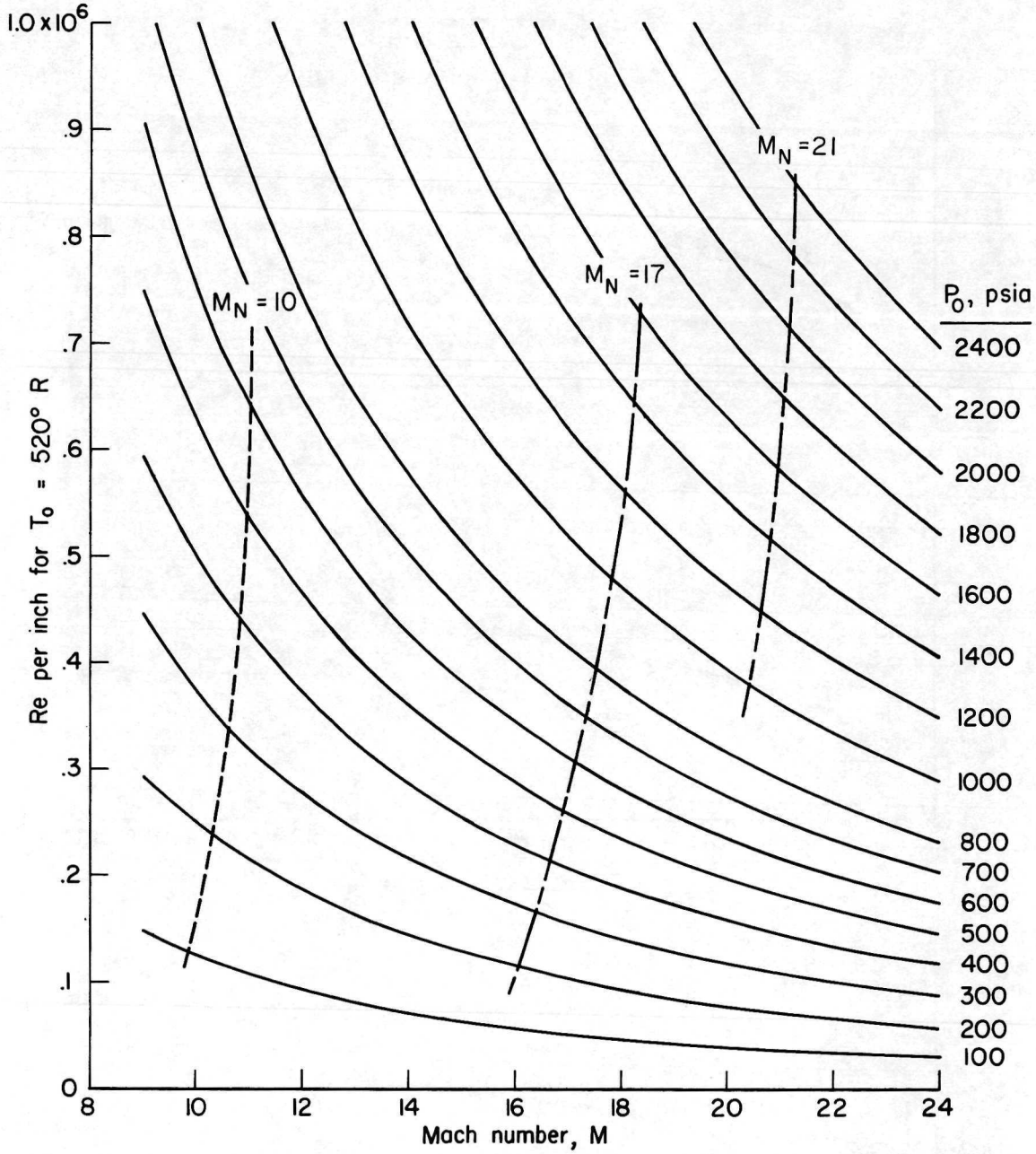

Figure 37.- Test-section Reynolds number per inch for $T_o = 520^\circ$ R.

CONFIDENTIAL

CONFIDENTIAL

CONFIDENTIAL